UNIVERSITÀ DEGLI STUDI DI PADOVA

Dipartimento di Fisica e Astronomia "Galileo Galilei"

Master Degree in Physics

Final Dissertation

Production of Hot Axions in the Early Universe

Thesis supervisors

Dr. Francesco D'Eramo

Prof. Alessio Notari

Candidate

Giovanni Pierobon

Accademic Year 2018/2019

Contents

Introduction

The Standard Model (SM) of particle physics is the most advanced theoretical framework, describing three fundamental forces of nature (strong, weak and electromagnetic) and all the elementary particles. Despite its remarkable and successful agreement with modern experiments, it leaves some phenomena unexplained and many inconsistencies suggest its failure of being a complete theory of fundamental interactions: it does not fully explain indeed the generation of baryon asymmetry, the inclusion of the gravitational interaction (well explained by General Relativity), the generation of neutrino masses recently observed and the dark matter (DM) abundance, among many other problems. At some high energy scale the theory needs to be extended and new physics beyond the Standard Model (BSM) should give the correct explanation of nature. In seeking a unified model that solves the problems presented, we will focus in this work on an hypothetical elementary particle known as *axion*, postulated in 1977 to dynamically solve the *strong CP problem*, that is the absence of CP violation in the strong interactions, within the framework of quantum chromodynamics (QCD). While the solution of this problem, discussed in detail in the first chapter, was a marvellous achievement (at least theoretically), already at the earliest days of the introduction of the QCD axion people realised that it also provides an incredibly promising DM candidate. The axion was later identified as the pseudo Goldstone boson of a new global axial symmetry, whose spontaneous breaking scale f_a defines the mass of the particle and the strength of the couplings with the other SM particles. In order to respect the observations and the limits set by various experiments axions should be very light and therefore very weakly coupled as well, and they were consequently dubbed *invisible* axions. As matter of fact, experimental constraints, also discussed in the work, force us to consider very high scales $f_a \gg 10^7$ GeV, corresponding to small masses $m_a \ll 1$ eV. The particles that we would like to solve our problems are therefore very elusive or very hard to detect, and we need to find possible smart ways to do it, also indirectly and via some theoretical predictions.

Our main goal is to calculate how many axions, if they exist, were thermally produced in the hot plasma of the early Universe. Such a population would not explain in reality the DM abundance, as modern cosmology requires a cold population of particles for the explanation of dark matter, nevertheless, the hot axions would give a contribution instead to the so-called *dark radiation* of the Universe, parameterised by the neutrino species and the quantity ΔN_{eff}, that we will properly introduce. We want to extend the works [26, 27] considering production of axions via model dependent couplings with heavy fermions with also corrections coming from the interaction with Electroweak (EW) particles, such as the Higgs boson. We want to discuss what are the possible values of f_a for every production process to thermalise and give detectable values of ΔN_{eff}. The forecasted sensitivity of future CMB-S4 experiments that measures this observable quantity is reaching an astonishing value $\Delta N_{\mathrm{eff}} \sim 0.01$, comparable to the contributions coming from hot axions. We are also going to briefly review the observational and experimental point of views in axion physics, as we want to establish the current exclusion bands in the parametric space of the axion decay constant and the status of the experiments. We want to assess whether a certain value of f_a could give detectable values of hot axions, but at the same time could fit in the axion cold dark matter models, also discussed in detail in the introductory chapters, and respect observations coming from astrophysics, cosmology and experiments in general.

The work is organised as follows: in the first chapter we explain in detail the strong CP problem and how our best solution is to consider the QCD axion. We also discuss its properties, such as mass and couplings, and the invisible models DFSZ and KSVZ. The second chapter focuses on the cosmological aspects of axions, as we discuss the thermal population and the more complicated cold production mechanisms: the misalignment contribution and topological defects. In chapter 3 and 4 our calculations are rigorously presented: we start from defining the starting lagrangian, we compute the various cross sections, and we then we calculated the axion abundance and the contribution ΔN_{eff}. In the last chapter we take into account all the population and constraints and we define the acceptable windows of values in the f_a parameter space for the invisible models.

Chapter 1

The QCD Axion

1.1 The $U(1)_A$ problem

Let us consider the QCD lagrangian in the low energy limit

$$\mathscr{L} = -\frac{1}{4}G_a^{\mu\nu}G^a_{\mu\nu} + \bar{q}(i\not{D} - m_q)q + \mathcal{O}(\text{heavy quarks})$$

where

$$q = \begin{pmatrix} u \\ d \\ s \end{pmatrix}, \qquad m_q = \begin{pmatrix} m_u & 0 & 0 \\ 0 & m_d & 0 \\ 0 & 0 & m_s \end{pmatrix},$$

and $G^a_{\mu\nu}$ is the gluon field strength of the non-abelian $SU(3)$ gauge group. If we consider massless the light quarks, i.e. $m_u = m_d = m_s = 0$, the lagrangian exhibits the global symmetry $U(N_f)_L \times U(N_f)_R$, with $N_f = 3$ in this case. The symmetry therefore consists of 3×3 unitary matrices in flavour space and can be written as

$$U(3)_L \times U(3)_R = U(1)_V \times U(1)_A \times SU(3)_L \times SU(3)_R. \tag{1.1}$$

In the first part $U(1)_V$ is the symmetry associated to baryon number of light quarks q and related to the vector current $q\gamma^\mu q$, while $U(1)_A$ is the axial symmetry broken by anomalies that will be of crucial importance in our discussion. In the second part we find $SU(3)_L \times SU(3)_R$, the so-called *chiral symmetry* which transforms left-handed and right-handed quarks as

$$q_{L,R} \to \Omega_{L,R}q_{L,R}, \qquad \Omega_{L,R} = \exp(-i\alpha^a_{L,R}t^a),$$

where t^a are the generators of $SU(3)$. The chiral symmetry is broken by the quark condensates $\langle\bar{q}q\rangle$ (basically because in general the rotation has $\alpha^a_L \neq \alpha^a_R$, but in the case where they are equal the subgroup $SU(3)_V$ is unbroken), meaning that at the energy of the QCD phase transition, around the so-called Λ_{QCD} scale, we have the spontaneous symmetry breaking

$$SU(3)_L \times SU(3)_R \to SU(3)_{V=L+R}.$$

It is easy to check that the condensate is invariant under $SU(3)_V$ and the 8 pseudo-Goldstone bosons* arising in the symmetry breaking mechanism are the pseudoscalar mesons $\pi^\pm$,π^0,$K^\pm$,K^0,$\bar{K}_0$ and η. In the two flavour case ($m_u = m_d = 0$)

*They are not Goldstone bosons because of the light quarks masses aren't really zero.

the symmetry breaking is related to $SU(2)_V$ and the three pseudo-Goldstone bosons are just the pions $\pi^{\pm}, \pi^0$. The dynamical degrees of freedom in low energy theory, called *chiral perturbation theory* (CHPT), are therefore the pseudo Nambu-Goldstone bosons (mesons), meaning that we can forget about the confined quarks. The most general, chirally invariant, effective Lagrangian density describing the dynamics of the mesons and with the minimal number of derivatives is [12, 14]

$$\mathscr{L}_\chi = \frac{f^2}{4}\mathrm{tr}\partial_\mu\Sigma\partial^\mu\Sigma^\dagger, \tag{1.2}$$

with

$$\Sigma = \exp\left(\frac{2i\pi(x)}{f}\right), \quad \pi(x) = \frac{1}{\sqrt{2}}\begin{pmatrix} \frac{1}{\sqrt{2}}\pi^0 + \frac{1}{\sqrt{6}}\eta & \pi^+ & K^+ \\ \pi^- & -\frac{1}{\sqrt{2}}\pi^0 + \frac{1}{\sqrt{6}}\eta & K^0 \\ K^- & \bar{K}^0 & -\frac{2}{\sqrt{6}}\eta \end{pmatrix},$$

for the $SU(3)$ case and where $f \approx 93$ MeV is a free parameter, associated to the pion decay constant [12]. The $SU(3)$ matrix π is nothing but the meson matrix

$$\pi(x) = \frac{1}{2}\sum_{a=1}^{8}\lambda_a\pi_a, \tag{1.3}$$

with λ_a the Gell-Mann matrices and π_a are linear combinations of the physical bosons, the latter being in the mass eigenstates. It is important to notice how π^0 and η get mixed because of the two diagonal generators $\pi_8 = \lambda_8/2$ and $\pi_3 = \lambda_3/2$, and the presence of the multiplicative constant $f^2/4$ is for the generation of the standard kinetic form (provided the expansion of the exponential $\Sigma = 1 + 2i\pi/f + \dots$) resulting in

$$\mathscr{L}_\chi = \frac{1}{2}\partial_\mu\pi_a\partial^\mu\pi_a + \mathscr{L}_{int}.$$

However, up until now, we have discussed an exact chiral symmetry without considering the quark masses: the latter are really small but different from zero, leading to an additional explicit breaking of the chiral symmetry. In the low energy limit we can see this breaking because mesons (pions, kaons and η) acquire mass, explaining why we can call them pseudo-particles. Let us see the spectrum in detail: the QCD quark mass term is

$$\mathscr{L}_m = -\bar{q}_L m_q q_R + \mathrm{h.c.} \tag{1.4}$$

and explicitly breaks the $SU(3)_L \times SU(3_R)$ symmetry. We can avoid this technical problem if m_q is an external field that transform under the chiral symmetry as [14]

$$m_q \to \Omega_L m_q \Omega_R^\dagger,$$

but this would change the lagrangian into

$$\mathscr{L}_\chi = \mu\frac{f^2}{2}\mathrm{tr}(\Sigma^\dagger m_q + m_q^\dagger\Sigma), \tag{1.5}$$

where μ is a free parameter that has to be matched by experiments and is related to the chiral quark condensate. Expanding now in small fluctuations around $\Sigma = 1$ we find the mass spectrum of the bosons π_a [14]

$$\mathscr{L}_m = -2\mu\mathrm{tr}(m_q\pi^2), \tag{1.6}$$

where π is the 3×3 matrix written in (1.3). The computation of the trace gives us the masses of charged pions and kaons

$$m_{\pi^\pm}^2=\mu(m_u+m_d),\qquad m_{K^\pm}^2=\mu(m_u+m_s),\qquad m_{K^0,\bar{K}^0}^2=\mu(m_d+m_s),$$

and the $\pi^0-\eta$ system is represented by its mixing matrix

$$\begin{pmatrix} m_u+m_d & \frac{m_u-m_d}{\sqrt{3}} \\ \frac{m_u-m_d}{\sqrt{3}} & \frac{1}{3}(m_u+m_d+4m_s)\end{pmatrix},$$

leading to the masses

$$m_{\pi^0}^2=\mu(m_u+m_d),\qquad m_\eta^2=\frac{\mu}{3}(m_u+m_d+4m_s). \tag{1.7}$$

Now we remember that in the initial symmetry (1.1) we also had $U(1)_V$ and $U(1)_A$; while the $U(1)_V$ is trivially verified (mesons have vanishing net baryon number), the anomalous symmetry is more important. It transforms quarks in the following way:

$$q\to e^{i\alpha\gamma_5/2}q,\qquad \bar{q}\to\bar{q}e^{i\alpha\gamma_5/2}, \tag{1.8}$$

and the Noether current associated to this transformation is the pseudo-vector

$$j_5^\mu=\bar{q}\gamma^\mu\gamma_5 q. \tag{1.9}$$

More importantly, having a diagonal generator $\pi_9=\mathbb{1}/2$, there will be another meson, called η', mixing with both π_0 and η. Recall that in the $SU(2)$ case, where we consider only the up and down quark, the π_8 generator is absent and so it is the η meson, but still in this simple case the π^0 would unavoidably mix with the η' meson, due to the presence of the $U(1)_A$ symmetry. Consequently in the more complete $SU(3)$ case there is a mixing between the π^0, the η and the η', and the presence of the latter can be seen in the matrix π that becomes

$$\pi=\frac{1}{\sqrt{2}}\begin{pmatrix} \frac{1}{\sqrt{2}}\pi^0+\frac{1}{\sqrt{6}}\eta+\sqrt{\frac{2}{3}}\eta' & \pi^+ & K^+ \\ \pi^- & -\frac{1}{\sqrt{2}}\pi^0+\frac{1}{\sqrt{6}}\eta+\sqrt{\frac{2}{3}}\eta' & K^0 \\ K^- & \bar{K}^0 & -\frac{2}{\sqrt{6}}\eta+\sqrt{\frac{2}{3}}\eta' \end{pmatrix}. \tag{1.10}$$

Without writing down a mixing matrix for the $\pi^0-\eta-\eta'$ system, we simply compute from (1.6) the mass of the additonal η' meson

$$m_{\eta'}^2=\frac{4}{3}\mu(m_u+m_d+m_d). \tag{1.11}$$

The masses from (1.7) point out the fact that $m_\eta>m_\pi$ because in the η meson we have the contribution coming from the strange quark, heavier than the both the up and down quarks. However, experimentally we find that[†] the mass of the η' meson vastly exceeds the pion mass

$$m_{\eta'}^2\gg m_\pi^2,$$

while from eq. (1.11) we should expect them to be roughly of the same order of magnitude. This points to an inconsistency historically dubbed by Weinberg [8] the $U(1)_A$ *problem*. This issue seems to be solved considering the anomaly itself and the non trivial topological structure of the QCD vacuum; it was first proposed by 't Hoof in 1986 [7].

[†]The measured values are $m_{\pi_0}\simeq 135$ MeV, $m_\eta\simeq 548$ MeV and $m_{\eta'}\simeq 958$ MeV [15,16].

1.1.1 Instantons solve the problem

The divergence of the axial current (1.9) associated with the $U(1)_A$ symmetry gets a contribution from quantum corrections, coming from the triangle loop diagram which connects it with two gluons [22] (the quarks are in the loop), explicitly

$$\partial_\mu j_5^\mu = -2im_q\bar{q}\gamma_5 q + \frac{N_f\alpha_s}{8\pi}G^a_{\mu\nu}\tilde{G}^{\mu\nu}_a,$$

where $\tilde{G}_{\mu\nu} = 1/2\epsilon^{\mu\nu\rho\sigma}G_{\rho\sigma}$. The second term is called anomaly because even for $m_q \to 0$, called *chiral limit*, it doesn't vanish. However the pseudoscalar density entering in the anomaly is a total derivative:

$$G^a_{\mu\nu}\tilde{G}^{\mu\nu}_a = \partial_\mu K^\mu, \qquad K^\mu = \epsilon^{\mu\nu\alpha\beta}A_{a\nu}\left(F^a_{\alpha\beta} - \frac{g_s}{3}f_{abc}A^a_\alpha A^b_\beta\right),$$

where f_{abc} are the structure constants of $SU(3)$. 't Hooft realized that being $SU(3)$ its gauge group, QCD has a non-abelian structure and there are topologically non-trivial field configurations, called *instantons*, that actually contribute to this operator. Thus, we would make a mistake neglecting the quantum corrections, and the latter explain the large mass of η' compared to the one of the pions and other mesons in general. Let us see how instantons lift $m_{\eta'}$ adding a term to the effective potential of mesons.

The classical vacuum corresponds to configurations with zero field strength, but it does not imply that the potential has to be constant, it just limits the fields to be in the so-called *pure gauge*, a particular orbit in configuration's space, composed by all the gauge transformations of the zero-field configuration:

$$|0\rangle \leftrightarrow A_\mu = 0, \qquad A'_\mu = U\partial_\mu U^\dagger, \tag{1.12}$$

where a particular choice of U can be written as [4] $U = \exp(-it^a n^a F(|\vec{x}|))$, t_a being the generators of the gauge group and F a spherically symmetric function. The correct boundary condition is the one where A_μ is a pure gauge field at spatial infinity, i.e. either $A_\mu = 0$ or a gauge transformation of 0. We use the matrix notation $A_\mu = A^a_\mu t^a$ and it is also useful to work in the temporal gauge $A_0 = 0$. $|0\rangle$ is a trivial configuration and does not correspond to the true vacuum of the theory, in addition we know that we can relate the $|0\rangle$ configuration to a generic $|n\rangle$ configuration by performing gauge transformations

$$\ldots|-1\rangle \to |0\rangle \to |1\rangle \ldots,$$

meaning that there is an infinite set of classical n-vacua, that characterise the real vacuum, enumerated by an integer n called the *Chern-Simons* number or topological charge [21]:

$$n = \frac{1}{16\pi^2}\int d^3x\epsilon^{ijk}\text{tr}[A_iA_jA_k]. \tag{1.13}$$

The anomalous part of the action can be written in terms of n as

$$\delta S = \int d^4x G\tilde{G} = \int d^4x\partial_\mu K^\mu = \int dt\partial_0 n = \Delta n,$$

where in the third step we exploited the temporal gauge, where only $K^0 \neq 0$:

$$K^0 \sim \epsilon_{ijk} \mathrm{tr} A^i A^j A^k .$$

The real QCD vacuum (or in general for $SU(N)$ theories) is called θ-vacuum and is a linear combination of the n-vacua described above

$$|\theta\rangle = \sum_n e^{in\theta} |n\rangle .$$

It is clearly gauge invariant‡ and the θ parameter characterize the vacuum itself. The meaning of this parameter can be understood with an analogy of a periodic potential in quantum mechanics, where we have a degeneracy in the ground state. In the finite barrier case the instantons are the configurations that allow a transition between two neighbouring vacua. If H is the Hamiltonian of the system this tunnelling possibility results in a non-zero overlap between two states $\langle n \pm 1|H|n\rangle = -\Delta$ that obviously depends on the barriers height. Computing the energy eigenvalues we find an additional term due to the instantons [3]:

$$H |\theta\rangle = (E_0 - 2\Delta \cos\theta) |\theta\rangle$$

and we know that Δ can be derived from the Euclidean action of the theory§

$$S_E = -\frac{1}{2g^2} \int d^4x \mathrm{Tr}[G_{\mu\nu} G^{\mu\nu}], , \tag{1.14}$$

and it can be proven [4] that the *self-duality* and *anti self-duality* equations

$$G_{\mu\nu} = \tilde{G}_{\mu\nu}, \quad n > 0 \tag{1.15}$$

$$G_{\mu\nu} = -\tilde{G}_{\mu\nu}, \quad n < 0 \tag{1.16}$$

satisfy the general Yang-Mills equations, coming from the action (1.14). Now, the minimum of the action over fields with a fixed topological charge n is a solution of the Yang–Mills equations and the instanton is the solution with $n = 1$¶ [4] shows a lower bound on the Euclidean action for fixed n

$$S \geq \frac{8\pi^2}{g_s^2} |n|, \tag{1.17}$$

meaning that the instanton action is the latter with $n = 1$. It is clear that the instanton configuration is not heavily suppressed only when g_s grows sufficiently below the the QCD scale, where perturbation theory fails. Our gauge filed, in the pure gauge definition (1.12) and with our ansatz on U (spherical symmetry) can be written as

$$A'_\mu = U A_\mu^{inst} U^\dagger + U \partial_\mu U^\dagger, \tag{1.18}$$

where A_μ^{inst} is the instanton configuration. Therefore the overlap Δ in the tunnelling amplitude must be proportional to action (1.17)

$$\Delta = k e^{-8\pi^2/g_s^2}, \tag{1.19}$$

‡Calling G the gauge transformation we know that $G|n\rangle = |n+1\rangle$, so $G|\theta\rangle = \sum_n e^{in\theta} |n+1\rangle = e^{-i\theta} \sum_{n'} e^{in'\theta} |n'\rangle = e^{-i\theta} |\theta\rangle$ and the phase is irrelevant.

§It is useful to define the gauge field as $A_\mu = -igt^a A_\mu^a$ and the Euclidean metric is implied.

¶The anti-instanton corresponds to the solution with $n = -1$.

giving

$$E(\theta) = -2ke^{-8\pi^2/g_s^2}\cos\theta. \tag{1.20}$$

Moreover, computing vacuum expectation values of an operator X on the θ-vacuum means solving the path integral

$$\langle\theta|X|\theta\rangle = \sum_{m,n}\langle m|Xe^{i(m-n)\theta}|n\rangle = \int \mathcal{D}A_\mu\mathcal{D}\psi\mathcal{D}\bar{\psi}X\exp\left[i\int\mathscr{L}_{\text{QCD}}d^4x + i(m-n)\theta\right],$$

but given the complexity of $|\theta\rangle$ we can avoid this technical problem by performing the integral in the easier $\theta = 0$ configuration, but changing the lagrangian:

$$\langle\theta|X|\theta\rangle|_{\mathscr{L}_{\text{QCD}}} = \langle\theta = 0|X|\theta = 0\rangle|_{\mathscr{L}'_{\text{QCD}}},$$

where

$$\mathscr{L}'_{\text{QCD}} = \mathscr{L}_{\text{QCD}} + \frac{\alpha_s}{8\pi}G_{\mu\nu}\tilde{G}^{\mu\nu}\theta_{\text{QCD}}.$$

This is a useful result, as we can acknowledge $\mathscr{L}'_{QCD}$ as the new QCD lagrangian that takes into account the complex structure of its vacuum. We finally have an additional term takes place in the η' sector of the meson potential

$$\delta V_{eff} = 2ke^{-8\pi^2/g_s^2}\cos\theta \simeq \Lambda^4\cos\theta, \tag{1.21}$$

explaining why the η' mass is much bigger than the other mesons' and solving the $U(1)_A$ problem

$$m_{\eta'}^2 \sim \frac{\Lambda^4}{f^2} \gg m_\pi^2.$$

1.2 Strong CP problem

The resolution of the $U(1)_A$ problem effectively adds an extra term to the QCD lagrangian because of the complicated vacuum structure

$$\mathscr{L}_\theta = \frac{\alpha_s}{8\pi}G_{\mu\nu}\tilde{G}^{\mu\nu}\theta, \tag{1.22}$$

calling $\theta \equiv \theta_{\text{QCD}}$. In addition, if we consider the weak interactions that the quark possess, we should also include the term

$$\mathscr{L}_m = -\bar{q}_{iR}M_{ij}q_{jL} + \text{h.c.}, \qquad M_{ij} = (m_q e^{i\theta_Y})_{ij}, \tag{1.23}$$

where m_q are the bare quark masses given by the interaction with the Higgs field. It is important to notice how both terms (1.22) and (1.23) are CP (T) violating; the $G\tilde{G}$ term violates parity and the time reversal symmetry but shows charge conjugation invariance, explicitly

$$G^a_{\mu\nu}\tilde{G}^{\mu\nu}_a = \vec{E}_a\cdot\vec{B}_a \xrightarrow{T} -\vec{E}_a\cdot\vec{B}_a, \qquad (\vec{E}_a \xrightarrow{T} -\vec{E}_a, \quad \vec{B}_a \xrightarrow{T} \vec{B}_a),$$

where $E_i^a = G_{0i}^a$ and $B_i^a = G_{ij}^a$ are the chromoelectric and chromomagnetic fields, respectively. The quark mass term is instead related to the CP violating phase of the weak sector within the Standard Model framework. It is convenient to use a physical basis, that can be reached by performing a chiral transformation, as in

(1.8), which changes θ by $ArgDetM$. In other words the physical contribution to the lagrangian multiplying the anomalous $G\tilde{G}$ term would be the combination

$$\bar{\theta} = \theta + ArgDetM = \theta + N_f\theta_Y, \tag{1.24}$$

where N_f is the number of active quarks we are considering in the theory, and we should consider the lagrangian (1.22) with the substitution $\theta \to \bar{\theta}$. The presence of the $\bar{\theta}$-term is crucial since it would give rise to an electric dipole moment (EDM) d_n for the neutron [10, 17]

$$\mathscr{L}_{EDM} = -\frac{d_n}{2}(\bar{\psi}_n i\gamma_5\sigma^{\mu\nu}\psi_n)F_{\mu\nu}, \qquad d_n \simeq e\bar{\theta}\frac{m_q}{m_N^2}.$$

Experimentally we have a strong constraint on this quantity (and that is why we can say that strong interactions don't violate CP):

$$|d_n| < 2.9 \times 10^{-26}\ e\ \text{cm}\ (90\%\ \text{C.L.}), \qquad |\bar{\theta}| \lesssim 10^{-10}.$$

The experimental bound on d_n is converted therefore into a strong constraint on the value of $\bar{\theta}$, that clearly represents a fine tuning issue, the famous *Strong CP problem*. There are two compelling possible solutions: the first one is to consider a *spontaneously broken CP symmetry* [10], setting $\theta = 0$ at classical level. However, if CP is spontaneously broken θ gets induced back at the loop-level and for values $\theta < 10^{-9}$ we would need a vanishing θ also at 1-loop. But the real problem with this scenario is that experimental data in excellent agreement with the CKM Model, where CP is explicitly, not spontaneously broken. The second viable solution is via introducing a *new chiral symmetry*, and it is believed to be a natural solution, because this additional symmetry would rotate θ away, solving the apparent inconsistency with experiments. Moreover, as physicists, we believe that small numbers are hinting at some dynamical processes, usually related to symmetries, enlightening new physics.

1.3 $U(1)_{PQ}$ and the QCD axion

In 1977 Peccei and Quinn introduced a new $U(1)$ global symmetry [9], later known as $U(1)_{PQ}$, promoting the CP violating $\bar{\theta}$ parameter to a spacetime dependent dynamical field, the *axion* ϕ. The Peccei-Quinn symmetry is spontaneously broken, meaning that the axion is a Goldstone boson and exhibits the shift symmetry

$$\phi \to \phi + \alpha f_a, \tag{1.25}$$

where α is a constant and f_a, called the *axion decay constant*, is the order parameter associated to the breaking of $U(1)_{PQ}$. The SM is augmented by an additional degree of freedom (the axion is a real scalar) and the lagrangian becomes

$$\mathcal{L} = \mathcal{L}_{SM} - \frac{1}{2}\partial_\mu\phi\partial^\mu\phi + \left(\bar{\theta} + \frac{N\phi}{f_a}\right)\frac{\alpha_s}{8\pi}G_{\mu\nu}\tilde{G}^{\mu\nu} + \mathcal{L}_{int},$$

where the last piece encodes the interaction terms that must satisfy the shift symmetry (1.25) and N is a constant known as *colour anomaly coefficient* (1.44). The $G\tilde{G}$ is explicitly violating the PQ symmetry via the anomaly and around Λ_{QCD}, where QCD non-perturbative effects (instantons) will become relevant, the axion acquires a mass. The anomalous part of the effective potential (1.21) becomes

$$\delta V_{eff} = \Lambda^4 \cos\left(\bar{\theta} + \frac{N\phi}{f_a}\right), \tag{1.26}$$

and the minimum of the potential is given by the condition $\partial_\phi V_{eff} = 0$, solved by

$$\langle\phi\rangle = -\frac{f_a \bar{\theta}}{N}.$$

In this way at the minimum the $\bar{\theta}$-term is cancelled out, if we write the lagrangian in terms of $\phi_{phys} = \phi - \langle\phi\rangle$, and this provides the requested dynamical solution of the strong CP problem. Around the Λ_{QCD} scale the axion is mixing with π^0 and the η' meson (and the η meson in the $N_f = 3$ case) in the following way

$$\eta'(x) = \pi_9(x) + \beta\phi(x),$$

$$\pi^0(x) = \pi_3(x) + \alpha\phi(x),$$

$$a(x) = \phi(x) - \alpha\pi_3(x),$$

where (see 1.3.1)

$$\beta = \frac{f}{2f_a}, \qquad \alpha = \frac{m_d - m_u}{2(m_u + m_d)}\frac{f}{f_a}.$$

Clearly $\eta'(x), \pi^0(x)$ and $a(x)$ are the mass eigenstates, namely the states of physical particles. However, usually people use the word axion for both ϕ and a, but here we will refer to a as the physical mass eigenstate, after the mixing. The mass of the axion can be found expanding V_{eff} in the minimum.

1.3.1 Zero temperature mass

The analytical expression of the effective potential and the mass at $T = 0$ can be computed with chiral perturbation theory. In the simple $SU(2)$ QCD case the three Goldstones are $\pi^\pm$ and π^0 and we recall the chiral lagrangian for the pions (1.5)

$$\mathscr{L}_\chi = \mu\frac{f^2}{2}\mathrm{tr}(\Sigma^\dagger m_q + m_q^\dagger \Sigma), \tag{1.27}$$

where now the π matrix is simply

$$\pi(x) = \frac{1}{2}\begin{pmatrix} \pi^0 & \sqrt{2}\pi^+ \\ \sqrt{2}\pi^- & -\pi^0 \end{pmatrix},$$

and τ^a are the three $SU(2)$ generators. Let us match the lagrangian (1.27) with the axion dependent part of the lagrangian, written without loss of generality as [19]

$$\mathscr{L}_a = \frac{1}{2}(\partial_\mu a)^2 + \frac{a}{f_a}\frac{\alpha_s}{8\pi}G_{\mu\nu}\tilde{G}^{\mu\nu} + \frac{1}{4}a g^0_{a\gamma\gamma}F_{\mu\nu}\tilde{F}^{\mu\nu} + c^0_q\frac{\partial_\mu a}{2f_a}\bar{q}\gamma^\mu\gamma_5 q. \tag{1.28}$$

$F_{\mu\nu}$ is the photon field strength, with the coupling

$$g^0_{a\gamma\gamma} = \frac{\alpha_{em}}{2\pi f_a}\frac{E}{N},$$

with E and N the electromagnetic and colour anomaly, respectively. These anomalies and the current $j^{\mu}_{a,0} = c^0_q \bar{q}\gamma^{\mu}\gamma_5 q$ are model dependent, see for instance section 1.4. Both the $F\tilde{F}$ term and the derivative coupling with matter are respecting the shift symmetry (1.25) that we used to eliminate the $\bar{\theta}$-term, therefore the only explicit violation comes from the pure QCD sector, i.e. the coupling with the gluons. The latter can be conveniently absorbed into the light quarks by a field redefinition

$$q \to e^{-i\frac{a(x)}{f_a}Q_a\gamma_5}q, \qquad \mathrm{Tr}(Q_a) = 1, \tag{1.29}$$

where $q = (u,d)^T$ in the simple $N_f = 2$ case. The lagrangian (1.28) becomes

$$\mathscr{L}_a = \frac{1}{2}(\partial_\mu a)^2 + \frac{1}{4} a g_{a\gamma\gamma} F_{\mu\nu}\tilde{F}^{\mu\nu} + \frac{\partial_\mu a}{2f_a} j^{\mu}_a - (\bar{q}_L M_a q_R + \mathrm{h.c.}), \tag{1.30}$$

where now

$$g_{a\gamma\gamma} = \frac{\alpha_{em}}{2\pi f_a}\left[\frac{E}{N} - 6\mathrm{tr}(Q_a Q^2)\right], \qquad j^{\mu}_a = j^{\mu}_{a,0} - \bar{q}\gamma^{\mu}\gamma_5 Q_a q, \qquad M_a = e^{i\frac{a}{2f_a}Q_a} m_q e^{i\frac{a}{2f_a}Q_a},$$

and $Q = \mathrm{diag}(2/3, -1/3)$ represents the electrical charge of the quarks. Now, coming back to the lagrangian (1.27) and looking at the neutral (diagonal) sector we obtain a potential similar to (1.21) [19]:

$$V_{eff}(a) = -f^2\Lambda\left[m_u \cos\left(\frac{\pi^0}{f} - \frac{a}{2f_a}\right) + m_d\left(\frac{\pi^0}{f} + \frac{a}{2f_a}\right)\right] \tag{1.31}$$

$$= -m_\pi^2 f_\pi^2 \sqrt{1 - \frac{4m_u m_d}{(m_u+m_d)^2}\sin^2\left(\frac{a}{2f_a}\right)}\cos\left(\frac{\pi^0}{f} - \varphi_a\right), \tag{1.32}$$

with

$$\tan\varphi_a = \frac{m_u - m_d}{m_u + m_d}\tan\left(\frac{a}{2f_a}\right),$$

but we know that on the vacuum π^0 acquires a VEV proportional to φ_a, so the last cosine is trivially equal to 1. Expanding to quadratic order we get the well-known formula for the axion mass in the $N_f = 2$ case:

$$m_a^2 = \frac{m_u m_d}{(m_u+m_d)^2}\frac{m_\pi^2 f_\pi^2}{f_a^2}. \tag{1.33}$$

It is important make a comment regarding the expression of the effective axion potential: when we introduced the instantons we ended up with the single cosine potential (1.21), however, as pointed out in [19], the potential (1.32) calculated with chiral perturbation theory is nowhere close to the potential suggested by the instanton calculation (see fig. 1.1). This is essentially because the latter relies on the semiclassical approximation.

With chiral PT is also possible to determine the relevant coupling with photons[‖]

$$g_{a\gamma\gamma} = \frac{\alpha_{em}}{2\pi f_a}\left[\frac{E}{N} - \frac{2}{3}\frac{4m_d + m_u}{m_d + m_u}\right] = \frac{\alpha_{em}}{2\pi f_a}\left[\frac{E}{N} - 1.92\right], \tag{1.34}$$

where the only model dependent part is the factor E/N, see section 1.4.

[‖] The coupling $g_{a\gamma\gamma}$ is not important for the solution of the strong CP problem but is relevant for axion detection. Almost all the detection techniques, including haloscopes and helioscopes [17], rely on the axion-photon effective coupling.

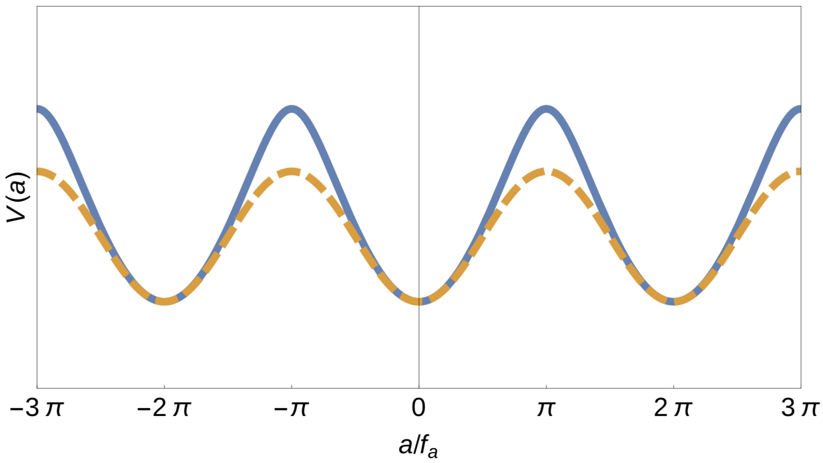

Figure 1.1: Comparison between the instanton potential (dashed line) and the effective potential computed with chiral perturbation theory (continuous line) [19].

1.3.2 Finite temperature

The axion mass we computed is valid in principle for $T = 0$, but effectively the zero temperature value is valid only for $T \lesssim \Lambda_{QCD}$, i.e. after the QCD phase transition has occurred. A power law dependence on the temperature can be found analytically if we recall the instantons and we consider the running of the coupling constant α_s. At high temperatures large gauge configurations are exponentially suppressed because of Debye screening, where at leading order the perturbative Debye mass is

$$m_D^2 = \left(\frac{N_c}{3} + \frac{N_f}{6}\right) g_s^2 T^2. \tag{1.35}$$

The axion potential has a dependence on T [18, 19]

$$V(\phi, T) = -f_a^2 m_a^2(T) \cos\left(\frac{\phi}{f_a}\right), \tag{1.36}$$

$$f_a^2 m_a^2(T) = 2 \int d\rho \, n(\rho, 0) e^{-\frac{2\pi^2}{g_s^2} m_D^2 \rho^2}, \tag{1.37}$$

where $n(\rho, 0) \propto e^{-8\pi^2/g_s^2}$ is the zero temperature instanton density and ρ is the instanton size appearing in the solution A_μ^{inst}. If we fix $N_c = 3$ and N_f to the number of active flavours at a given temperature, then the integral can be solved within the saddle point approximation, and the functional dependence on T of (1.37) is a power law $T^{-\alpha}$, where $\alpha \approx 7 + N_f/3$ is only fixed by the QCD β function $\beta(\alpha_s) \simeq b_0 \alpha_s^2$. However, even tough it shows a power-law dependence, the calculation is not really reliable because it is based on the dilute instanton gas approximation that works at finite temperature perturbative QCD [19].

Therefore we need direct computations from non-perturbative methods such as lattice QCD, where recent calculations show a power-law dependence on T for the axion mass,at high temperatures ($T > 1$ GeV) [23]

$$m_a^2(T) = \alpha_a \frac{\Lambda_{QCD}^3 m_u}{f_a^2} \left(\frac{T}{\Lambda_{QCD}}\right)^{-n}. \tag{1.38}$$

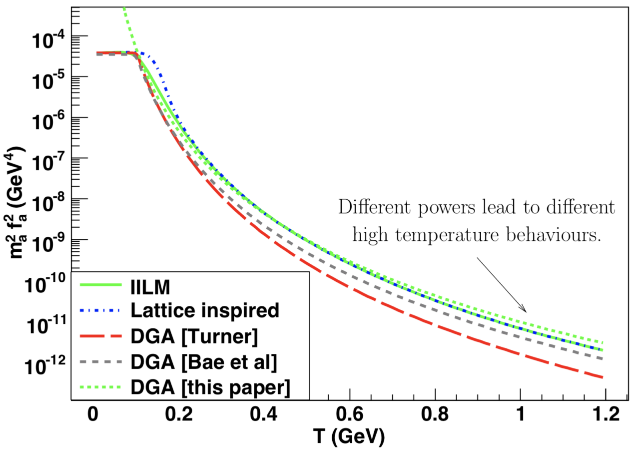

Figure 1.2: Numerical simulations of the axion temperature mass around the GeV scale. The IILM [24] is represented by the green continuous line.

The fit from the so called *interacting instanton liquid model* (IILM) [24] gives $n = 6.68$ and $\alpha_a = 1.68 \times 10^{-7}$. As we can see in fig. 1.2 the zero temperature mass value is reached for $T \lesssim 200$ MeV, after the QCD phase transition, and is usually written in the literature [25]

$$m_a \simeq 5.7 \times 10^{-3}\ \text{eV} \left(\frac{10^9\ \text{GeV}}{f_a}\right). \tag{1.39}$$

For high values of temperature our knowledge of axion properties gets worse because there are no lattice results available. Our power-law behaviour (1.38) just shows that for $T \gg 1$ GeV the value of the mass is indeed irrelevant, as we know that near the scale of PQ breaking f_a (we will see in the next chapter what ranges of f_a we should consider) the axion is a massless degree of freedom.

1.4 Invisible axion models

In the last section we computed in the low energy limit the axion potential and mass, but up until now we only discussed the effective theory for energies below the spontaneous symmetry breaking of the PQ symmetry. The $\phi G\tilde{G}$ operator is 5-dimensional and therefore non-renormalizable, meaning that for high energies ($E > f_a$) the model needs a so-called *UV completion*, in order to describe the correct physics. Let us mention the proposed models that extend the SM:

- ◇ PQWW: the Peccei-Quinn-Weinberg-Wilczek axion, which introduces one additional complex scalar field only, tied to the EW Higgs sector.
- ◇ DSFZ: the Dine-Fischler-Srednicki-Zhitnitsky axion, which introduces an additional Higgs field as well as the PQ field.
- ◇ KVSZ: the Kim-Shifman-Vainshtein-Zakharov axion, which introduces heavy quarks as well as the PQ field.

The PQWW was historically the first QCD axion model, introducing a single additional complex scalar field, φ, to the standard model as a second Higgs doublet.

Just like the Higgs it features a symmetry breaking potential

$$V(\varphi) = \lambda \left(|\varphi|^2 - \frac{f_a^2}{2} \right)^2 , \tag{1.40}$$

that takes the VEV $\langle \varphi \rangle = f_a/\sqrt{2}$ at the electroweak scale. This means that after electroweak symmetry breaking (EWSB) we are left with two additional EM neutral scalars, which are the heavy radial part $\rho(x)$ and the angular field $\phi(x)$

$$\varphi = \rho(x) e^{i\frac{\phi(x)}{f_a}} , \tag{1.41}$$

and ϕ is indeed the axion field, as the Goldstone boson of the spontaneously broken $U(1)_{PQ}$. In this model the axion couples to the SM via the chiral rotations (as we have seen in 1.3.1), the chiral anomaly induces couplings to the gauge bosons $G^a_{\mu\nu}, F_{\mu\nu}$ and all the couplings are suppressed by f_a. Nevertheless the PQWW model is excluded by experiments because f_a (set at the EW scale) is relatively small and therefore couplings too large. In the KSVZ and DFSZ models φ is introduced independently of the energy scale and f_a is a free parameter with a lower bound, in order to avoid couplings excluded by whichever type of experiment. This is why the KSVZ and DFSZ models are called *invisible models*.

The DFSZ model

The DFSZ model is similar to the PQWW, but the field φ is introduced as a standard model singlet and couples to it via the Higgs sector, that contains two Higgs doublets H_u, H_d like in the PQWW model [23],

$$\mathscr{L}_H = \lambda_H \varphi^2 H_u H_d.$$

Consequently in oder to be PQ invariant the model assigns PQ charge $+1$ to φ and -1 to both the Higgs doublets. The latter also couple to SM fermions via the Yukawa coupling

$$\mathscr{L}_Y = y_u \bar{q}_L H_u u_R + \ldots ,$$

meaning that the SM fermions have to be charged under $U(1)_{PQ}$ as well, leading to a large colour anomaly coefficient $N = 6$. In addition in the DSFZ model there are tree-level couplings between the axion and standard model fermions, via the chiral term in mass matrix, as opposed to KSVZ, where there are 1-loop couplings via new heavy quarks. The DSFZ model is very important in our work when we consider (see chapter 3) thermal axion production by scattering and annihilation of heavy SM quarks (mostly t, b) with the tree-level coupling $\phi\bar{q}q$

$$\mathscr{L}_{\phi\bar{q}q} = \frac{\partial_\mu \phi}{2 f_a} \sum_q c_q \bar{q}_f \gamma^\mu \gamma_5 q. \tag{1.42}$$

In the derivative basis of the lagrangian (3.1) the coefficient c_q is the PQ charge of the quark (or fermion in general) considered.

The KSVZ model

The KSVZ is instead the simplest invisible axion model, its lagrangian is

$$\mathscr{L}_{KSVZ} = \mathscr{L}_{SM} + \bar{Q} i \not{D} Q + \partial_\mu \varphi^* \partial^\mu \varphi - V(\varphi^* \varphi) - (y \bar{Q}_L \varphi Q_R + \text{h.c.}), \tag{1.43}$$

where φ is also a SM singlet, but in this model we are introducing a new heavy quark doublet Q that is a weak singlet, colour charged and PQ-charged. These new quarks induce the anomaly through the loop diagram of the $G\tilde{G}$ term, see fig. 1.3.

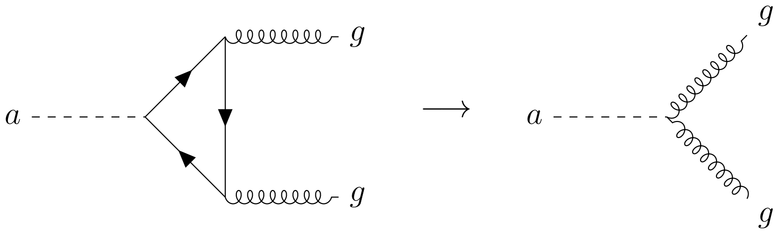

Figure 1.3: Feynman diagram of the anomalous axion coupling with gluons. In the KSVZ model the new heavy quarks Q are running in the loop.

The lagrangian is $U(1)_{PQ}$ symmetric, i.e. invariant under the transformations

$$Q \rightarrow e^{iQ_{PQ}\gamma_5/2} Q, \qquad \varphi \rightarrow e^{-iQ_{PQ}} \varphi,$$

where Q_{PQ} is the PQ charge. At low energies, after PQ symmetry breaking by the VEV of φ, the Q fields obtain a large mass due to the last term in the lagrangian (1.43), $m_Q \sim y f_a$. It is then possible to integrate them out, meaning that for much lower energies ($E \ll m_Q$) the coupling of the axion is directly to gluons. The latter is proportional to $\sim N/f_a$, and the colour anomaly N is defined as

$$N\delta_{ab} = 2\mathrm{Tr} T_a T_b Q_{PQ}, \tag{1.44}$$

where T_a, T_b are the $SU(3)$ generators. The coupling with the photons (1.34) is the same replacing the gluons with two photons ($\rightarrow$), and the EM anomaly is therefore

$$E = 2\mathrm{Tr} Q_{EM}^2 Q_{PQ}.$$

We can then see how for example the KSVZ and DFSZ models differ: the E/N term in the $g_{a\gamma\gamma}$ expression is equal to 0 for the KSVZ and 8/3 for the DFSZ.

Chapter 2

Axion Cosmology

Let us review the general picture for axion particles given in the previous chapter, focusing now on the cosmology of the very early Universe. Two important physical processes determine the behaviour of axions: spontaneous symmetry breaking occurs at some high scale f_a, establishing the axion as a Goldstone boson and non-perturbative effects, QCD *instantons*, becomes relevant at some temperature $T_{NP} \ll f_a$, providing an effective potential for the axion. The axion field ϕ (before mixing with pions), related to the angular degree of freedom of a complex scalar, shows a shift symmetry $\phi \to \phi + const$ and is massless to all orders in perturbation theory. The scale of non-perturbative physics is called Λ and the potential induced must respect a residual shift symmetry $\phi \to \phi + 2\pi n f_a/N_{DW}$, for some integer n. In other words the explicit breaking by NP physics can be written as $U(1)_{PQ} \to Z(N_{DW})$, where N_{DW} is and integer called *domain-wall* number. A particularly simple, but not unique, choice for the potential is [23]

$$V(\phi) = \Lambda^4(t)\left[1 - \cos\left(\frac{N_{DW}\phi}{f_a}\right)\right], \tag{2.1}$$

where we can write $\Lambda^4(t) = f_a^2 m_a^2(t)$, and the time-dependence on the mass is accounted because of the increasing NP effects when decreasing the temperature of the Universe*. The relic density of axions can be written as $\rho_a = \Omega_a \rho_c$ with

$$\rho_c = \frac{3H_0^2}{8\pi G},$$

and is given by the sum of the relic axion populations that can arise in the early Universe. These are:

- ◇ Hot thermal axions.
- ◇ Cold axions from vacuum realignment (pre- and post-inflationary scenarios).
- ◇ Cold axions from decay of topological defects (strings, domain-walls).

In the next chapters we are going to discuss in detail the production of thermal axions at the electroweak scale, where the axion is essentially massless and the only scale of interest is f_a. Hot axions are generically dubbed *Dark Radiation* (DR). The effective potential instead becomes relevant when we will describe the axion field evolution for cold populations. The latter are widely interpreted, as we shall see, as a promising Dark Matter (DM) candidate.

*In the first chapter we saw the temperature dependence of the axion mass (1.38), but as we know time and temperature are inversely proportional and related by the Friedmann equations.

2.1 Thermal Axions

Thermal production is by far the easiest way to produce a relic population: the contact with SM particles in the thermal bath of early stages creates and annihilates axions by processes

$$x_1 + x_2 \leftrightarrow x_3 + \phi, \quad x_1 \to x_2 + \phi \tag{2.2}$$

where x_1, x_2 and x_3 are generic SM particles. The number density of thermal axions solves the Boltzmann equation [1, 27]

$$\frac{dn_\phi}{dt} + 3Hn_\phi = \left(\sum_S \bar{\Gamma}_S + \sum_D \bar{\Gamma}_D\right)(n_\phi^{eq} - n_\phi), \tag{2.3}$$

where $H(t)$ is the Hubble expansion rate and we can compute the axion density at thermal equilibrium as

$$n_\phi^{eq} = \frac{1}{(2\pi)^3}\int_0^\infty \frac{4\pi p^2 dp}{\exp(p/T) - 1} = \frac{\zeta(3)}{\pi^2}T^3, \tag{2.4}$$

with the T dependence typical of radiation and $\zeta(3) = 1.202\ldots$, the Riemann zeta function of argument 3. Both scattering and decay processes affect the axion number density: for a the processes in (2.2) the scattering and decay rate can be respectively written as [27]

$$\bar{\Gamma}_S = \frac{n_1^{eq} n_2^{eq}}{n_\phi^{eq}} \langle \sigma_S v_{rel} \rangle\,, \tag{2.5}$$

$$\bar{\Gamma}_D = \frac{n_1^{eq}}{n_\phi^{eq}} \Gamma_D \frac{K_1(m_1/T)}{K_2(m_1/T)}, \tag{2.6}$$

where v_{rel} is the Moeller velocity, K_1 and K_2 the modified Bessel functions of the second kind and $\langle \sigma_s v_{rel} \rangle$ is thermally averaged cross section. In the present work we will focus only on scattering processes. Based on the QCD axion and the coupling $\phi G\tilde{G}$ the simplest (model independent) scattering processes that can thermalize the axion are the following (the detailed treatment can be found in section 2.1.1):

$$\phi + q(\bar{q}) \leftrightarrow g + q(\bar{q}), \qquad \phi + g \leftrightarrow q + \bar{q}, \qquad \phi + g \leftrightarrow g + g, \tag{2.7}$$

and where first computed in [28]. Their corresponding tree-level diagrams are depicted in figure 2.1. A rough estimate of the cross section and production rate are given by

$$\sigma \sim \frac{\alpha_s^3}{8\pi^2 f_a^2}, \qquad \Gamma \propto \frac{T^3}{f_a^2} \tag{2.8}$$

since we know that the QCD vertex $g\bar{q}q$ has a $\sqrt{\alpha_s}$ contribution and the ϕgg vertex goes as $\sim \alpha_s/f_a$. At temperatures $T > 1$ TeV both the quarks and the gluons are relativistic, thus their equilibrium number density can be written as [32]

$$n_q = n_{\bar{q}} = 27\frac{\zeta(3)}{\pi^2}T^3, \qquad n_g = 16\frac{\zeta(3)}{\pi^2}T^3.$$

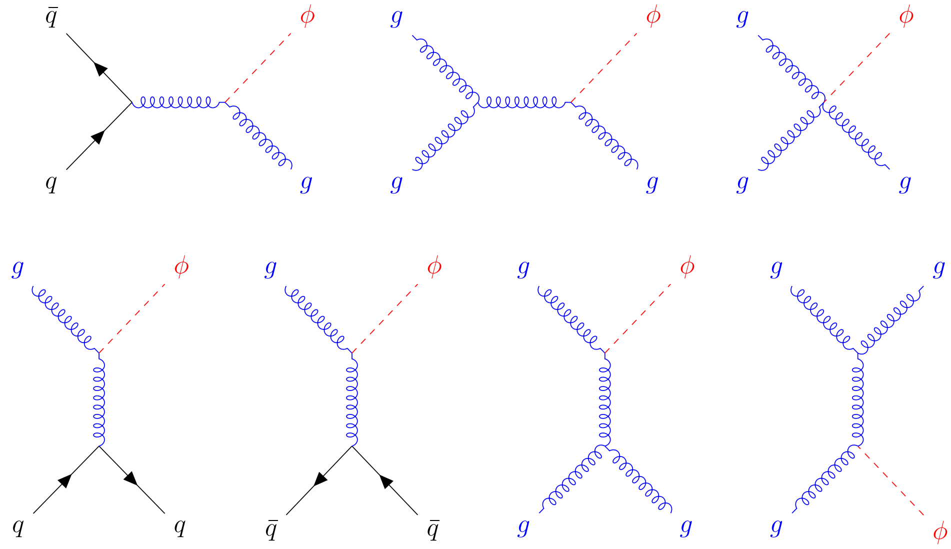

Figure 2.1: Feynman diagrams of the processes (2.7) with the axion coupling to gluons. Axions are depicted with red dashed lines, gluons with blue lines and quarks and antiquarks with black lines.

The Hubble parameter in the radiation era is

$$H^2 = \frac{1}{3M_{pl}^2}\left(\mathcal{N}_b(T) + \frac{7}{8}\mathcal{N}_f(T)\right)\frac{\pi^2}{30}T^4, \tag{2.9}$$

$M_{pl} = \sqrt{\hbar c/(8\pi G)}$ being the reduced Planck mass and $\mathcal{N}_{b,f}(T)$ the relativistic degrees of freedom of bosons and fermions respectively. The latter depend on the temperature, as heavy particles get progressively Boltzmann suppressed because of the decreasing of temperature. Above the TeV scale all the SM d.o.f are present,

$$\mathcal{N}_{SM}^{full} = \frac{7}{8}\left(\underbrace{6\cdot 3\cdot 2\cdot 2}_{q_i} + \underbrace{3\cdot 2\cdot 2}_{e,\mu,\tau} + \underbrace{3\cdot 2}_{\nu_i}\right) + \underbrace{8\cdot 2}_{G_\mu^\alpha} + \underbrace{3\cdot 2}_{W_\mu^\alpha} + \underbrace{2}_{B_\mu} + \underbrace{4}_{\Phi} = 106.75$$

and assuming only an additional one due to the axion field ϕ we obtain $\mathcal{N} = 107.75$. From the condition $\Gamma \sim H$ we can say (setting $\alpha_s \simeq 0.03$ [28]) that the processes of Fig. 2.1 maintain axions in thermal equilibrium with the plasma till the decoupling temperature

$$T_D \simeq 2\cdot 10^{11}\ \text{GeV}\left(\frac{f_a}{10^{12}\ \text{GeV}}\right)^2, \tag{2.10}$$

where in the computation effects of running of the coupling constant $\alpha_s(\mu)$ are taken into account [29]. It is important to stress the fact that for temperatures $T \gtrsim N f_a$ the PQ symmetry is restored and the calculation is not valid. It also suggests [28, 32] that for values

$$f_a \lesssim 2N\cdot 10^{12}\ \text{GeV} \tag{2.11}$$

thermalization is reached and a hot population of axions is created. Nevertheless an inflationary period with reheating temperature $T_R < T_D$ may wipe out the axions, consequently it is also important to search for processes that may re-establish a thermal axion population later. We stress the fact that the role of T_R is of great importance with respect to f_a and T_D, both for thermal axions and cold axions, that we will see later on.

As pointed out in [30] the axion gluon coupling is a loop level effect, proportional to α_s, and suppressed compared to the tree-level couplings (1.42) of the DSFZ model. Therefore if we allow the existence of axion couplings to matter we can obtain axion production rates much bigger that the one in (2.8), calculated in detail in [28]. This is why in chapter 3 we will focus on axion interactions with heavy fermions of the standard model at the EW scale and we will point out if a thermal population of such kind can be detected in future CMB experiments, see section 2.1.2.

2.1.1 Model independent thermalization

A relic density of thermally produced axions can be computed by solving the Boltzmann equation (2.3) for n_ϕ. Leaving the detailed computations of cross sections and thermal averages in the next chapters we can solve the equation with these quantities as parameters that depend on the process that we want to consider and within the model independent coupling ϕgg there are two cases of axion production that can be also found on the literature: the large f_a in the very early Universe where the axion interact with massless quarks and gluons and the small f_a case where the axion mostly interact with pions in the hadronic plasma.

Early Universe: large f_a

First of all, it is important to define comoving variables that will allow us to rewrite eq. (2.3) into a much simpler equation. The dimensionless comoving axion number and entropy density are defined as

$$Y_\phi = \frac{n_\phi}{s}, \qquad s = \frac{2\pi^2}{45} g_{*s} T^3,$$

and we rewrite the equilibrium number density of axions

$$n_\phi^{eq} = \frac{\zeta(3)}{\pi^2} T^3.$$

We will refer to x as a convenient time variable based on the process considered: it can be written for example as

$$x^{(1)} = \frac{f_a}{T}, \qquad x^{(2)} = \frac{m_i}{T}.$$

The first case is useful for the processes described in figure 2.1, where the axion production starts after the PQ breaking around f_a, while the second case will be useful in the scattering with heavy fermions at lower scales, where m_i is the mass of the heaviest particle considered in the scattering. In this section we want to give a precise estimate of axions produced only with the $gg\phi$ coupling, setting therefore $x = x^{(1)}$. In this way the Boltzmann equation becomes

$$sHx\frac{dY_\phi}{dx} = \left(1 - \frac{1}{3}\frac{d\ln g_{*s}}{d\ln x}\right)\gamma_a \left(1 - \frac{Y_\phi}{Y_\phi^{eq}}\right), \tag{2.12}$$

where now $\gamma_a = n_\phi^{eq}\bar{\Gamma}_S$. In the simple case where we neglect the temperature dependence on g_* and g_{*s} and focusing only on scattering processes the equation we want to solve becomes

$$sHx\frac{dY_\phi}{dx} = \gamma_a\left(1 - \frac{Y_\phi}{Y_\phi^{eq}}\right), \tag{2.13}$$

and the comoving equilibrium abundance and the scattering rate (2.8) [28] are

$$Y_\phi^{eq} = \frac{n_\phi^{eq}}{s} \simeq \frac{0.277}{g_{*D}}, \qquad \bar{\Gamma}_S \equiv \Gamma \simeq 7.1\times 10^{-6}\frac{T^3}{f_a^2}$$

where g_{*D} is the value of g_{*s} at $T = T_D$. Using now the variable $y = Y_\phi/Y_\phi^{eq}$ we can rewrite Boltzmann equation (2.13) in the following way

$$x^2\frac{dy}{dx} = k(1-y), \qquad k = x\frac{\Gamma}{H}, \tag{2.14}$$

and since $H \propto T^2$, k is a constant. The solution of the ordinary differential equation can be easily found

$$y(x) = 1 - Ae^{k/x}, \tag{2.15}$$

where A is the integration constant. At $x = k$ (when $\Gamma = H$) axions decouple, if we are assuming they only interact with the ϕgg coupling, and their number density stays constant in a comoving volume. This instant is associated to the decoupling temperature T_D written in eq. (2.10); the latter, together with T_R and the scale f_a define the thermal history of the Universe that affects the relic abundance of axions. As a matter of fact, looking at figure 2.2 we have six different regions (I-VI) in the $f_a - T_R$ plane.

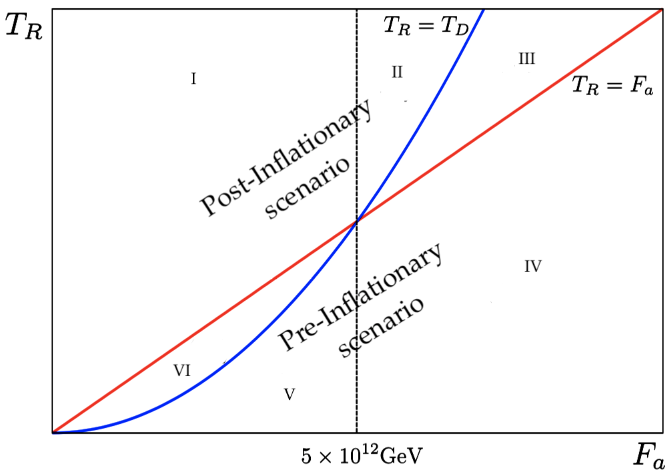

Figure 2.2: Different regions defined by T_R, T_D and f_a. Only for regions I and VI thermalization is achieved [41].

For case I we have $T_R > f_a > T_D$ and the solution (2.38) can completely written

$$y(x) = 1 - e^{k(1/x-1)}, \tag{2.16}$$

and as initial condition we set $y(1) = 0$, as axions are not produced for $T \geq f_a$. Requiring that the deviation from the thermal spectrum at the time of decoupling is less than 5% [28] we find

$$\frac{Y_D}{Y_{eq}} = y(x=k) = 1 - e^{1-k} > 0.95, \qquad \leftrightarrow \qquad k > 4,$$

meaning that axions enter into thermal equilibrium before they decouple from the plasma; in other words we obtain the same condition on f_a found in (2.11), with $N = 1$,

$$f_a \lesssim 10^{12}\ \text{GeV}.$$

The other case where thermalization is reached is the region VI of figure 2.2, where $f_a > T_R > T_D$ and the PQ symmetry is broken before inflation, as opposed to case I. In the case of cold axions, that we shall discuss later, the distinction between the cases $T \lesseqgtr f_a$ is of great importance. In case VI instead we have to be careful and change the initial conditions: we set $y(x) = 0$ for $T > T_R$ (if thermal axions were produced during inflation, they would be suppressed by the driving expansion), leading to the solution

$$y(x) = 1 - e^{k(1/x - 1/x_R)},$$

where $x_R = f_a/T_R$. In the cases II, III, IV and V thermalization is never reached.

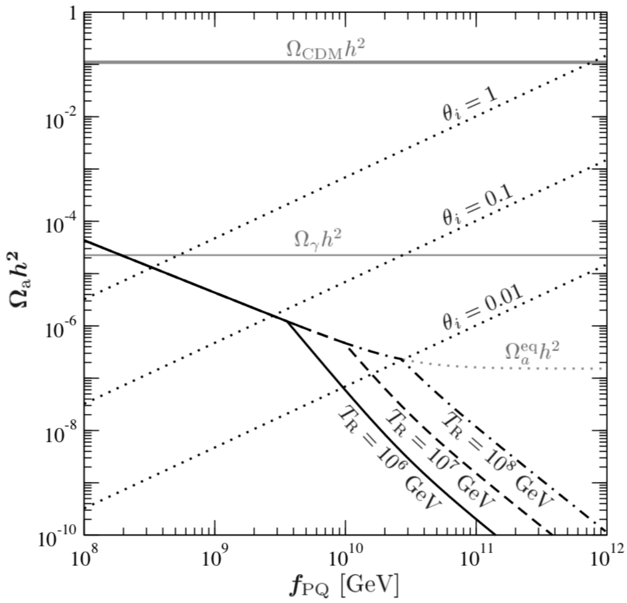

Figure 2.3: The axion relic density from thermal processes for different values of T_R and the one from the misalignment mechanism (see section 2.2.1) for $\theta_i = 1, 0.1, 0.01$. The density parameters for thermal relic axions, photons, and cold dark matter are indicated, respectively, by $\Omega_a^{eq}h^2$, $\Omega_\gamma h^2$ and $\Omega_{CDM}h^2$ [29].

For case I and VI we can compute today's relic abundance, since it is determined by Y_{eq} and does not depend on the initial conditions

$$n_\phi(t_0) = Y_{eq}s_0 = \frac{0.277}{g_*(T_D)}s_0 \simeq 7.8\ \text{cm}^{-3}\left(\frac{100}{g_*(T_D)}\right), \tag{2.17}$$

and we can compute the relic density parameter from thermal processes [29]

$$\Omega_a^{th}h^2 \simeq \frac{\sqrt{\langle p_{\phi,0}\rangle + m_\phi^2}\,n_\phi(t_0)h^2}{\rho_c} \simeq 10^{-9}\left(\frac{100}{g_*(T_D)}\right)\left(\frac{10^{12}\ \text{GeV}}{f_a}\right), \tag{2.18}$$

where $\langle p_{\phi,0}\rangle$ is the present average momentum of axions. Figure 2.3 graphically explains what is written in eq. (2.18): even for the small values of f_a (10^8 GeV) model

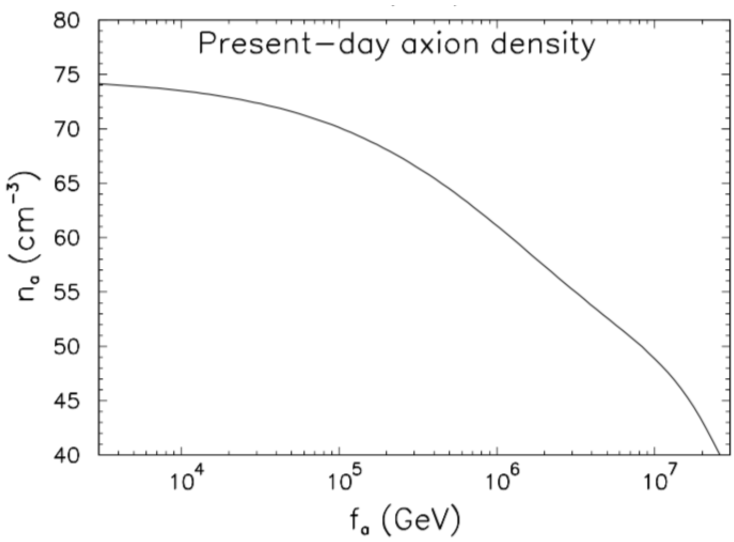

Figure 2.4: Axion number density calculated by the thermalization of the process $\pi\pi \leftrightarrow \pi a$. It is only relevant in the window $f_a \lesssim 10^7$ GeV [37]

.

independent axion production is too small to explain dark matter. Moreover, for typical values of f_a compatible with cold dark matter axions (region 10^{10-12} GeV), the population is way smaller than the one of photons or neutrinos.

Hadronic plasma: small f_a

At low energies, below Λ_{QCD}, instantons become important and hadrons replace quarks. As mentioned in the first chapter the axion mixes with the neutral pions and we expect among the axion couplings with hadrons that the one of particular relevance is responsible for the processes $\pi\pi \leftrightarrow \pi a$, where a is now the mass eigenstate axion†. Its coupling can be read recalling lagrangian of CHPT (1.2) and exploiting once again the filed redefinition (1.29). Consequently the interaction between axion and pions can be written as [39]

$$\mathscr{L}_{a\pi} = C_{a\pi}\frac{\partial_\mu a}{f_a f_\pi}(\pi^0\pi^+\partial^\mu\pi^- + \pi^0\pi^-\partial^\mu\pi^+ - 2\pi^+\pi^-\partial^\mu\pi^0), \tag{2.19}$$

and at $T \sim m_\pi$ the cross section is roughly $\sigma_\pi \sim 1/f_a^2$. Hence the thermal equilibrium condition ($\Gamma \gtrsim H$) is satisfied by

$$\frac{n_\pi \sigma_\pi}{H} \sim \frac{m_\pi M_{pl}}{f_a^2} \gtrsim 1,$$

and numerically by [35]

$$f_a \lesssim 5 \times 10^8 \text{ GeV}. \tag{2.20}$$

This axion population is DR, or Hot dark matter (HDM), and its number density can be compared (same order of magnitude) to the one of neutrinos, as seen in fig. 2.4. This hot population cannot account for the dark matter in the Universe, not

†We don't include nucleons because of their scarcity with respect to pions [37].

only because of the cosmological constraints of large scale structures, but because the relic density of this thermalization process [35]

$$\Omega_a^{th.} \simeq \frac{m_a}{130 \text{ eV}},$$

if matched to the DM relic density would imply an axion lifetime shorter than the age of the Universe‡. However, the constraint (2.20) is in contradiction with astrophysical and cosmological bounds (see for example [17, 38]) that suggest

$$f_a > 6 \times 10^8 \text{ GeV}. \tag{2.21}$$

The problem is that the latter is obtained by looking at interactions that are mostly model dependent, meaning that in principle we could have for example a model where the axion coupling to photons is arbitrary small [37]. In the last chapter we will discuss with more details the astro/cosmo exclusion bounds.

Nevertheless in the development of our work we will consider the f_a range that respects the observational constraint (2.21), neglecting the axion production in hot hadronic gas.

2.1.2 Dark radiation and N_{eff}

Let us now show how this can affect some important cosmological observables. The axion energy density from thermal production is directly connected to the effective number of neutrinos N_{eff}, that quantifies the energy density of radiation via the following expression

$$\rho_r = \sum_{i=\gamma,\nu,\phi} \rho_i = \left[1 + \frac{7}{8}\left(\frac{T_\nu}{T_\gamma}\right)^4 N_{\text{eff}}\right] \rho_\gamma. \tag{2.22}$$

The contribution of ρ_ν and ρ_ϕ can be called *dark radiation* and is encoded on the value N_{eff}. The latter has a precise value without considering any physics beyond the SM, $N_{\text{eff}}^{(\text{SM})} = 3.046$§, namely considering only neutrinos. However the presence of axions can result in a deviation of this quantity

$$\Delta N_{\text{eff}} = N_{\text{eff}} - N_{\text{eff}}^{(\text{SM})} = \frac{8}{7}\left(\frac{1}{4}\right)^{4/3} \frac{\rho_\phi}{\rho_\gamma}, \tag{2.23}$$

where we used the relation $T_\nu/T_\gamma = (4/11)^{1/3}$ due to neutrino decoupling around the temperatures of e^+e^- annihilation [1]. Now we notice that the ratio ρ_ϕ/ρ_γ is proportional to $Y_\phi^{4/3}$ and we can write the thermal axion contribution as

$$\Delta N_{\text{eff}} \simeq 12.15\, (g_{*s} Y_\phi)^{4/3}. \tag{2.24}$$

The value of g_* and g_{*s} and their temperature dependences are of great importance, and are depicted in fig. 2.5. In expression (2.24) we can write for instance the late Universe value of g_{*s}

$$g_{*s}(T \lesssim 0.5\text{MeV}) = 2 + \frac{7}{8} \times 2 \times 3 \times \frac{4}{11} = \frac{43}{11} \simeq 3.909,$$

‡The axion lifetime is calculated based on the decay width of the process $a \to \gamma\gamma$, see [35].

§The SM value is not exactly equal to 3 because the neutrino decoupling is not instantaneous.

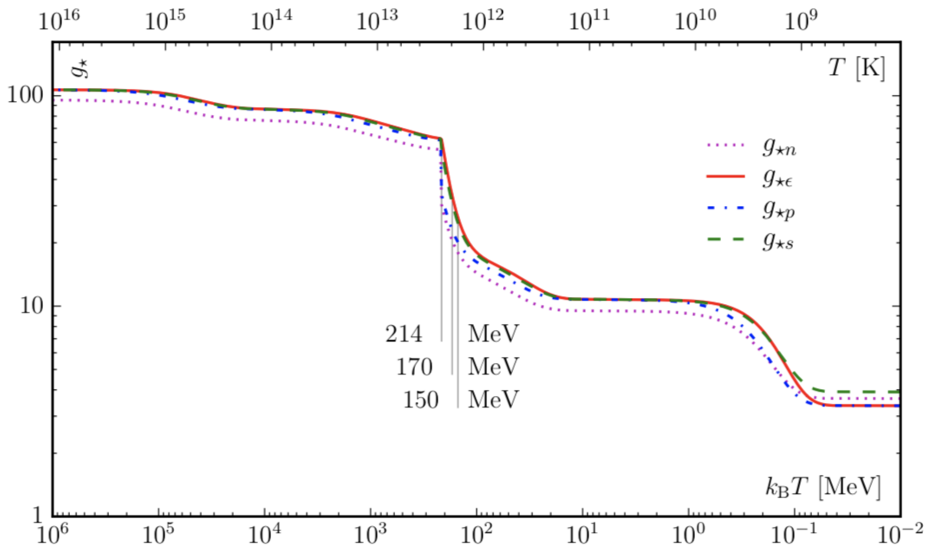

Figure 2.5: The evolution of g_* and g_{*s} as a function of temperature. They are with the continuous red line and green dashed line, respectively [31].

and in this way it simply becomes [27]

$$\Delta N_{\rm eff} \simeq 74.82\,(Y_\phi)^{4/3}. \tag{2.25}$$

It is also useful to give a semi-analytical solution to eq. (2.13) that we can plug into the expression of $\Delta N_{\rm eff}$, within the approximation where g_* and g_{*s} are constant. We refer to the time variable $x = x^{(2)} = m_i/T$, where m_i is the heavy fermion considered in the scattering/annihilation process (for example we will set in Chapter 3 $m_i = m_t$, where t is the top quark) and we have the following x dependences

$$H = H(m_j)x^{-2}, \qquad s = s(m_j)x^{-3}, \qquad \gamma_S = \gamma_S(m_j)x^{-4}e^{-x}.$$

Using $Y_\phi = 0$ for $x \to 0$ then we can analytically solve (2.13):

$$Y_\phi = Y_\phi^{eq}[1 - e^{-(1-e^{-x})r}], \tag{2.26}$$

defining $r = (\bar{\Gamma}_S/H)_{T=m_i}$. The result that we want to obtain is the asymptotic value at small temperatures ($x \to \infty$), where the term e^{-x} becomes irrelevant

$$Y_\phi = Y_\phi^{eq}(1 - e^{-r}), \tag{2.27}$$

and only depends on r, i.e. the scattering rate. Plugging in the expression of Y_ϕ into (2.24) we obtain the contribution to $N_{\rm eff}$

$$\Delta N_{\rm eff} \simeq \frac{4}{7}\left(\frac{43}{4g_{*s}}\right)^{4/3}[1 - e^{-r}]^{4/3}. \tag{2.28}$$

In other words, for large values of $r = (\bar{\Gamma}_S/H)_{T=m_j}$ the axions reach thermal equilibrium and their contribution to $N_{\rm eff}$ depends only on the value of g_{*s} at decoupling. For small values of r instead, valid for the large f_a case when axions do not thermalize, we can expand the exponential and obtain

$$\Delta N_{\rm eff} \simeq \frac{4}{7}\left(\frac{43}{4g_{*s}}\right)^{4/3}\left[\frac{\bar{\Gamma}_S}{H}\right]^{4/3}_{T=m_i} \propto \left(\frac{c_i}{f_a}\right)^{8/3}. \tag{2.29}$$

However, due to the complicate temperature dependence of both g_* and g_{*s}, it would be better to solve Boltzmann equation (2.13) numerically. N_{eff} can be indirectly measured by CMB experiments, and the future CMB-S4 experiment as enough forecasted sensitivity to probe some of the models of thermal axion production [26, 42]. For example, assuming only the additional existence of the axion above the EW scale, the predicted change in N_{eff} due to axions would be

$$\Delta N_{\text{eff}} = \frac{4}{7}\left(\frac{43}{4g_{*s}(T_D)}\right)^{4/3} \simeq 0.027. \tag{2.30}$$

2.2 Axion field evolution

The thermal axions discussed in the last section are *quantum fluctuations* about the average background axion field, but before turning into the discussion of cold populations of axions we should examine the time evolution of the axion field ϕ in an expanding Universe. We emphasize again that ϕ is the field before mixing with pions and has random initial conditions. The dynamics of the axion field evolution relies on the scale of PQ breaking f_a, as we have to consider two different cases, if we accept the inflationary scenario and we know that the size of the causal horizon is hugely modified during cosmological inflation. In the first case, called *pre-inflationary* scenario, the PQ symmetry is spontaneously broken before inflation, in other words the reheating temperature is smaller than the breaking scale, $T_R < f_a$. In this simple case the axion field can be considered spatially homogeneous and the evolution of this zero momentum mode is easy to compute. The second case is called *post-inflationary* scenario, where the PQ symmetry is broken during or after inflation. The axion field has in this case non zero modes (in addition to the zero mode of the first case) and also carries topological defects like *cosmic strings* and *domain walls.*

We then recall the dynamics, i.e. the equations of motion in the FRW metric that minimize the following action

$$S = \int d^4x\sqrt{-g}\left[\frac{1}{2}\partial_\mu\phi\partial^\mu\phi - V(\phi)\right], \tag{2.31}$$

where the determinant of the metric is $\sqrt{-g} = R^3(t)$, $R(t)$ being the scale factor, and the potential $V(\phi)$ is the one written in (2.1). The equations of motion are

$$\ddot{\phi} - \frac{(\nabla\phi)^2}{R^2} + 3H\dot{\phi} + \frac{dV}{d\phi} = 0, \tag{2.32}$$

where $H = \dot{R}/R$ and the dot represents the usual time derivative. In the first case (that we will refer as *zero mode*), with the PQ phase transition occurring before inflation the axion field only depends on time and eq. (2.32) changes into

$$\ddot{\phi} + 3H\dot{\phi} + V'(\phi) = 0, \tag{2.33}$$

where at leading order in the potential (and setting $N_{DW} = 1$) the last term of the equation is $V'(\phi) \approx m_a^2\phi$. Now we have the equation of a dumped harmonic oscillator, because of the H friction term due to the expansion of the Universe and we can split the solution into two different regimes. In the *frozen regime*, where the friction is stronger than the force, i.e. $m_a \ll H$, the equation becomes

$$\ddot{\phi} + 3H\dot{\phi} = 0,$$

and $\phi =$ const. is the solution and the initial value of the axion field that freezes due to a strong friction term. Then there is the *fast oscillation regime*, where the potential term (or the mass equivalently) becomes relevant and is stronger than the friction. The equation is therefore the full damped harmonic oscillator (2.33), and the zero mode energy density and pressure of the axion field are (taking $V(\phi) = m_\phi^2\phi^2/2$):

$$\rho_\phi = \frac{1}{2}\dot{\phi}^2 + \frac{1}{2}m_\phi^2\phi^2, \qquad P_\phi = \frac{1}{2}\dot{\phi}^2 - \frac{1}{2}m_\phi^2\phi^2. \tag{2.34}$$

They describe a coherent state of axions at rest with number density $n_\phi = \rho_\phi/m_\phi$, where the number of zero momentum axions per co-moving volume is conserved. Consequently, this can give rise to a cold population of axions, via the so-called *misalignment mechanism* (see 2.2.1), that can account for the dark matter relic abundance.

In the more general *non-zero mode* post-inflationary scenario instead the axion field ϕ depends on all the spacetime coordinates and now the solution of eq. (2.32) is a linear superposition of modes

$$\phi(x) = \int d^3k\ \phi(\mathbf{k}, t)e^{i\mathbf{k}\cdot\mathbf{x}}, \tag{2.35}$$

where $\phi(\mathbf{k}, t)$, in a radiation dominated Universe where $R \propto \sqrt{t}$, satisfies

$$\left(\partial_t^2 + \frac{3}{2t}\partial_t + \frac{k^2}{R^2} + m_\phi^2\right)\phi(\mathbf{k}, t) = 0. \tag{2.36}$$

The wavelength of the modes is stretched because of Hubble expansion and increases with the scale factor, $\lambda(t) = 2\pi/kR(t)$, and in a period of inflation when the growth of $R(t)$ is exponential it is important to distinguish between modes with wavelength outside ($\lambda(t) > t$) or inside ($\lambda(t) < t$) the horizon, i.e. whether they are in causal connection or not.

A cold population of particles is what we expect due to structure formation [1] if we want to explain the dark matter in the Universe. The production of such population can be achieved via non-thermal productions such as the misalignment mechanism, both for zero and non-zero modes, and topological defects in the case of post-inflationary scenario. In the pre-inflationary scenario instead only the zero momentum mode contributes.

2.2.1 Misalignment mechanism

The misalignment mechanism is the simplest way to produce cold axions and gives a very reasonable explanation to CDM. The mechanism involves the relaxation of the $\bar{\theta}$ angle towards the minimum of the potential, the CP conserving value. Today we believe that $\bar{\theta} = 0$, or at least a value compatible with zero with great precision, as we pointed out in the first chapter. However, at temperatures around f_a the axion is essentially massless and therefore the initial value $\bar{\theta}_i$ is not expected to be zero, but random value instead; technically we can say that the axion field is initially *misaligned* with the minimum of its potential. In addition, as mentioned above, the misalignment mechanism has to be distinguished between pre- and post-inflationary scenarios.

Zero mode

The pre-inflationary scenario is the easiest case to solve, as the universe was made homogeneous by inflation after the PQ phase transition and the initial value of the axion field was casual and the same everywhere in the Universe: $\phi_i = f_a\bar{\theta}_i$. If we now look back at eq. (2.33),

$$\ddot{\phi} + 3H\dot{\phi} + m_\phi^2\phi = 0, \tag{2.37}$$

the first two terms are proportional to t^{-2} and this means that the axion mass $m_a(T)$ is only relevant when it becomes of order t^{-1}, or equivalently when it is comparable to H. There is a critical time t_1 where this happens [32]

$$m_\phi(t_1)t_1 = 1,$$

and the temperature T_1 corresponds to the time t_1. We find

$$\frac{T_1^2}{M_p} \approx \left(\frac{m_\pi f_\pi}{f_a}\right)\left(\frac{\Lambda_{QCD}}{T_{osc}}\right)^{n/2}, \qquad T_1 \approx 1.18\left(\frac{10^{12}\text{GeV}}{f_a}\right)^{0.185}\text{GeV},$$

meaning that for reasonable values of the axion decay constant f_a the axion field starts oscillating a $T_1 \sim$ few GeV. For $t > t_1$ the solution of (2.33), for a radiation dominated Universe, can be written as [23]

$$\phi(t) = R^{-3/2}(t/t_i)^{1/2}[C_1 J_n(m_\phi t) + C_2 Y_n(m_\phi t)], \tag{2.38}$$

where $n = (3p-1)/2$ ($p = 1/2$ in this case), J_n and Y_n are Bessel functions of the first and second kind and t_i is the initial time. C_1 and C_2 are dimensionful and determined by initial conditions and the solution is depicted in fig. 2.6. However, when both matter and radiation are important, eq. (2.37) has to be solved with approximations or numerically. A useful valid approximation in this case is the *WKB method*, that gives the solution [23]

$$\phi(t) = \mathcal{A}(t)\cos\left(\int^t \omega(t')dt'\right), \qquad \omega^2(t) = \frac{3}{2t}\partial_t + m_\phi^2, \tag{2.39}$$

where the most important role is played by the amplitude $\mathcal{A}(t)$. Within the approximation we find $\mathcal{A}^2(t)m_\phi(t) \propto R^{-3/2}$, where $R(t)$ is the scale factor. If we now recall the expression of the axion energy density (2.34) we can make use of the virial theorem that simplifies the expression

$$\rho_\phi = \langle\dot{\phi}^2\rangle = \langle m_\phi^2\phi^2\rangle\,, \tag{2.40}$$

where the brackets mean the average value in the oscillations. Taking now the

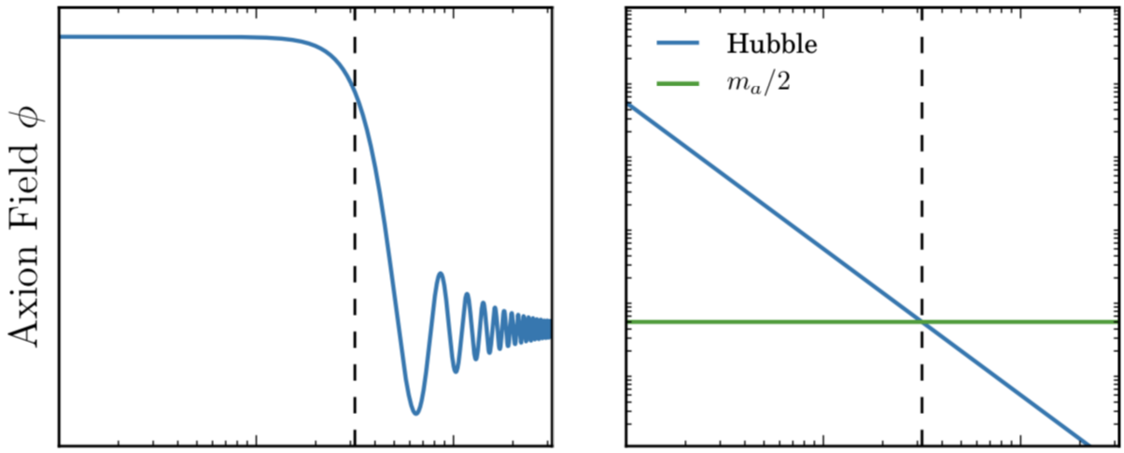

Figure 2.6: Time evolution of the axion field. The dotted line represents the time t_1 where the axion mass is comparable with the Hubble parameter (we assumed that around t_1 the axion mass already reached its constant zero temperature value).

time derivative of the energy density we find the differential equation

$$\dot{\rho}_\phi = \left(\frac{\dot{m}_\phi}{m_\phi} - 3H\right)\rho_\phi,$$

solved by

$$\rho_\phi = \text{const.}\frac{m_\phi(T)}{R^3}. \tag{2.41}$$

This means that when the axion field settles down to its zero temperature value the evolution of the energy density scales with $\propto R^{-3}$ and reflects how a coherent population of axions, with number density $n_\phi = m_\phi \mathcal{A}^2/2$, behaves like non-relativistic (NR) matter. With this mechanism we achieved a cold population of light bosons, that will condensate and could explain dark matter structures, such as clusters; it is important to stress how we can have a NR population without a dependence on axion mass, that can therefore be very small. Another key feature of this mechanism is that, looking at eq.(2.41), the energy density does not scale as R^{-3}, if the mass changes with the temperature; however $n_\phi = \rho_\phi/m_\phi$ does it, meaning that the number of axions per comoving volume is conserved. The energy density today (t_0) can be therefore written as

$$\rho_\phi^{pre}(t_0) = \rho_\phi(t_1)\frac{m_\phi}{m_\phi(t_1)}\left(\frac{R(t_1)}{R(t_0)}\right)^3, \qquad \rho_\phi(t_1) = m_\phi^2(t_1) f_a^2 \bar{\theta}_i^2, \tag{2.42}$$

$\rho_\phi(t_1)$ is the energy density value at the beginning of oscillations. The result depends on the fundamental parameters f_a and in this case (pre-inflationary) a crucial role is played by the initial misalignment angle $\bar{\theta}_i$:

$$\Omega_a^{pre} \approx 0.27\left(\frac{0.7^2}{h^2}\right)\left(\frac{f_a}{10^{11}\text{ GeV}}\right)^{1.18}\bar{\theta}_i^2. \tag{2.43}$$

Because of the presence of $\bar{\theta}_i$ the right DM relic abundance can be obtained by a wide range of f_a values, as opposed to the case of post-inflationary model. In the latter scenario there is also a contribution of the zero momentum mode, but in this case we have different random values of $\bar{\theta}_i$ around different causal patches in the Universe, because of inflation. Being the average of $\bar{\theta}_i^2$ over different regions of order one, the energy density can be written as

$$\rho_\phi^{post}(t_0) \sim f_a^2 m_\phi m_\phi(t_1) \left(\frac{R_1}{R_0}\right)^3 . \tag{2.44}$$

Non-zero modes

In the more complicated case where the PQ breaking occurs after inflation non-zero modes and topological defects appear. In this section we will compute the relic density of non-zero modes within the misalignment mechanism without considering topological defects (they will be discussed in section 2.2.2). As we have already seen, in this case the axion field is spatially varying and the equation we want to solve is (2.36), where we neglect the axion mass term till $t \sim t_1$. For modes outside the horizon, $\lambda(t) \gg t$, the general solution is

$$\phi(\mathbf{k}, t) = \phi_0(\mathbf{k}) + \phi_1(\mathbf{k}) t^{-1/2},$$

meaning that the axion field is "frozen by causality". For modes in causal connection instead ($\lambda(t) \ll t$) the solution is

$$\phi(\mathbf{k}, t) = \frac{\text{cost}}{R(t)} \cos\left(\int^t \omega(t')dt'\right), \tag{2.45}$$

where now $\omega^2(t) \simeq k^2/R^2$. Let us now call $dn_\phi/d\omega(\omega, t)$ the axion number density in physical and frequency space of wavelengths $\lambda = 2\pi/\omega$, with $\omega > t^{-1}$. The number and energy density of axions read [32]

$$n_\phi(t) = \int_{t^{-1}} d\omega \frac{dn_\phi}{d\omega}(\omega, t), \qquad \rho_\phi(t) = \int_{t^{-1}} d\omega \frac{dn_\phi}{d\omega}(\omega, t)\omega, \tag{2.46}$$

and during radiation domination we can write [32]

$$\frac{dn_\phi}{d\omega}(\omega, t) \sim \frac{N^2 f_a^2}{2t^2\omega^2},$$

where we remember $N = v_\phi/f_a$ is the colour anomaly. Integrating over $w > t^{-1}$ the number density at the beginning of oscillations can be written as

$$n_\phi(t_1) \sim \frac{N^2 f_a^2}{t_1} \sim N^2 f_a^2 m_\phi(t_1),$$

and today energy density due higher momentum modes is

$$\rho_\phi^{post,n}(t_0) \sim m_\phi m_\phi(t_1) N^2 f_a^2 \left(\frac{R_1}{R_0}\right)^3 . \tag{2.47}$$

This result is exactly the same of the zero momentum mode in the post scenario (2.44), with the only difference in the N^2 factor. In the post inflationary scenario we have to sum the contributions of zero and higher momentum modes in the misalignment mechanism but also topological defects like strings and domain walls.

2.2.2 Topological defects

Depending on the nature of symmetry breakdown, topological defects of various type are believed to have formed in the early Universe during cosmological phase transitions:

- ◇ *Magnetic monopoles*, cube-like defects that form when a spherical symmetry is broken and are predicted to have magnetic charge.
- ◇ *Cosmic strings*, one-dimensional lines that form due to the breaking of an axial symmetry.
- ◇ *Domain walls*, two-dimensional membranes that arise in a discrete symmetry breaking.

In the case of axions, cosmic strings are relevant in the breaking of $U(1)_{PQ}$, where a phase transition at $T \sim f_a$ is occurring. Domain walls are also relevant, but during the QCD phase transition, where the instanton potential (2.1) shows a discrete symmetry. We will follow the cosmological evolution of the Peccei-Quinn field φ with lagrangian density

$$\mathscr{L} = -\frac{1}{2}|\partial_\mu \varphi|^2 - V_{eff}(\varphi, T),$$

where φ is a complex scalar field, previously introduced in the invisible axion models, while $V_{eff}(\varphi, T)$ is the effective potential of the field that takes into account effects of finite temperature. As a matter of fact, for high temperatures ($T \gtrsim f_a$) we have a symmetry restoration and φ is in thermal equilibrium and the potential can be written as

$$V_{eff}(\varphi, T) = \lambda \left(|\varphi|^2 - \frac{f_a^2}{2} \right)^2 + \frac{\lambda}{6}|\varphi|^2 T^2, \tag{2.48}$$

without considering other possible interactions for simplicity. The PQ transition occurs at $T \sim T_c \equiv \sqrt{6} f_a$, and after that φ gets a VEV and $U(1)_{PQ}$ is broken. When the temperature of the universe becomes comparable to the QCD scale Λ we should add to (2.48) the following potential

$$V(\phi) = \Lambda^4(t) \left[1 - \cos\left(\frac{N_{DW}\phi}{f_a} \right) \right], \qquad \varphi = \rho(x) \exp\left(i\frac{\phi(x)}{f_a} \right).$$

Cosmic strings

Cosmic strings are extended objects which arise in field theories when a symmetry G is broken, $G \to H$, and the quotient space G/H has nontrivial π_1 homotopy [5]. The simplest case is when a complex scalar field has a $U(1)$ symmetry and its potential (1.40) leads to SSB. In this case the vacuum manifold is a circle S^1 and its first homotopy group is $\pi_1(S^1) = \mathbb{Z}$. In the post-inflationary scenario the field initially makes the choice of symmetry breaking direction in a casual independent way at widely separated points in space, leading to string type defects, like in the Kibble mechanism [1]. Even tough it will be destroyed around the QCD scale by non-perturbative effects, a network of axionic cosmic strings could play a dominant role in the early Universe, establishing a populations of cold axions.

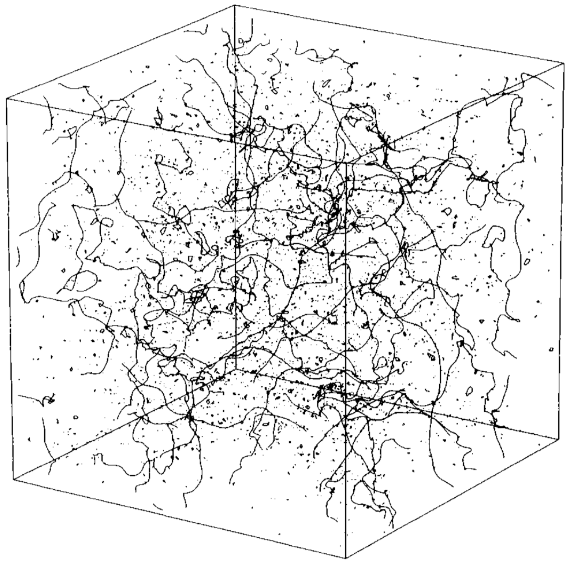

Figure 2.7: A numerical simulation of a cosmic string network. It consists of infinite strings and finite string loops [1].

If we want to take into account the possibility of a production of axions by string decay is important to introduce the energy per unit length of a string

$$\mu_s = \pi N f_a^2 \ln(f_a L), \tag{2.49}$$

where L is the characteristic distance between strings. For infinitely long strings this quantity is logarithmically divergent as opposed to the local case, where there is the gauge field contribution. We expect that the axionic string network will rapidly approach a scaling solution [32], where

$$\rho_s = \xi \frac{\mu_s}{t^2}, \tag{2.50}$$

where $\xi \sim \mathcal{O}(1)$ is called the *scaling parameter*. Usually a cosmic string network is made up by long pieces of infinite strings (i.e. that stretch across the horizon) and small finite loops, see fig. 2.7, and the system is sustainable as strings are constantly cutting themselves into loops that dissipate energy into gravitational waves. However in the case of axionic strings the dissipation is mainly achieved by radiation coming from axion decay, leading to a population of axions and maintaining the scaling solution. This production of action takes place in the time interval between t_c and t_1, where t_c is the instant that corresponds to $T_c = \sqrt{6} f_a$, and if we assume a massless axion in this time interval the evolution of energy densities is described by the differential equations [50]

$$\frac{d\rho_s}{dt} = -2H\rho_s - \left.\frac{d\rho_s}{dt}\right|_{emiss.}, \tag{2.51}$$

$$\frac{d\rho_\phi}{dt} = -4H\rho_\phi + \left.\frac{d\rho_s}{dt}\right|_{emiss.}. \tag{2.52}$$

Inserting (2.49) and (2.50) we obtain

$$\left.\frac{d\rho_s}{dt}\right|_{emiss.} = \frac{\xi \pi N f_a^2}{t^3}\Big[\ln(f_a L) - 1\Big], \tag{2.53}$$

and defining the comoving energy of axions radiated from strings

$$E_\phi(t) = R^4(t)\rho_\phi(t),$$

its time derivative reads

$$\frac{dE_\phi}{dt} = R^4(t)\left.\frac{d\rho_s}{dt}\right|_{emiss.}.$$

Therefore the comoving number of axions produced by string decay can be written as [50]

$$N_\phi(t > t_1) = \int_{t_c}^{t_1} dt' \frac{1}{R(t')\langle\omega_\phi(t')\rangle}\frac{dE_\phi}{dt'} \tag{2.54}$$

$$= \int_{t_c}^{t_1} dt' \frac{R^3(t')}{\langle\omega_\phi(t')\rangle}\frac{\xi\pi N f_a^2}{t'^3}\left[\ln(f_a t') - 1\right], \tag{2.55}$$

where $\langle\omega_\phi(t)\rangle$ is the mean energy of radiated axions. In order to compute N_ϕ we should specify ω_ϕ, or in other words we have to interpret the spectrum of radiated axions. Here is where the discussion begins: according to [33] (scenario A) the wavelength of radiated axions is given by the size of the horizon, hence

$$\langle\omega_\phi(t)\rangle^{(A)} \sim \frac{2\pi}{t}.$$

Integrating, the axion number density today is in this case

$$n_\phi^{(A)}(t_0) \simeq \left(\frac{R_1}{R_0}\right)^3 \frac{N^2 f_a^2 \xi}{t_1}\ln(f_a t_1); \tag{2.56}$$

it is easy to see how this expression is greater than the one of misalignment mechanism by a factor of $\ln(f_a t_1) \sim \mathcal{O}(10^2)$. However, according to [32, 34] instead (scenario B), the radiated axions have a $1/k$ spectrum, meaning that

$$\langle\omega_\phi(t)\rangle^{(B)} \sim \frac{2\pi}{t}\ln(f_a t),$$

leading to

$$n_\phi^{(B)}(t_0) \simeq \left(\frac{R_1}{R_0}\right)^3 \frac{N^2 f_a^2 \xi}{t_1}, \tag{2.57}$$

which is exactly the expression of the misalignment production. Even tough the scenario A and B differ by a the logarithmic factor we acknowledge the fact that either way we have to consider axionic string decay, as their energetic contribution is at least of the same order of magnitude than the coherent oscillation of the field itself. The energy density today reads in general

$$\rho_\phi(t_0) \gtrsim m_\phi m_\phi(t_1)\xi N^2 f_a^2 \left(\frac{R_1}{R_0}\right)^3. \tag{2.58}$$

Domain walls

The existence of the QCD potential explicitly breaks the original $U(1)_{PQ}$ symmetry down to its discrete subgroup $Z(N_{DW})$, namely the axion at $T \lesssim \Lambda_{QCD}$ possesses the shift symmetry $\phi \to \phi + 2\pi n f_a/N_{DW}$, creating defects called domain walls.

Because of the large hierarchy $f_a \gg \Lambda_{QCD}$ the formation of domain walls occur much later than the formation of cosmic strings. Domain walls arise as topological defects because the discrete group is also spontaneously broken, leading to a N_{DW} degeneracy in the vacuum configuration. The domain wall is in fact the minimum energy field configuration which interpolates between neighbouring vacua (they are equidistant to each other), as in the Kibble mechanism [1]. When the axion

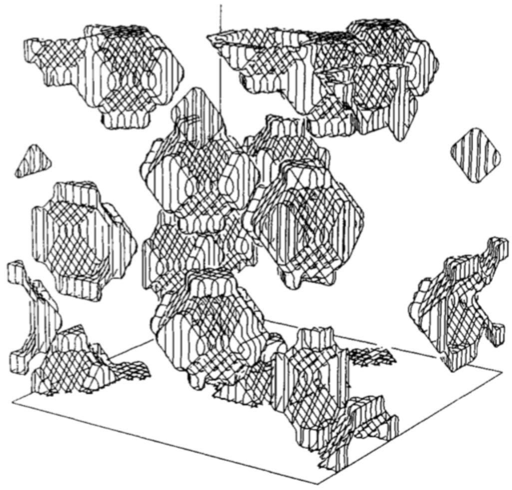

Figure 2.8: A domain wall network formed in a numerical simulation of a spontaneously broken Z_2 symmetry. The contour lines indicate the domain walls that separate the regions of different vacua [1].

mass becomes important at t_1, each axion string becomes the edge of the N_{DW} domain walls and the latter represent a cosmological disaster in the post-inflationary scenario, unless $N_{DW} = 1$[¶]. Let us see how. In the case where $N_{DW} \geq 2$ there two or more degenerate vacua and their values in regions outside each other's casual horizon are independent. This means that there is at least on the order of one domain wall per causal horizon, whose size is t. Hence the energy density stored in domain walls can be written as

$$\rho_{\mathrm{w}}(t) = \mathcal{A}\frac{\sigma_{\mathrm{w}}}{t},$$

where $\mathcal{A} \sim \mathcal{O}(1)$ and σ_{w} is the energy wall density per unit surface [32]

$$\sigma \simeq 9 f_a^2 m_\phi \simeq 5.5 \times 10^{10}\ \mathrm{GeV}^3 \left(\frac{f_a}{10^{12}\ \mathrm{GeV}}\right).$$

This expression would lead to an energy density today that exceeds by many orders of magnitude the critical energy density ρ_c, in complete disagreement with cosmological observations. This is generally known as the *domain wall problem* and there are three possible approaches towards the solution: the first two consist in postulating the pre-inflationary scenario or $N_{DW} = 1$, while the last one is introducing a small explicit breaking of the $Z(N_{DW})$ symmetry [32]. While solving the domain wall problem is important for obvious cosmological consistencies, we will focus only on the axion production due to wall decay. The case of interest is $N_{DW} = 1$, since according to [41] for $N_{DW} > 1$ the predominant decay of the

[¶]We note that there are domain walls even when $N_{DW} = 1$, where both sides of the domain wall are in the same and only vacuum.

axion walls is trough gravitational radiation. The energy of the *string-wall* system at $t > t_1$ is

$$\rho_{sw}(t) = \left[\mathcal{A}_1 \frac{\sigma_{\rm w}(t_1)}{t_1} + \xi_1 \frac{\mu_s(t_1)}{t_1^2}\right] \left(\frac{R(t_1)}{R(t)}\right)^3, \tag{2.59}$$

where $\mathcal{A}_1$ and ξ_1 are the scaling parameters defined at t_1. It can be shown by simulations [50] that the axion contribution from wall decay is subdominant relative to those from string decay and the misalignment mechanism.

2.2.3 Axion cold dark matter

In this final section we try to give an estimation of the cosmological relic density of axions and compare it to the observed dark matter abundance. It depends on two important parameters thoroughly discussed, namely f_a and N_{DW}, and we have also seen along the chapter that it is important to distinguish whether the PQ symmetry breaking occurs before or after inflation.

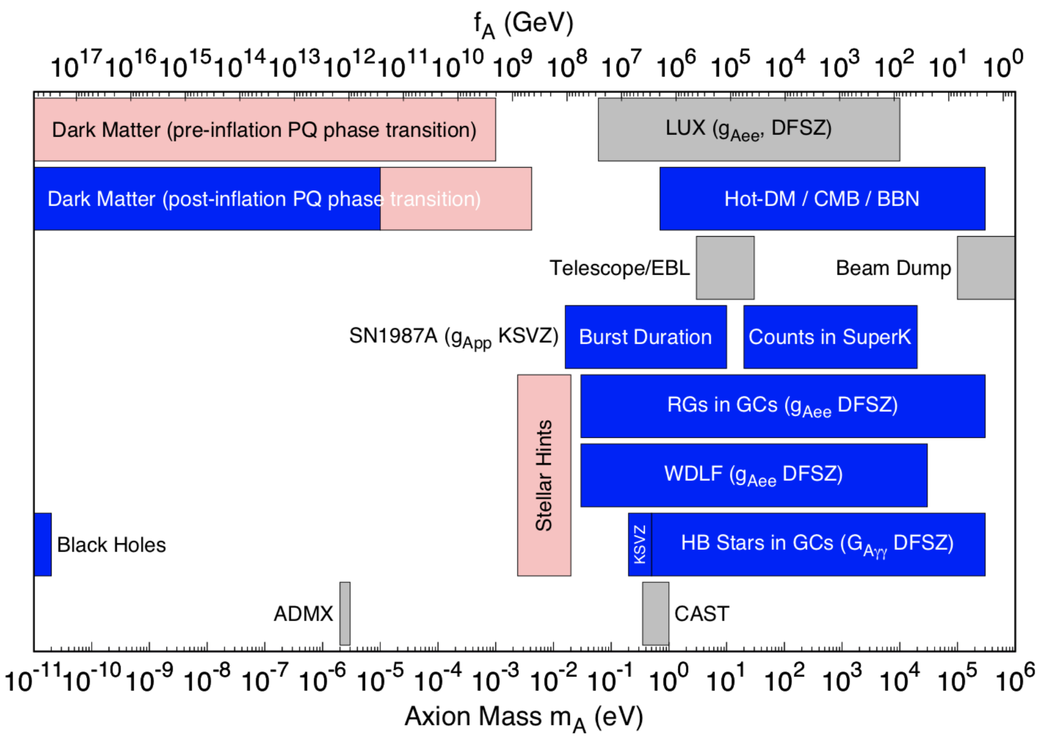

Figure 2.9: Exclusion bands, discussed in detail in the last chapter and possible windows for the axion decay constant and the axion mass [25].

Pre-inflationary scenario

In this simple case the axion energy density is dominated by the coherent oscillation of the axion field, namely the misalignment mechanism. The population of topological defects is wiped away beyond the horizon scale, and there is no domain wall problem. The relic density can be simply written as

$$\Omega_a^{pre} h^2 \sim 0.15 \left(\frac{f_a}{10^{11}\,\text{GeV}}\right)^{1.18} \bar{\theta}_i^2. \tag{2.60}$$

This means that if we believe axion are dark matter, in order to match the right relic abundance the axion decay constant f_a is constraint to be in a very high range

$$f_a \gtrsim 10^{10}\ \text{GeV}, \tag{2.61}$$

and possibly lying in the so-called *anthropic window*, where for tuned values $\bar{\theta}_i \to 0$, we could have an arbitrarily high PQ scale, $f_a \gg 10^{12}$ GeV.

Post-inflationary scenario

In the more complicated post-inflationary scenario higher momentum modes in the misalignment production and topological defects are taken into account, hence the relic density is the sum of all the possible productions

$$\Omega_a^{post} h^2 = \Omega_{a,mis}^{post} h^2 + \Omega_{a,strings}^{post} h^2 + \Omega_{a,walls}^{post} h^2.$$

We have found previously the energy density of the zero momentum mode in the misalignment (2.44)

$$\rho_\phi^{post,0}(t_0) = f_a^2 m_\phi m_\phi(t_1) \langle \bar{\theta}_i^2 \rangle \left(\frac{R_1}{R_0}\right)^3,$$

where $\langle \bar{\theta}_i^2 \rangle$ is the the order one average over the possible misalignment angles of different causal regions, that we discussed previously. We can compute it, following the argument of [1], doing a root mean square average of a uniform distribution of initial values over the possible angles, using the harmonic approximation

$$\langle \bar{\theta}_i^2 \rangle = \frac{1}{2\pi} \int_{-\pi}^{\pi} d\theta_i \theta_i^2 = \frac{\pi^2}{3}. \tag{2.62}$$

Similarly, the energy densities for higher momentum modes and string decay read

$$\rho_\phi^{post,n}(t_0) \sim N_{DW}^2 \rho_\phi^{post,0}(t_0), \qquad \rho_\phi^{post,s}(t_0) \gtrsim \xi N_{DW}^2 \rho_\phi^{post,0}(t_0).$$

The final relic abundance for the post inflationary scenario can be written numerically as (using string production of [50]):

$$\Omega_a^{post} h^2 \sim 0.7 \left(\frac{f_a}{10^{11}\ \text{GeV}}\right)^{1.18}. \tag{2.63}$$

As we can see in figure 2.9 the axion decay constant is constrained to be (for $N_{DW} = 1$) in the range $10^9 - 10^{11}$ GeV.

Chapter 3

Production of Hot Axions

3.1 The effective lagrangian

In this chapter we are going to write in detail the lagrangians for the axion thermal production. The aim is to compute the cross sections of interesting processes in order to quantify the thermal abundance of axions in the early Universe. The QCD axion model of interest is the DFSZ, since it does not require extra fermionic fields, but only the SM content; the generic full effective lagrangian reads

$$\mathscr{L} = \mathscr{L}_{SM} + \frac{1}{2}(\partial_\mu \phi)^2 + \frac{\phi}{f_a}\sum_X \frac{\alpha_X}{8\pi} C_{XX} \mathrm{tr} X_{\mu\nu}\tilde{X}^{\mu\nu} + \frac{\partial_\mu \phi}{2f_a}\sum_\psi c_\psi \bar{\psi}\gamma^\mu\gamma_5\psi, \tag{3.1}$$

where $\mathscr{L}_{SM}$ is written and discussed in full detail in the appendix A. Let us make some comments about what we have written above. First of all, the axion field is ϕ, i.e. the one before the mixing with mesons; as a matter of fact, we will only consider processes that thermalize axions way above the QCD phase transitions, where the axion mass and potential are negligible. Secondly, in agreement the lagrangian (1.28), written in the first chapter, we are expressing the axion interactions with matter in the so-called *derivative basis*, where we have an explicit dependence on the derivative $\partial_\mu \phi$. The sum is intended over all the fermions, namely all the quarks (not confined above 1 GeV) and all the leptons. The other interaction are with gauge bosons X_μ: for temperatures above the EW scale the sum contains $G^a_{\mu\nu}$, $W^i_{\mu\nu}$ and $B_{\mu\nu}$, while after the phase transition it refers to $G^a_{\mu\nu}$ and $F_{\mu\nu}$, namely the gluon and the photon. The coupling constants C_{XX} and c_ψ are dimensionless (they belong to 5-dim. operators, but the suppression scale is f_a) and for convention we can set $C_{gg} = 1$; also, according to what we found $C_{\gamma\gamma} = E/N - 1.92 \simeq 0.75$ and c_ψ are the PQ charges in the DFSZ model.

It is also important to notice that the derivative basis is expressed with Dirac fermions ψ, but in principle we could write, using the notation of [30], the simpler coupling

$$\mathscr{L} \supset \frac{\partial_\mu \phi}{2f_a}\sum_\chi c_\chi \bar{\chi}\gamma^\mu \chi, \tag{3.2}$$

where $\chi = \{Q, U, D, L, E\}$ are Weyl left-handed spinors representing the SM fermions. According to the relation (A.6) of Appendix A the relation between the coupling constants is

$$c_\psi = -c_\chi.$$

Nevertheless we will only use in this work Dirac spinors $\psi = \{q_L, u_R, d_R, l_L, e_R\}$. As pointed out in [30] if we consider the coupling of axions with fermions it is convenient to exploit the PQ symmetry in the phase redefinition of SM matter fields

$$\psi \to \exp\left(\frac{ic_\psi \gamma_5 \phi}{2f_a}\right)\psi. \tag{3.3}$$

In this way, at first order in ϕ in the exponential, the derivative coupling disappears from the lagrangian (3.1). However the transformation (3.3) introduces an axion phase in the Yukawa couplings of $\mathscr{L}_{SM}$: recalling eq. (A.5) of the appendix we obtain the transformation

$$y_\psi \to y_\psi \exp\left(\frac{ic_\psi \gamma_5 \phi}{f_a}\right) \tag{3.4}$$

in the Yukawa lagrangian. Again, at first order in ϕ, a new interaction is generated

$$\mathscr{L}_{int} = i\frac{c_\psi y_\psi}{f_a}\phi\left(\frac{v+h}{\sqrt{2}}\right)\bar{\psi}\gamma_5\psi, \tag{3.5}$$

and when at the EW scale the Higgs field gets VEV v the interaction is clearly proportional to the fermion mass

$$m_\psi = v y_\psi/\sqrt{2}. \tag{3.6}$$

We will use the vertex in the Yukawa basis (see table 3.1), as the computation of cross sections is vastly simplified; also, we will check the equivalence of the two basis in the calculations. At linear order in h, the excitation of the Higgs field, a new interaction is depicted in table 3.1, in the four-legs vertex with the Higgs particle; the only difference with the axion-fermion vertex is the presence of v in the denominator.

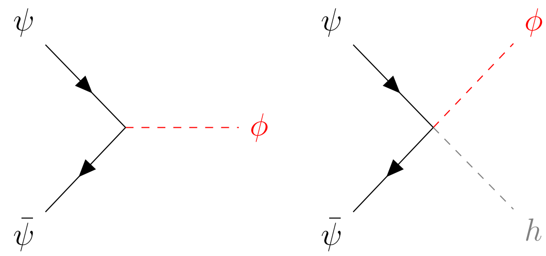

Derivative basis	$c_\psi \gamma^\mu \gamma_5/2f_a$	
Yukawa basis	$ic_\psi m_\psi \gamma_5/f_a$	$ic_\psi m_\psi \gamma_5/vf_a$

Table 3.1: Axion-fermion vertex in the two basis, and axion-Higgs-fermion vertex in the Yukawa basis.

As a matter of fact in the four-legs coupling we can insert the expression of the mass (3.6) and express it with only the Yukawa constant y_ψ:

$$\mathscr{L}^{(4)}_{\bar{\psi}\psi\phi h} = i\frac{c_\psi y_\psi}{\sqrt{2}f_a}\phi h\bar{\psi}\gamma_5\psi, \tag{3.7}$$

that can also be seen from the general interacting lagrangian (3.5).

3.2 Thermal axion production

As pointed out in [27] scattering and decay processes can give a contribution to N_{eff} possibly detectable by future CMB experiments (CMB-S4 [42]). However we want consider in this work similar processes using also particles at the Electroweak scale ($\sim 10^2$ GeV): heavy quarks, EW bosons and Higgs boson. For the sake of simplicity we can consider only one generation of quarks and we focus in the case $q = \{t, b\}$, the heaviest quarks of the SM*. The processes we will consider are annihilation and scattering producing thermal axions ϕ and can be generalised as the following:

$$\psi(p1) + \bar{\psi}(p2) \leftrightarrow X(p3) + \phi(k), \qquad \psi(p1) + X(p2) \leftrightarrow \psi(p3) + \phi(k), \tag{3.8}$$

$$\psi \equiv q = \{t, b\}, \qquad X = \{g, \gamma, Z, W^{\pm}, h\}.$$

We will use and express the results in terms of the *Mandelstam* variables, see below. In the annihilation processes we have three topologically different diagrams: the s-channel, t-channel and u-channel. However, as pointed out in the previous chapters and in the lagrangian (3.1), in the s-channel the coupling comes from the anomalous 5-dimensional operator

$$\mathscr{L} \supset \frac{\phi}{f_a}\frac{\alpha_s}{8\pi}C_{gg}\mathrm{tr}G_{\mu\nu}\tilde{G}^{\mu\nu}, \tag{3.9}$$

whereas the t and u channels are represented by the recently introduced Yukawa coupling

$$\mathscr{L} \supset i\frac{c_\psi m_\psi}{f_a}\phi\bar{\psi}\gamma_5\psi. \tag{3.10}$$

As we said earlier we want to focus also on model dependent couplings, meaning that we don't want to only consider the axion-gluon coupling, but also the other operators (3.10) and $X_{\mu\nu}\tilde{X}^{\mu\nu}$. The strength of the latter is proportional to α_X/f_a, that is a suppression due to the α_X of the SM, in comparison with the masses of the fermions in the Yukawa couplings. But this is only true for temperatures around the fermion masses and more importantly below the EW scale, where the SM fermions have masses thanks to Higgs mechanism. As a matter of fact, accordingly to [30], we could consider all the possible couplings, and therefore included also the axion couplings with matter, and compute their production rates for very high temperatures, even much above the TeV scale. While the latter computation has already been made, we focus on what we can understand from it. First of all the axion coupling with matter, that can be written as† [30]

$$\mathscr{L} \supset ic_\psi y_\psi \frac{\phi}{f_a}\chi_i H \chi_j, \tag{3.11}$$

is quantified in this case by the Yukawa of the SM fermions, and we then acknowledge that the only interesting process comes with the top Yukawa coupling y_t, orders of magnitude bigger than the others. But more importantly, if we are to compute the cosmological axion yield and the possibles CMB signatures through

*Eventually we will also consider other heavy fermions like the τ and μ leptons, see in the following sections.

†In the notation of [30] the matter fields are Weyl fermions χ, and that is why we previously introduced them. Also, H is the $SU(2)_L$ invariant Higgs field.

the observable ΔN_{eff}, [30] found out that even considering the strongest effect on the axion production rate, that comes from y_t process (3.11), the computation implies that axions decouple at temperature above the EW scale. This means that all the SM particles are still relativistic, and once they gradually become non-relativistic they will annihilate heating only photons and neutrinos. The limit on ΔN_{eff} is the same that we found in (2.30)

$$\Delta N_{\text{eff}} = 0.0264 \frac{Y_\phi}{Y_\phi^{eq}}. \tag{3.12}$$

Therefore we want to extend the work in [30] by using all the possible axion couplings using only the operator (3.10) and for temperatures around, but also below the EW scale. We will consider only the t and u contribution in the annihilation, neglecting the s-channel. For the scattering the contributions come only from the s and u channels. The diagrams are depicted in figure 3.1.

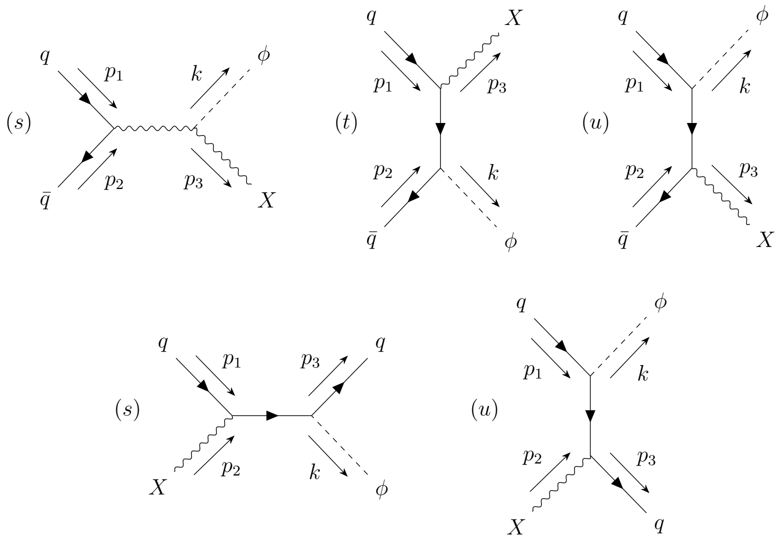

Figure 3.1: Feynman diagrams for the generic processes (3.8). In the first row s, t and u channels of the annihilation, in the second row the s and u diagrams of the scattering.

It is relevant to discuss an important property of the diagrams we are considering that will crucially simplify the amount of the computations. Indeed, if we look at the diagrams, we notice that passing from the annihilation to the scattering we would need a replacement in the momenta:

$$p_1 \to p_1, \qquad p_2 \to -p_3, \qquad p_3 \to -p_2, \qquad k \to k, \tag{3.13}$$

meaning that the square amplitude of the processes will satisfy a *crossing symmetry*. If we look at the definition of the Mandelstam variables,

$$s = (p_1 + p_2)^2 = (p_3 + k)^2,$$
$$t = (p_1 - p_3)^2 = (p_2 - k)^2,$$
$$u = (p_1 - k)^2 = (p_2 - p_3)^2,$$

and accordingly to the notation of the momenta in the diagrams of 3.1, the crossing symmetry is reflected in the replacements

$$s \to t, \qquad t \to s, \qquad u \to u.$$

We are going to exploit this feature by only computing explicitly the squared amplitude $|\mathcal{M}_{\text{ann}}|^2$ for the annihilation process and then for the scattering

$$|\mathcal{M}_{\text{sca}}|^2 = |\mathcal{M}_{\text{ann}}|^2(s \to t, t \to s).$$

List of processes

After having discussed the general properties of the diagrams let us look in detail the processes we will consider in this work. Table 3.2 refers to every annihilation and scattering process following a temperature increasing order: we basically know that the production rate will be peaked around the fermion mass and we can list the processes by the mass hierarchy of the SM fermions. As it can be seen from table 3.2 the first processes consider the μ and τ leptons as the SM fermions, this is because in order to have a complete and full description of thermal axion production within the SM we also have to consider the QED sector and their heaviest particles, originally discussed in [27]. However most of the other processes have production rates that become interesting at temperatures around the EW scale and will be our major focus. Process 19 and 20 are the only exceptions as they rely on beyond the SM physics, that is the UV completed KSVZ model described in section 1.4. In the latter the production rate is peaked at very high temperatures, in principle arbitrarily higher than the EW scale; as a lower bound, for example from colliders like the LHC at CERN, we should consider energies bigger than a few TeV, see in detail section 3.4

	Process	Couplings	Temperature [GeV]
1	$\mu^+\mu^- \to \gamma\phi$	e	$\sim m_\mu = 0.105$
2	$\mu^\pm\gamma \to \mu^\pm\phi$	e	"
3	$\tau^+\tau^- \to \gamma\phi$	e	$\sim m_\tau = 1.777$
4	$\tau^\pm\gamma \to \tau^\pm\phi$	e	"
5	$b\bar{b} \to g\phi$	g_s	$\sim m_b = 4.180$
6	$b(\bar{b})g \to b(\bar{b})\phi$	g_s	"
7	$b\bar{b} \to \gamma\phi$	e	"
8	$b(\bar{b})\gamma \to b(\bar{b})\phi$	e	"
9	$t\bar{t} \to g\phi$	g_s	$\sim m_t = 173.4$
10	$t(\bar{t})g \to t(\bar{t})\phi$	g_s	"
11	$t\bar{t} \to \gamma\phi$	e	"
12	$t(\bar{t})\gamma \to t(\bar{t})\phi$	e	"
13	$t\bar{b} \to W^+\phi$	g_W	~ 200 (EW scale)
14	$tW^+ \to \bar{b}\phi$	g_W	"
15	$b\bar{b} \to Z\phi$	g_W	"
16	$t\bar{t} \to Z\phi$	g_W	"
17	$t\bar{t} \to h\phi$	y_t	"
18	$t(\bar{t})h \to t(\bar{t})\phi$	y_t	"
19	$Q^\star\bar{Q}^\star \to g\phi$	g_s	$\gtrsim 1000$
20	$Q^\star(\bar{Q}^\star)g \to Q^\star(\bar{Q}^\star)\phi$	g_s	$\gtrsim 1000$

Table 3.2: Thermal axion production processes at different scales.

3.3 Cross Sections

3.3.1 Gluons

The easiest interactions that we can compute are the ones considering massless bosons, gluons and photons. The case of the gluons is more interesting because of the presence of α_s, in contrast with α_{em}. Nevertheless we will also discuss the processes involving photons, as the computation of the squared amplitude is exactly the same.

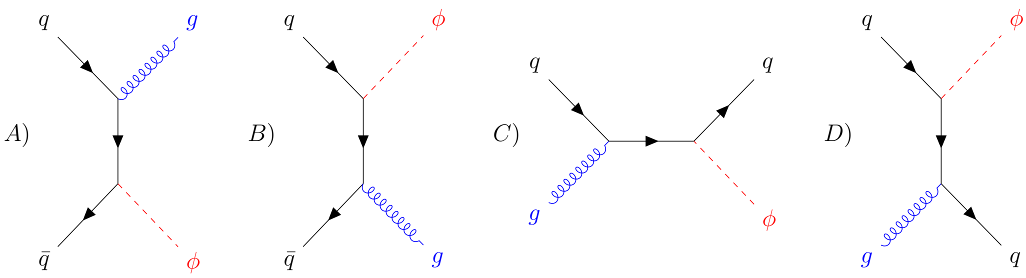

Figure 3.2: Feynman diagrams involving gluons. The quarks are both t and b.

In figure 3.4 are depicted the 4 diagrams (A, B for annihilation and C, D for scattering). We therefore consider first the annihilation processes

$$t\bar{t} \to g\phi, \qquad b\bar{b} \to g\phi,$$

with matrix element

$$\mathcal{M}_{q\bar{q}\to g\phi} = \mathcal{M}_A + \mathcal{M}_B, \tag{3.14}$$

where

$$\mathcal{M}_A = \frac{ic_q m_q g_s}{f_a}\epsilon^*_\mu(p_3,\lambda)\bar{v}(p_2)\gamma_5\frac{\not{p}_1 - \not{p}_3 + m_q}{t - m_q^2}\gamma^\mu u(p_1)t^a_{ij}, \tag{3.15}$$

$$\mathcal{M}_B = \frac{ic_q m_q g_s}{f_a}\epsilon^*_\mu(p_3,\lambda)\bar{v}(p_2)\gamma^\mu\frac{\not{p}_1 - \not{k} + m_q}{u - m_q^2}\gamma_5 u(p_1)t^a_{ij}. \tag{3.16}$$

We notice how the computation is proportional to the quark mass m_q and the charge c_q (remember we are in the DSFZ model), meaning that in the massless quark limit the cross section vanishes. The other quantities entering in the prefactor are the coupling constant $g_s = \sqrt{4\pi\alpha_s}$, that in general will have a temperature dependence, and the fundamental PQ scale f_a. t^a_{ij} is the *color factor*, coming from the QCD vertex and λ is taking into account the helicity of the gluons, that will be summed in the expression of the averaged squared amplitude:

$$|\bar{\mathcal{M}}_{q\bar{q}\to g\phi}|^2 = \Pi_i \sum_s |\mathcal{M}_{q\bar{q}\to g\phi}|^2,$$

where s are the spins of the final state particles, while the prefactor Π_i is just an average over the initial state polarizations. Using the sums

$$\sum_s u_s(p)\bar{u}_s(p) = \not{p} + m, \qquad \sum_s v_s(p)\bar{v}_s(p) = \not{p} - m, \qquad \sum_\lambda \epsilon_\mu(k)\epsilon^*_\nu(k) = -g_{\mu\nu},$$

and the trace computations we obtain

$$|\bar{\mathcal{M}}_{q\bar{q}\to g\phi}|^2 = \left(\frac{c_q m_q g_s}{f_a}\right)^2 |t^a_{ij}|^2 \frac{s^2}{(s+t-m_q^2)(m_q^2-t)}. \tag{3.17}$$

For the computation of the cross section we make use of the expression of appendix B, where the phase-space integration can be done in the CM (center of mass) frame. In the latter is possible to express the Mandelstam variable t in terms of the scattering angle θ [27]

$$t|_{\text{ann}} = m_q^2 - \frac{s}{2}\left(1 - L(s)\cos\theta\right), \qquad L(s) = \sqrt{1 - \frac{4m_q^2}{s}},$$

leading to the result

$$\sigma_{q\bar{q}\to g\phi}(s) = \frac{1}{32\pi\sqrt{s}L(s)} \int_{-1}^{1} d\cos\theta |\bar{\mathcal{M}}_{q\bar{q}\to g\phi}|^2 \tag{3.18}$$

$$= \left(\frac{c_q m_q g_s}{f_a}\right)^2 |t^a_{ij}|^2 \frac{\tanh^{-1}(L(s))}{4\pi(s-4m_q^2)}. \tag{3.19}$$

For the scattering processes involving the t and b quarks (diagrams C and D of figure 3.4) we can write

$$\mathcal{M}_C = \frac{ic_q m_q g_s}{f_a} \epsilon_\mu(p_2,\lambda)\bar{u}(p_3)\gamma_5 \frac{\not{p}_1 - \not{p}_2 + m_q}{s - m_q^2} \gamma^\mu u(p_1) t^a_{ij}, \tag{3.20}$$

$$\mathcal{M}_D = \frac{ic_q m_q g_s}{f_a} \epsilon_\mu(p_2,\lambda)\bar{u}(p_3)\gamma^\mu \frac{\not{p}_1 - \not{k} + m_q}{u - m_q^2} \gamma_5 u(p_1) t^a_{ij}. \tag{3.21}$$

As we anticipated earlier it is easy to see that $\mathcal{M}_C$ and $\mathcal{M}_D$ differ from $\mathcal{M}_A$ and $\mathcal{M}_B$ by the replacement (3.13), respectively. Therefore the squared amplitude is just

$$|\bar{\mathcal{M}}_{q\gamma\to q\phi}|^2 = \left(\frac{c_q m_q g_s}{f_a}\right)^2 |t^a_{ij}|^2 \frac{t^2}{(s+t-m_q^2)(m_q^2-s)}. \tag{3.22}$$

The cross section can be then computed using the relation [27]

$$t|_{\text{sca}} = -\frac{s}{2}\left(1 - \frac{m_q^2}{s}\right)^2 (1-\cos\theta), \tag{3.23}$$

giving

$$\sigma_{qg\to q\phi}(s) = \frac{1}{32\pi\sqrt{s}} \int_{-1}^{1} d\cos\theta |\bar{\mathcal{M}}_{qg\to q\phi}|^2 \tag{3.24}$$

$$= \left(\frac{c_q m_q g_s}{f_a}\right)^2 |t^a_{ij}|^2 \frac{2s^2\log(s/m_q^2) - 3s^2 + 4m_q^2 s - m_q^4}{32\pi s^2(s-m_q^2)}. \tag{3.25}$$

It is important to notice how after the integration in $\cos\theta$ the only dependence of the cross section relies on the Mandelstam variable s, meaning that the expressions (3.19) and (3.25) are Lorentz invariant. It is left to compute the color factors $|t^a_{ij}|^2$ for the two cases.

Color factors

The specification of a quark state in QCD requires not only the Dirac spinor $u_s(p)$ (momentum and spin), but also the color c_i, a three-column vector that can be *red*, *blue* or *green*:

$$|r\rangle = \begin{pmatrix}1\\0\\0\end{pmatrix}, \quad |b\rangle = \begin{pmatrix}0\\1\\0\end{pmatrix}, \quad |g\rangle = \begin{pmatrix}0\\0\\1\end{pmatrix}.$$

For the annihilation case we have a quark-antiquark interaction and the color factor in the matrix element reads (for both t and u channels):

$$t^a_{ij} = c_i^\dagger t^a c_j \equiv \frac{1}{2}\langle i|\lambda^a|j\rangle = \frac{1}{2}\sum_a (\lambda^a)_{c_i c_j},$$

and it depends on the color state of the interacting quarks. A typical octet state is $r\bar{b}$ (but any of the others would lead to the same result) meaning that the incoming quark is red, the incoming antiquark is antiblue and the outgoing gluon is red-antiblue because of color conservation. In this case we identify $|i\rangle \equiv |r\rangle$, $|j\rangle \equiv |b\rangle$ and then write

$$t^{a,\alpha}_{ij} = \frac{1}{2}\begin{pmatrix}1 & 0 & 0\end{pmatrix}\lambda^a \begin{pmatrix}0\\1\\0\end{pmatrix} = \frac{1}{2}(1-i).$$

Therefore the color factor in the squared amplitude and in the cross section for the generic $q\bar{q}$ is just

$$|t^{a,\alpha}_{ij}|^2 = \frac{1}{4}|1-i|^2 = \frac{1}{2}. \tag{3.26}$$

The configuration we chose was a red-antiblue gluon, but we should include all the different configurations of gluons in oder to take into account the color structure; therefore the full color factor in the cross sections will just be the sum over the gluons

$$|t^a_{ij}|^2 = \sum_{\alpha=1}^{8} |t^{a,\alpha}_{ij}|^2 = \frac{1}{2} \times 8 = 4. \tag{3.27}$$

In the case of the scattering processes we notice that the matrix element is exactly the same in the color space (where the kets $|r\rangle, |b\rangle, |g\rangle$ live), and the color factor is therefore the same.

It is easy now to generalize the computations to the same identical processes but replacing gluons with photons, as depicted in figure 3.3. The computations is exactly the same as the gluon and photon polarization are the same, being massless. The only difference comes from the coupling constant, as we have the replacement $g_s \to Q_q e$, where Q_q is the electric charge of the considered quark and e the electric charge of leptons. Moreover the color factor is obviously disappearing. The change in the coupling constant is crucial if we want to determine for which values of f_a the process reaches thermalization. The electromagnetic coupling e is indeed much weaker than g_s at the GeV scale, meaning that the process of scattering and annihilation considering heavy quarks and photons are irrelevant compared to the ones with gluons. Anyway in the case of photons we could consider the heavy leptons μ, τ of the QED sector and calculate the same process of annihilation and scattering, and this is what we are going to do in next section.

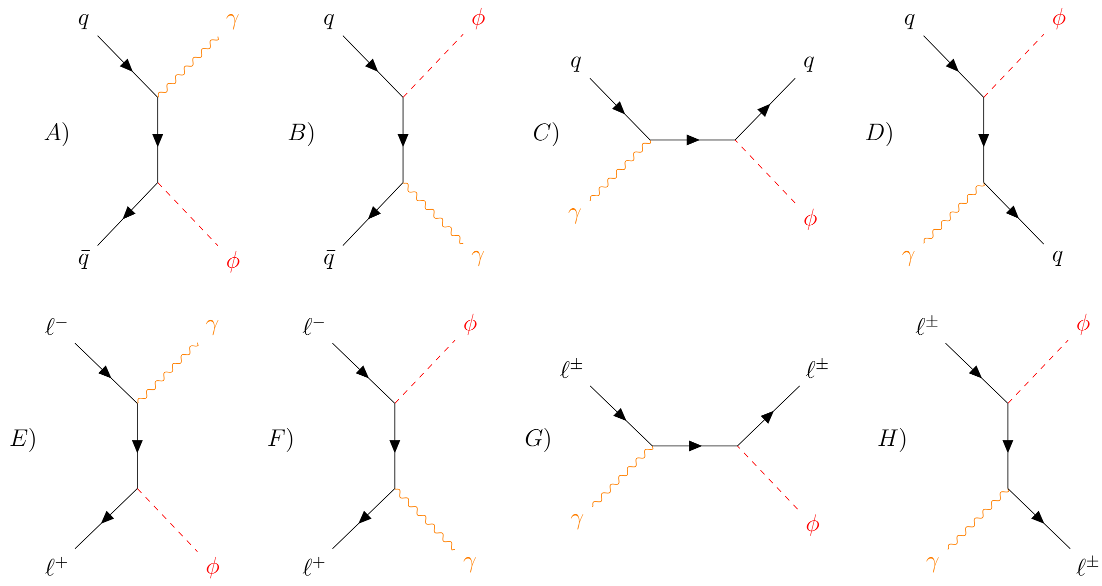

Figure 3.3: Feynman diagrams involving photons. The quarks are both t and b, the leptons can μ and τ.

3.3.2 Photons

As we commented earlier it is interesting to look at the processes with leptons. We first consider the annihilation processes

$$\ell^+\ell^- \to \gamma\phi,$$

where $\ell = \{\mu, \tau\}$ depicted in diagrams E) and F) in figure 3.3 and with matrix elements

$$\mathcal{M}_{\ell^+\ell^-\to\gamma\phi} = \mathcal{M}_E + \mathcal{M}_F, \tag{3.28}$$

$$\mathcal{M}_E = \frac{ic_\ell m_\ell e}{f_a}\epsilon^*_\mu(p_3,\lambda)\bar{v}(p_2)\gamma_5\frac{\not{p}_1 - \not{p}_3 + m_\ell}{t - m_\ell^2}\gamma^\mu u(p_1), \tag{3.29}$$

$$\mathcal{M}_F = \frac{ic_\ell m_\ell e}{f_a}\epsilon^*_\mu(p_3,\lambda)\bar{v}(p_2)\gamma^\mu\frac{\not{p}_1 - \not{k} + m_\ell}{u - m_\ell^2}\gamma_5 u(p_1). \tag{3.30}$$

The coupling constant is now the electrical charge $e = \sqrt{4\pi\alpha_{em}}$, that shows a running due to renormalization. Altough it is the only coupling that grows in strength as the temperature increases, below the EW scale is weaker than both g_s and g_W. We notice that the trace calculation is exactly the same as the quark-gluon process, and also the cross section will be the same: we are just considering leptons instead of quarks, but the only things that changes besides the coupling (and the absence of the colour factor of course) is the fermion mass. We can then write

$$|\bar{\mathcal{M}}_{q\bar{q}\to\gamma\phi}|^2 = \left(\frac{c_\ell m_\ell e}{f_a}\right)^2\frac{s^2}{(s+t-m_\ell^2)(m_\ell^2 - t)}, \tag{3.31}$$

and the cross sections, following the exactly same steps and integration as in the case of gluons, turns out to be

$$\sigma_{\ell^+\ell^-\to\gamma\phi}(s) = \left(\frac{c_\ell m_\ell e}{f_a}\right)^2\frac{\tanh^{-1}(L(s))}{4\pi(s - 4m_\ell^2)}. \tag{3.32}$$

Now for the scattering process

$$\ell^{\pm}\gamma \to \ell^{\pm}\phi,$$

we write the matrix elements for the diagrams G) and H) of figure 3.3:

$$\mathcal{M}_G = \frac{ic_\ell m_\ell e}{f_a}\epsilon_\mu(p_2,\lambda)\bar{u}(p_3)\gamma_5\frac{\not{p}_1 - \not{p}_2 + m_\ell}{s - m_\ell^2}\gamma^\mu u(p_1), \tag{3.33}$$

$$\mathcal{M}_H = \frac{ic_\ell m_\ell e}{f_a}\epsilon_\mu(p_2,\lambda)\bar{u}(p_3)\gamma^\mu\frac{\not{p}_1 - \not{k} + m_\ell}{u - m_\ell^2}\gamma_5 u(p_1), \tag{3.34}$$

and analogously we write down the squared amplitude

$$|\bar{\mathcal{M}}_{\ell^\pm\gamma\to\ell^\pm\phi}|^2 = \left(\frac{c_\ell m_\ell e}{f_a}\right)^2 \frac{t^2}{(s+t-m_\ell^2)(m_\ell^2 - s)}, \tag{3.35}$$

and the cross section

$$\sigma_{\ell^\pm\gamma\to\ell^\pm\phi}(s) = \left(\frac{c_\ell m_\ell e}{f_a}\right)^2 \frac{2s^2\log(s/m_\ell^2) - 3s^2 + 4m_\ell^2 s - m_\ell^4}{32\pi s^2(s - m_\ell^2)} \tag{3.36}$$

We can then summarize the cross sections for the processes with gluons and photons, both for quarks and leptons:

$$\sigma_{q\bar{q}\to g\phi}(s) = 4\left(\frac{c_q m_q g_s}{f_a}\right)^2 F_1(s; m = m_q), \tag{3.37}$$

$$\sigma_{qg\to q\phi}(s) = 4\left(\frac{c_q m_q g_s}{f_a}\right)^2 F_2(s; m = m_q), \tag{3.38}$$

$$\sigma_{t\bar{t}\to\gamma\phi}(s) = \frac{4}{9}\left(\frac{c_t m_t e}{f_a}\right)^2 F_1(s; m = m_t), \tag{3.39}$$

$$\sigma_{t\gamma\to t\phi}(s) = \frac{4}{9}\left(\frac{c_t m_t e}{f_a}\right)^2 F_2(s; m = m_t), \tag{3.40}$$

$$\sigma_{b\bar{b}\to\gamma\phi}(s) = \frac{1}{9}\left(\frac{c_b m_b e}{f_a}\right)^2 F_1(s; m = m_b), \tag{3.41}$$

$$\sigma_{b\gamma\to b\phi}(s) = \frac{1}{9}\left(\frac{c_b m_b e}{f_a}\right)^2 F_2(s; m = m_b), \tag{3.42}$$

$$\sigma_{\ell^+\ell^-\to\gamma\phi}(s) = \left(\frac{c_\ell m_\ell e}{f_a}\right)^2 F_1(s; m \equiv m_\ell), \tag{3.43}$$

$$\sigma_{\ell^\pm\gamma\to\ell^\pm\phi}(s) = \left(\frac{c_\ell m_\ell e}{f_a}\right)^2 F_2(s; m \equiv m_\ell), \tag{3.44}$$

where

$$F_1(s) = \frac{\tanh^{-1}(L(s))}{4\pi(s - 4m^2)}, \qquad F_2(s) = \frac{2s^2\log(s/m^2) - 3s^2 + 4m^2 s - m^4}{32\pi s^2(s - m^2)},$$

3.3.3 EW gauge bosons

$W^\pm$ processes

Now let us focus on the electroweak processes with $W^\pm$ and Z bosons. As described in appendix A the coupling of fermions with the W boson is flavour changing because of the charged current, therefore the processes we are interested in are:

$$t\bar{b} \to W^+\phi, \qquad b\bar{t} \to W^-\phi, \qquad tW^+ \to \bar{b}\phi, \qquad bW^- \to \bar{t}\phi \tag{3.45}$$

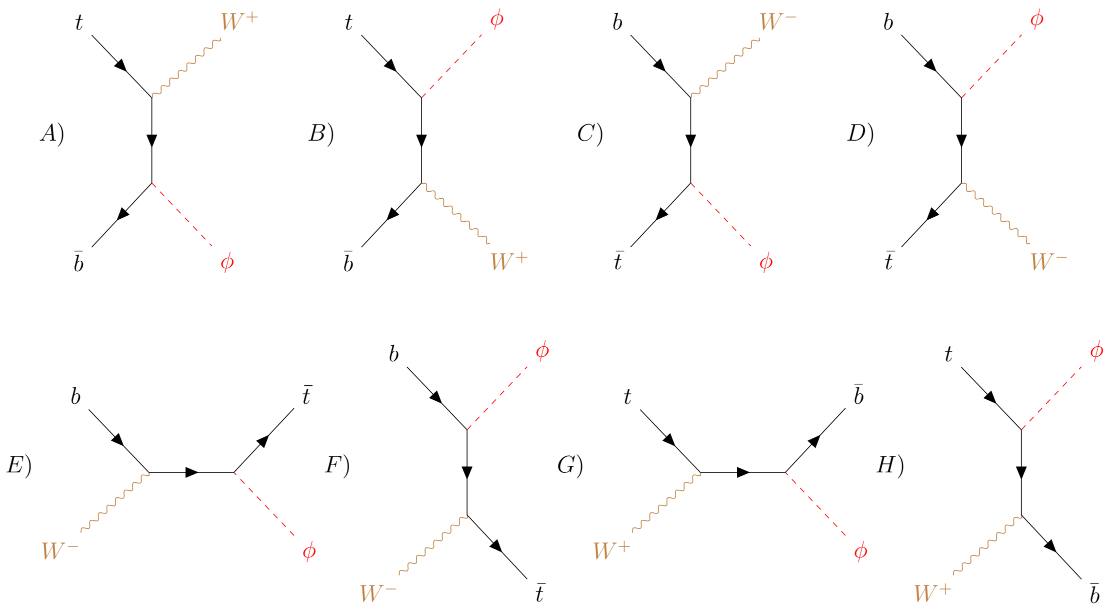

Figure 3.4: Feynman diagrams of annihilation and scattering involving $W^\pm$ bosons.

For all the four processes considered there is one leading diagram and one sub-dominant one. The latter comes from the $b\bar{b}\phi$ coupling proportional to m_b that is considerably lower than the temperatures we want to consider ($T \gtrsim 100$ GeV). Therefore diagrams A, D, F and G give only a correction to the squared amplitude.

The first annihilation case $t\bar{b} \to W^+\phi$ is depicted in diagrams A, B, with matrix elements

$$\mathcal{M}_A = \frac{ic_b m_b g_W}{2\sqrt{2}f_a}\epsilon^*_\mu(p_3,\lambda)\bar{v}(p_2)\gamma_5\frac{\not{p}_1 - \not{p}_3 + m_b}{t - m_b^2}\gamma^\mu(1-\gamma_5)u(p_1), \tag{3.46}$$

$$\mathcal{M}_B = \frac{ic_t m_t g_W}{2\sqrt{2}f_a}\epsilon^*_\mu(p_3,\lambda)\bar{v}(p_2)\gamma^\mu(1-\gamma_5)\frac{\not{p}_1 - \not{k} + m_t}{u - m_t^2}\gamma_5 u(p_1), \tag{3.47}$$

where we have used the SM coupling of fermions with the $W^\pm$ bosons and setting $V_{ij} = 1$ in the case of one generation. g_W replaces g_s as coupling constant and in addition the sum over the spins of the polarization tensors changes due to the presence of the mass

$$\sum_\lambda \epsilon_\mu(k)\epsilon^*_\nu(k) = -g_{\mu\nu} + \frac{k_\mu k_\nu}{M_W^2}, \tag{3.48}$$

complicating the computation of the squared amplitude. The latter can be written as

$$|\bar{\mathcal{M}}|^2 = \frac{1}{4}|\mathcal{M}_A^2 + \mathcal{M}_B^2 + 2\mathcal{M}_A^*\mathcal{M}_B| \sim \frac{1}{4}|\mathcal{M}_B^2|, \tag{3.49}$$

because of the presence of the bottom quark mass. In other words, without considering the factors coming from the traces we could write

$$|\bar{\mathcal{M}}|^2 \propto \frac{1}{4}\left(\frac{c_t m_t g_W}{2\sqrt{2}f_a}\right)^2 \left[1 + \underbrace{\left(\frac{c_b m_b}{c_t m_t}\right) + \left(\frac{c_b m_b}{c_t m_t}\right)^2}_{\text{corrections}}\right], \tag{3.50}$$

where $m_b/m_t \sim 10^{-2}$ and $m_b^2/m_t^2 \sim 10^{-4}$. The computation of the trace gives

$$|\bar{\mathcal{M}}|^2_{t\bar{b}\to W^+\phi} = \frac{c_t^2 m_t^2 g_W^2}{8f_a^2}\left[\frac{2t - m_t^2 + s(2m_t^2 + M_W^2 - t - s)/4M_W^2}{m_t^2 + M_W^2 - t - s}\right]. \tag{3.51}$$

Like in the case of gluons and photons the computation of the cross section is given by integrating on the angular variable θ, that is

$$\sigma(s) = \frac{1}{32\pi I}\int_{-1}^{1} |\bar{\mathcal{M}}|^2 \left(1 - \frac{M_W^2}{s}\right) d\cos\theta, \tag{3.52}$$

where we are neglecting the bottom mass‡. The prefactor I can be written

$$I = \frac{sL(s)}{2}, \qquad L(s) = \sqrt{1 - \frac{2m_t^2}{s} + \frac{m_t^4}{s^2}}, \tag{3.53}$$

and in the expression of the squared amplitude we have to express the t variable according to the following

$$t|_{\text{ann}} = m_t^2 + m_Z^2 - \frac{s}{2}(1 - L(s)\cos\theta).$$

For the computation of the cross section we had to separate all the terms of the squared amplitude and integrate them one by one before summing all the contributions, using the software *Mathematica*; the cross section reads

$$\sigma_{t\bar{b}\to W^+\phi}(s) = \frac{c_t^2 m_t^2 g_W^2 (M_W^2 - s)}{512\pi f_a^2 L^2(s) M_W^2 s^3} F_3(s), \tag{3.54}$$

where the expression of $F_3(s)$ can be found in (B.5) of the appendix B.

Exploiting now the crossing symmetry we can then write the squared amplitude for the scattering process $tW^+ \to \bar{b}\phi$:

$$|\bar{\mathcal{M}}|^2_{tW^+\to\bar{b}\phi} = \frac{c_t^2 m_t^2 g_W^2}{8f_a^2}\left[\frac{2s - m_t^2 + t(2m_t^2 + M_W^2 - t - s)/4M_W^2}{m_t^2 + M_W^2 - t - s}\right]. \tag{3.55}$$

Analogously we integrate analytically the angular variable, obtaining

$$\sigma_{tW^+\to\bar{b}\phi}(s) = \frac{c_t^2 m_t^2 g_W^2}{1024\pi f_a^2 L^2(s) M_W^2 s^3} F_4(s), \tag{3.56}$$

‡It is reasonable, since involving the $W^\pm$ bosons and the top quark, both way more massive than the b quark, we are expecting that the process dominates for temperatures $\gtrsim$ 100 GeV.

where now

$$L(s) = \sqrt{1 - \frac{m_t^2 + M_W^2}{s} + \frac{(m_t^2 - M_W^2)^2}{s^2}},$$

and the explicit expression of $F_4(s)$ is in appendix B. We see how the two cross sections (3.54) and (3.56) have the same prefactor, being proportional to m_t^2/f_a^2. We can also notice the presence of the W mass in the denominator that is reflected in the shape of the rate: based on dimensional analysis we can expect such a rate with the following dependences around the EW scale, where m_t are relevant

$$\Gamma = n\,\langle\sigma v\rangle \sim T^3 \frac{m_t^2}{M_W^2 f_a^2} \sim T^3, \qquad \Gamma/H \sim T, \qquad T \sim T_{EW}. \tag{3.57}$$

Z processes

For the Z boson instead we have the diagrams depicted in figure (3.5):

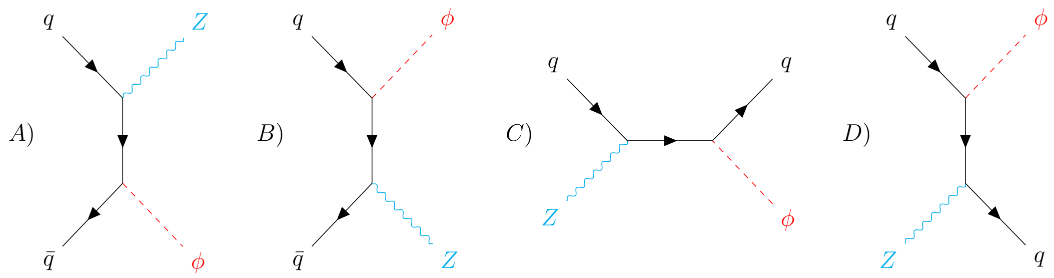

Figure 3.5: Feynman diagrams of annihilation and scattering involving the Z boson.

The annihilation process $q\bar{q} \to Z\phi$ is depicted in diagrams A, B, with matrix elements

$$\mathcal{M}_A = \frac{ic_q m_q g_W}{2\cos\theta_W f_a}\epsilon^*_\mu(p_3,\lambda)\bar{v}(p_2)\gamma_5 \frac{(\not{p}_1 - \not{p}_3 + m_q)}{t - m_q^2}\gamma^\mu(c_V^{(q)} - c_A^{(q)}\gamma_5)u(p_1), \tag{3.58}$$

$$\mathcal{M}_B = \frac{ic_q m_q g_W}{2\cos\theta_W f_a}\epsilon^*_\mu(p_3,\lambda)\bar{v}(p_2)\gamma^\mu(c_V^{(q)} - c_A^{(q)}\gamma_5)\frac{(\not{p}_1 - \not{k} + m_q)}{u - m_q^2}\gamma_5 u(p_1), \tag{3.59}$$

where we have now in the coupling the presence of the *Weinberg angle* θ_W[§], and the presence of the factors $c_V^{(q)}$ and $c_A^{(q)}$, defined in appendix A as

$$c_V^{(q)} = T_{3L,q} - 2Q_f \sin^2\theta_W, \qquad c_A^{(q)} = T_{3L,q}.$$

The values for the considered quarks can be easily calculated:

	$c_V^{(q)}$	$c_A^{(q)}$
$q = t$	$-1/2 - 4/3\sin^2\theta_W$	$-1/2$
$q = b$	$1/2 + 2/3\sin^2\theta_W$	$1/2$

Therefore we can write the squared amplitude in the following way:

$$|\bar{\mathcal{M}}|^2_{q\bar{q}\to Z\phi} = -\frac{1}{4}\left(\frac{c_q m_q g_W}{2\cos\theta_W f_a}\right)^2\left(-g_{\mu\nu} + \frac{p_{3\mu}p_{3\nu}}{M_Z^2}\right)\mathcal{D}^{\mu\nu}, \tag{3.60}$$

[§]Experimentally we have the numerical result $\sin^2\theta_W \approx 0.23$ [].

where $\mathcal{D}^{\mu\alpha}$ is the trace of γ functions

$$\mathcal{D}^{\mu\nu} = \mathrm{tr}\Bigg[(\not{p}_1 + m_q)\left(\frac{\gamma_\star^\nu(\not{p}_1 - \not{p}_3 + m_q)\gamma_5}{t - m_q^2} + \frac{\gamma_5(\not{p}_1 - \not{k} + m_q)\gamma_\star^\nu}{u - m_q^2}\right)\times$$
$$(\not{p}_2 - m_q)\left(\frac{\gamma_5(\not{p}_1 - \not{p}_3 + m_q)\gamma_\star^\mu}{t - m_q^2} + \frac{\gamma_\star^\mu(\not{p}_1 - \not{k} + m_q)\gamma_5}{u - m_q^2}\right)\Bigg],$$

with the definition

$$\gamma_\star^\mu = \gamma^\mu(c_V^{(q)} - c_A^{(q)}\gamma_5).$$

The result of the squared amplitude comes from a long and tedious computation and the result can be found in (B.2) of appendix (B). In the computation of the cross section we isolated all the terms in the squared amplitude, integrated them one by one and then summed them, all this with *Mathematica*. The result can be written as

$$\sigma_{q\bar{q}\to Z\phi}(s) = \left(\frac{c_t m_t g_W}{f_a}\right)^2 \frac{F_5(s)}{4\pi M_Z^2 L^2 s^4 (L^2 - 1)(M_Z^2 - S)^2}, \tag{3.61}$$

where

$$L(s) = \sqrt{1 - \frac{4m_q^2}{s}}.$$

We also calculated, using the crossing symmetry the squared amplitude and the cross section of the scattering process

$$tZ \to t\phi,$$

however, being also a long and mechanical calculation, we leave the cross section for this process with the couplings dependence and a the function $F_6(s)$, that we are not reporting for the sake of simplicity. We can finally summarize the cross sections for the processes with the EW gauge bosons, where thermalization can occur around the EW scale:

$$\sigma_{t\bar{b}\to W^+\phi}(s) = \left(\frac{c_t m_t g_W}{f_a}\right)^2 \frac{(M_W^2 - s)F_3(s)}{512\pi L^2(s) M_W^2 s^3} \tag{3.62}$$

,

$$\sigma_{tW^+\to\bar{b}\phi}(s) = \left(\frac{c_t m_t g_W}{f_a}\right)^2 \frac{F_4(s)}{1024\pi L^2(s) M_W^2 s^3}, \tag{3.63}$$

$$\sigma_{t\bar{t}\to Z\phi}(s) = \left(\frac{c_t m_t g_W}{f_a}\right)^2 \frac{F_5(s)}{4\pi M_Z^2 L^2 s^4 (L^2 - 1)(M_Z^2 - S)^2}, \tag{3.64}$$

$$\sigma_{b\bar{b}\to Z\phi}(s) = \left(\frac{c_b m_b g_W}{f_a}\right)^2 \frac{F_5(s)}{4\pi M_Z^2 L^2 s^4 (L^2 - 1)(M_Z^2 - S)^2}, \tag{3.65}$$

$$\sigma_{tZ\to t\phi}(s) = \left(\frac{c_t m_t g_W}{f_a}\right)^2 F_6(s), \tag{3.66}$$

$$\sigma_{bZ\to b\phi}(s) = \left(\frac{c_b m_b g_W}{f_a}\right)^2 F_6(s), \tag{3.67}$$

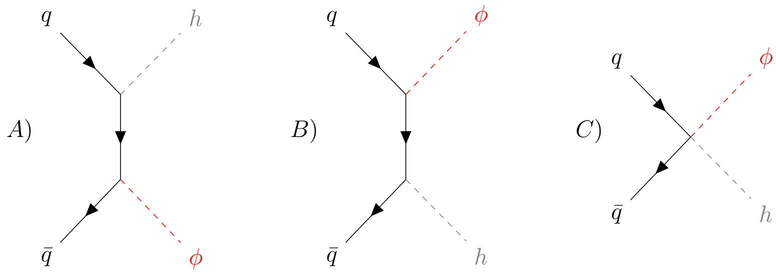

Figure 3.6: Feynman diagrams of the annihilation process involving the Higgs boson particle.

3.3.4 Higgs boson

Involving the Higgs particle we are looking at the two processes

$$t\bar{t} \to h\phi, \qquad t(\bar{t})h \to t(\bar{t})\phi,$$

and we start by computing the cross section for the annihilation process. The matrix elements reads

$$\mathcal{M}_{t\bar{t}\to h\phi} = \mathcal{M}_A + \mathcal{M}_B + \mathcal{M}_C,$$

where

$$\mathcal{M}_A = \frac{ic_t m_t^2}{v_{EW} f_a} \bar{v}(p_2)\gamma_5 \frac{\not{p}_1 - \not{p}_3 + m_t}{t - m_t^2} u(p_1), \tag{3.68}$$

$$\mathcal{M}_B = \frac{ic_t m_t^2}{v_{EW} f_a} \bar{v}(p_2) \frac{\not{p}_1 - \not{k} + m_t}{u - m_u^2} \gamma_5 u(p_1), \tag{3.69}$$

$$\mathcal{M}_C = \frac{ic_t y_t}{\sqrt{2} f_a} \bar{v}(p_2)\gamma_5 u(p_1) \tag{3.70}$$

However we have to take into account the fact the fact that around $T \simeq T_{EW} \simeq 250$ GeV, the Higgs mechanism provides the Electroweak phase transition, meaning that for higher temperatures all the fermions and bosons of the SM are massless. If we look at the couplings where the axion is present, above the EWPT only the C diagram is present, because it involves the y_t coupling constant, and not directly the top quark mass. We also have to specify that above the phase transition the Higgs scalar particle h has to be replaced by the $SU(2)_L$ invariant Higgs field H, that contains 4 degrees of freedom (it is a complex doublet). The latter case, as we discussed previously, has already been discussed in [30], while the case below the EWPT, with the physical and massive scalar h is the focus of our work. The trace calculation in the for the annihilation matrix element gives

$$|\mathcal{M}_{t\bar{t}\to h\phi}|^2 = \left(\frac{c_t m_t y_t}{f_a}\right)^2 \frac{(8m_t^4 - 4m_t^2 m_h^2 - 2m^2 s + m_h^4 - m_h^2 s + s^2)}{(m_t^2 - t)\,(m_t^2 - u)}, \tag{3.71}$$

where¶

$$y_t = \frac{m\sqrt{2}}{v_{EW}}, \qquad u = 2m_t^2 + M_Z^2 - t - s,$$

¶We used the numerical values $m_h = 125$ GeV, and $v_{EW} = 246$ GeV.

based on the relations of Mandelstam variables. The integration of the cross section now follows the same steps we did before, and in the case of annihilation it reads

$$\sigma_{t\bar{t}\to h\phi}(s) = \frac{c_t^2 m_t^2 y_t^2 F_7(s)}{16\pi f_a^2 L(s)^2 s^3}, \tag{3.72}$$

where

$$L(s) = \sqrt{1 - \frac{4m_t^2}{s}},$$

and the function $F_7(s)$ can be found in appendix B.

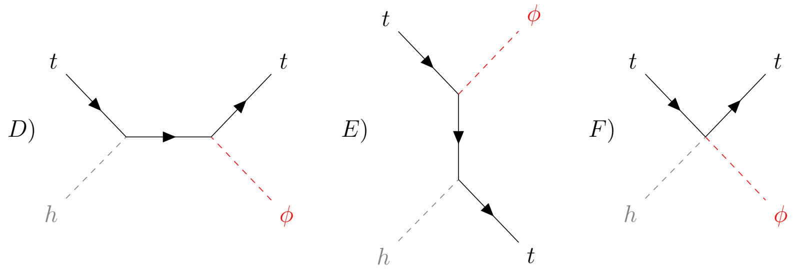

Figure 3.7: Feynman diagrams of the scattering process involving the Higgs boson particle.

For the more interesting case of the scattering $th \to t\phi$, depicted in figure 3.7, we write the matrix elements

$$\mathcal{M}_{th\to t\phi} = \mathcal{M}_D + \mathcal{M}_E + \mathcal{M}_F,$$

where

$$\mathcal{M}_D = \frac{ic_t m_t^2}{v_{EW} f_a}\bar{u}(p_3)\gamma_5 \frac{\not{p}_1 - \not{p}_2 + m_t}{s - m_t^2} u(p_1), \tag{3.73}$$

$$\mathcal{M}_E \frac{ic_t m_t^2}{v_{EW} f_a}\bar{u}(p_3) \frac{\not{p}_1 - \not{k} + m_t}{u - m_u^2}\gamma_5 u(p_1), \tag{3.74}$$

$$\mathcal{M}_F = \frac{ic_t y_t}{\sqrt{2} f_a}\bar{u}(p_3)\gamma_5 u(p_1), \tag{3.75}$$

that leads to

$$|\mathcal{M}_{th\to t\phi}|^2 = \left(\frac{c_t m_t y_t}{f_a}\right)^2 \frac{(8m_t^4 - 4m_t^2 m_h^2 - 2m^2 t + m_h^4 - m_h^2 t + t^2)}{(m_t^2 - t)\,(m_t^2 - u)}, \tag{3.76}$$

also achievable with the crossing symmetry. In the cross section the factor $L(s)$ changes into

$$L(s) = \sqrt{1 - \frac{m_t^2 + m_h^2}{s} + \frac{(m_t^2 - m_h^2)^2}{s^2}},$$

leading to the result

$$\sigma_{th\to t\phi}(s) = \frac{c_t^2 m_t^2 y_t^2 F_8(s)}{64\pi f_a^2 L(s)^2 (m_t^2 - s) s^3}, \tag{3.77}$$

As before, the expression of $F_8(s)$ can be found in appendix B. In addition the results can be generalised to the bottom quark case, with the replacements $c_t \to c_b$ and $m_t \to m_b$.

3.3.5 Hierarchy of the processes

Within the SM, we considered all the possible axion thermal production processes, using the axion coupling with fermions

$$\mathcal{L}_{\phi\bar{\psi}\psi} = \frac{ic_\psi m_\psi}{f_a}\phi\bar{\psi}\gamma_5\psi, \tag{3.78}$$

meaning that all the cross sections, as we have seen in the calculations, are proportional to m_ψ^2/f_a^2. It is clear now, being y_t the biggest by orders of magnitude, that the highest production rate based on these assumptions is the one involving the top quark, and this is why we decided to consider heavy quarks in the first place. Nevertheless, concerning the CMB signatures, we obtained the relation[‖] (2.28)

$$\Delta N_{\text{eff}} \simeq \frac{4}{7}\left(\frac{43}{4g_{*s}}\right)^{4/3}[1-e^{-\Gamma/H}]^{4/3}, \tag{3.79}$$

and this means that if axions reach thermal equilibrium ($\Gamma/H > 1$) then the value ΔN_{eff} only depends on the value of g_{*s} evaluated at the decoupling temperature. Consequently, for production processes involving lighter fermions, like the bottom quark or the heaviest lepton τ, we could obtain larger contributions on N_{eff} that we could observe. Still, the best way to thermalize axions is using the top-axion coupling (operator (3.78) with $\psi = t$) and exploiting a SM coupling in the matrix element: now the hierarchy of the cross sections relies on the strength of the coupling we are using in the non-axionic vertex. Based on this argument the cross sections can be generically written as

$$\sigma \simeq \frac{m_t^2\alpha_X}{f_a^2}, \qquad \alpha_X = \frac{g_X^2}{4\pi}, \tag{3.80}$$

including $\alpha_t = y_t^2/(4\pi)$. The numerical values can be roughly written as

$$\alpha_s \simeq 10^{-1}, \quad \alpha_W \simeq 10^{-2}, \quad \alpha_t \simeq 10^{-1},$$

neglecting α_{em}, that is smaller than the weak coupling. Our best choice would be gluons and the strong coupling α_s, the latter being the biggest, followed by the top Yukawa coupling in the Higgs process. The weak coupling and the electromagnetic coupling are expected to give smaller cross sections, even tough in the case of α_{em} we could obtain large values of ΔN_{eff}, for relatively small ($f_a \lesssim 10^7$ GeV) axion decay constants, due to the difficulty in reaching thermalization. Considering the scattering processes[**] of the top-axion coupling we write the expected hierarchy for the rates and therefore in the thermalization:

$$\begin{array}{lll} 1) & tg \to t\phi, & \sigma \sim \alpha_s m_t^2 \\ 2) & th \to t\phi, & \sigma \sim y_y^2 m_t^2 \\ 3) & tZ \to t\phi, & \sigma \sim \alpha_W m_t^2. \end{array}$$

The first process is also dominant due to the colour factor, basically because we have 8 different types of gluons. We expect that is order will also be respected in the CMB signatures (see section 4.3), as the first process should cover detectable regions for higher values of f_a. At lower temperature, processes with lighter fermions will be dominant, but the coupling will at the same time be proportional to a smaller mass.

[‖] Γ is thermally averaged production rate, see section 4.1 for the details.

[**] Due to the thermal average in section 4.1 the scattering rate is dominant with respect to the annihilation rate.

3.4 New heavy quarks

Up to now we considered processes with SM particles, but we also want to extend our work by considering new degrees of freedom within theories beyond the SM. In the first chapter we discussed the invisible axion models (1.4), and we used the PQ charges c_ψ in our calculation, accordingly with the DFSZ model. Hence in the latter, as we already discussed, there was no need of introducing new particles, as the charges of the new axial symmetry are carried by the SM fermions. In the KSVZ model the PQ charges are carried by new heavy quarks,[††] that can be integrated out at the EW energy scale. As a lower bound we take

$$m_{Q^\star} > 1\ \text{TeV},$$

and we consider the processes, depicted in figure 3.8,

$$Q^\star \bar{Q}^\star \to g\phi, \qquad Q^\star g \to Q^\star \phi,$$

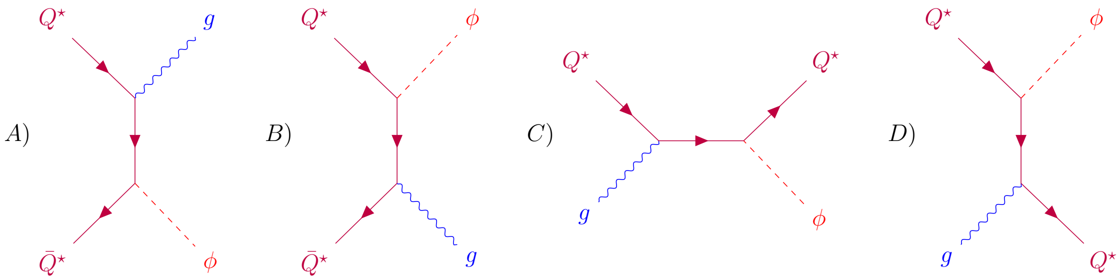

Figure 3.8: Feynman diagrams of the scattering and annihilation processes with heavy quarks.

The matrix elements read

$$\mathcal{M}_{Q^\star \bar{Q}^\star \to g\phi} = \mathcal{M}_A + \mathcal{M}_B, \tag{3.81}$$

$$\mathcal{M}_{Q^\star g \to Q^\star \phi} = \mathcal{M}_C + \mathcal{M}_D, \tag{3.82}$$

where

$$\mathcal{M}_A = \frac{i c_{Q^\star} m_{Q^\star} g_s}{f_a} \epsilon^*_\mu(p_3, \lambda) \bar{v}(p_2) \gamma_5 \frac{\not{p}_1 - \not{p}_3 + m_{Q^\star}}{t - m^2_{Q^\star}} \gamma^\mu u(p_1) t^a_{ij}, \tag{3.83}$$

$$\mathcal{M}_B = \frac{i c_{Q^\star} m_{Q^\star} g_s}{f_a} \epsilon^*_\mu(p_3, \lambda) \bar{v}(p_2) \gamma^\mu \frac{\not{p}_1 - \not{k} + m_{Q^\star}}{u - m^2_{Q^\star}} \gamma_5 u(p_1) t^a_{ij}, \tag{3.84}$$

$$\mathcal{M}_C = \frac{i c_{Q^\star} m_{Q^\star} g_s}{f_a} \epsilon_\mu(p_2, \lambda) \bar{u}(p_3) \gamma_5 \frac{\not{p}_1 - \not{p}_2 + m_{Q^\star}}{s - m^2_{Q^\star}} \gamma^\mu u(p_1) t^a_{ij}, \tag{3.85}$$

$$\mathcal{M}_D = \frac{i c_{Q^\star} m_{Q^\star} g_s}{f_a} \epsilon_\mu(p_2, \lambda) \bar{u}(p_3) \gamma^\mu \frac{\not{p}_1 - \not{k} + m_{Q^\star}}{u - m^2_{Q^\star}} \gamma_5 u(p_1) t^a_{ij}. \tag{3.86}$$

We are assuming that the new heavy quarks couple to the QCD sector like SM quarks, therefore in the $\bar{Q}^\star Q^\star g$ vertex we have to consider the strong coupling

[††]We call them quarks because are charged under the $SU(3)_C$ gauge group, therefore they have colour.

constant g_s. The trace computation is now very easy, as we can treat the new quarks as SM quarks, and the squared amplitude is exactly the same (including the color factor) as the one we previously calculated, with the replacement $m_q \to m_{Q^\star}$. Therefore the result on the cross sections for both the annihilation and scattering are, respectively

$$\sigma_{Q^\star \bar{Q}^\star \to g\phi}(s) = \left(\frac{c_{Q^\star} m_{Q^\star} g_s}{f_a}\right)^2 |t^a_{ij}|^2 \frac{\tanh^{-1}\left(\sqrt{1-\frac{4m^2_{Q^\star}}{s}}\right)}{4\pi(s-4m^2_{Q^\star})}, \tag{3.87}$$

$$\sigma_{Q^\star g \to Q^\star \phi}(s) = \left(\frac{c_{Q^\star} m_{Q^\star} g_s}{f_a}\right)^2 |t^a_{ij}|^2 \frac{2s^2\log(s/m^2_{Q^\star}) - 3s^2 + 4m^2_{Q^\star}s - m^4_{Q^\star}}{32\pi s^2(s-m^2_{Q^\star})}. \tag{3.88}$$

Based on the cross sections we are expecting a very high production rate

$$\Gamma \sim \frac{m^2_{Q^\star}\alpha_s}{f_a^2} T,$$

but also a high decoupling temperature. Thus we are not going to obtain values $\Delta N_{\text{eff}} > 0.027$, but the latter could be achieved for high values of f_a.

Chapter 4

Numerical results

In the following chapter we are going to present the numerical computations based on the cross sections we calculated. We finally want to describe for which range of values of f_a, or more precisely of f_a/c_ψ, the value ΔN_{eff} can be measured by the next CMB surveys. We will first discuss the production rate Γ, defined in (2.5), that will be our model dependent input for the solution of the Boltzmann equation, later depicted for every process. The final graphs will show the values of ΔN_{eff} in the parametric axis of the axion decay constant, again for each process studied.

4.1 Production rates

In this section we will present the ratio Γ/H for different values of the temperature and for every process considered, but before presenting our graphical results we discuss how we thermally averaged the cross sections for the computation of the rate Γ.

Thermally averaged rates

Now that we have the expressions for the cross sections we can calculate the annihilation and scattering rates $\Gamma_i = n_i \langle \sigma v \rangle$, defined also as [26]

$$\Gamma_i = \frac{1}{n_\phi^{eq}} \int \frac{d^3 p_a}{(2\pi)^3 2E_a} \frac{d^3 p_b}{(2\pi)^3 2E_b} f_a(E_a) f_b(E_b)(4\sigma_i E_a E_b), \tag{4.1}$$

where a, b label the incoming states. However within the Boltzmann approximations, that is $f_a = \exp(-E_a/T)$, we can write a general Lorentz invariant expression for the thermal average [27]

$$\langle \sigma_{x_1 x_2 \to x_3 \phi} v \rangle = \frac{\int_{s^*}^{\infty} ds \lambda(s, m_{x_1}, m_{x_2}) s^{-1/2} \sigma_{x_1 x_2 \to x_3 \phi}(s) K_1(\sqrt{s}/T)}{8 K_2(m_{x_1}/T) K_2(m_{x_2}/T) m_{x_1}^2 m_{x_2}^2 T}, \tag{4.2}$$

where

$$\lambda(x, y, z) = [x - (y + z)^2][x - (y - z)^2], \tag{4.3}$$

$$s^* = (m_{x_1} + m_{x_2})^2, \tag{4.4}$$

the lower integration extremum is present for obvious kinematic reasons. In addition for the cases where we have a massless particle in the initial state, like in the scattering with gluons and photons, (4.2) can be written (setting $m_{x_2} = 0$) as

$$\langle \sigma_{x_1 x_2 \to x_3 \phi} v \rangle = \frac{\int_{m_{x_1}^2}^{\infty} ds \lambda(s, m_{x_1}, 0) s^{-1/2} \sigma_{x_1 x_2 \to x_3 \phi}(s) K_1(\sqrt{s}/T)}{16 K_2(m_{x_1}/T) m_{x_1}^2 T^3}. \tag{4.5}$$

In the expression of the rate we have then to multiply by the equilibrium densities

$$\Gamma = \frac{n_1^{eq} n_2^{eq}}{n_\phi^{eq}} \langle \sigma v \rangle , \tag{4.6}$$

where in the last relation we have to consider the internal degrees of freedom g of the particles and the statistics of fermions. The expression of n_ϕ^{eq} is always the one we found in (2.4), since the axion is massless at the temperatures we consider, while the expression of n_1^{eq} and n_2^{eq} changes. In general for massive particles we can write its full expression

$$n_f^{eq} = \frac{3g}{4} \frac{m^2 T K_2[m/T]}{2\pi^2}, \tag{4.7}$$

where g are internal degrees of freedom and the factor $3/4$ comes from the statistics of fermions. As it can be seen from figure 4.1, the expression we wrote perfectly match the solutions in the classical and relativistic limits, in their respective ranges of validity:

$$n_{f,T\gg 1}^{eq} = \frac{\zeta(3) T^3}{\pi^2}, \qquad n_{f,T\ll 1}^{eq} = \left(\frac{mT}{2\pi}\right)^{3/2} e^{-m/T}. \tag{4.8}$$

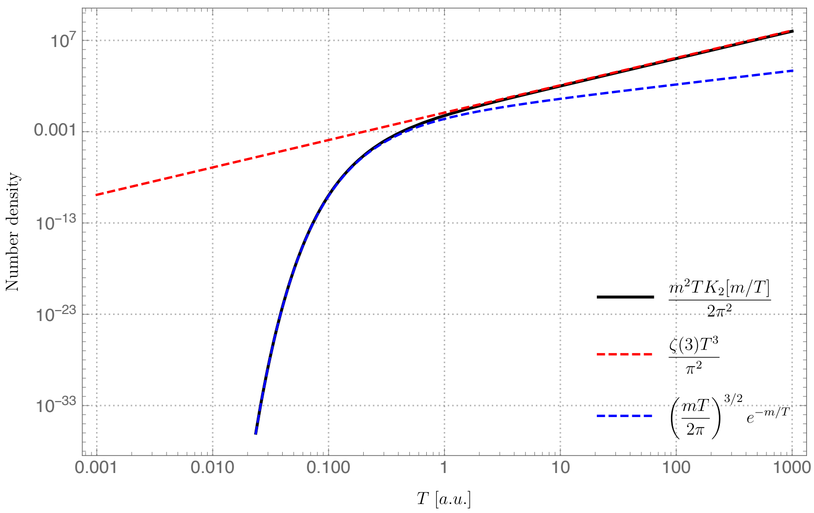

Figure 4.1

It is useful to compare the rate Γ with the Hubble parameter H in order to quantify for which valus of the axion decay constant f_a the processes reach thermalization and the axions achieve thermal equilibrium in the primordial plasma. The ratios Γ/H * are plotted for different parametric values of f_a.

*In the expression of H we used the numerical values $g_* = 106.75$ and $M_{pl} = 2.4 \times 10^{18}$ GeV.

Massless bosons

Here we present the results for the processes involving massless bosons: gluons and photons, both for the quarks and the leptons.

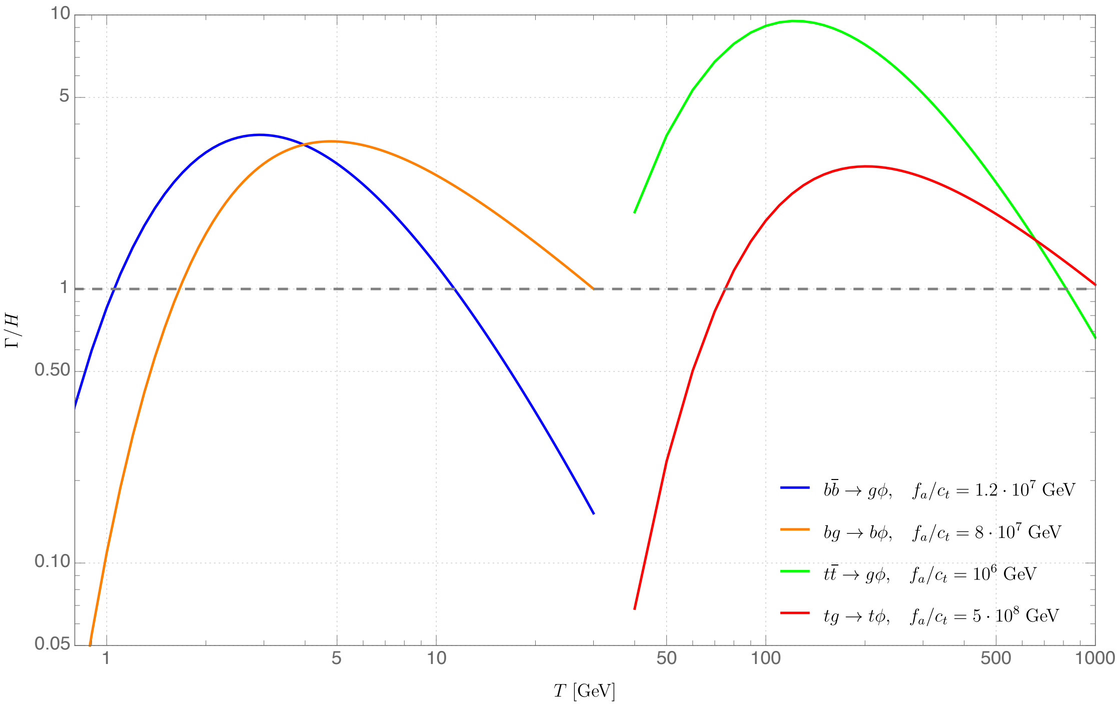

Figure 4.2: Log-Log graph for the comparison of both the scattering and annihilation for the bottom and top processes with gluons.

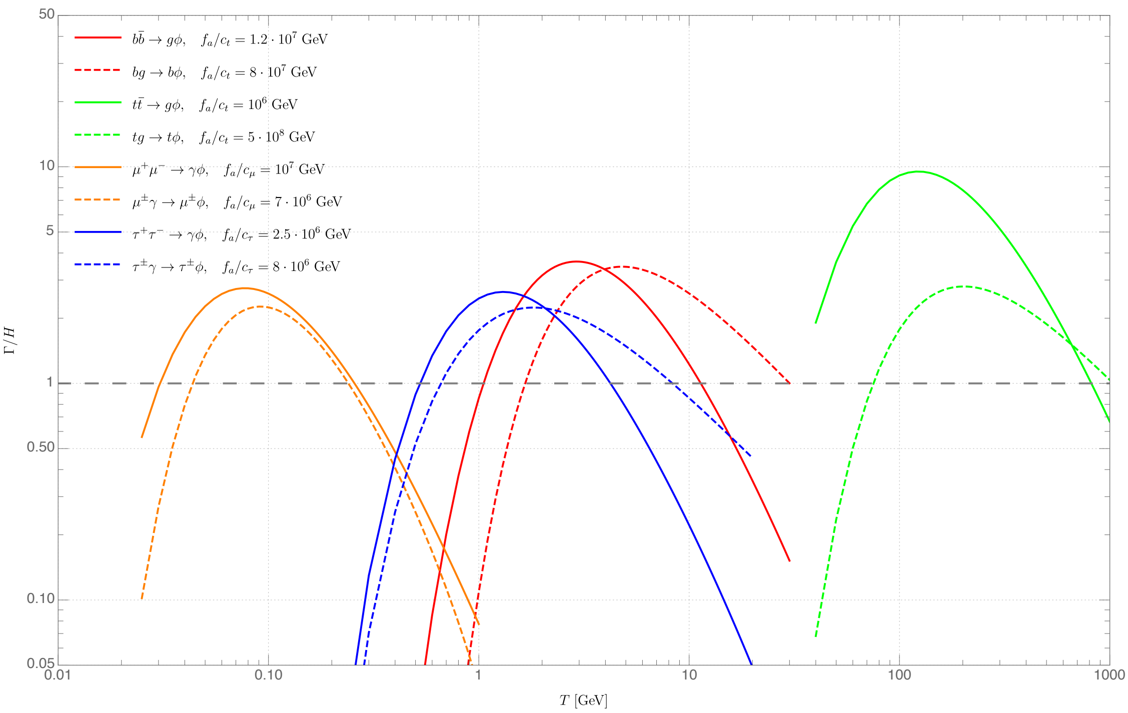

Figure 4.3: Log-Log graph for the comparison of both the scattering and annihilation for the bottom and top processes with gluons and the μ and τ processes with photons.

EW bosons

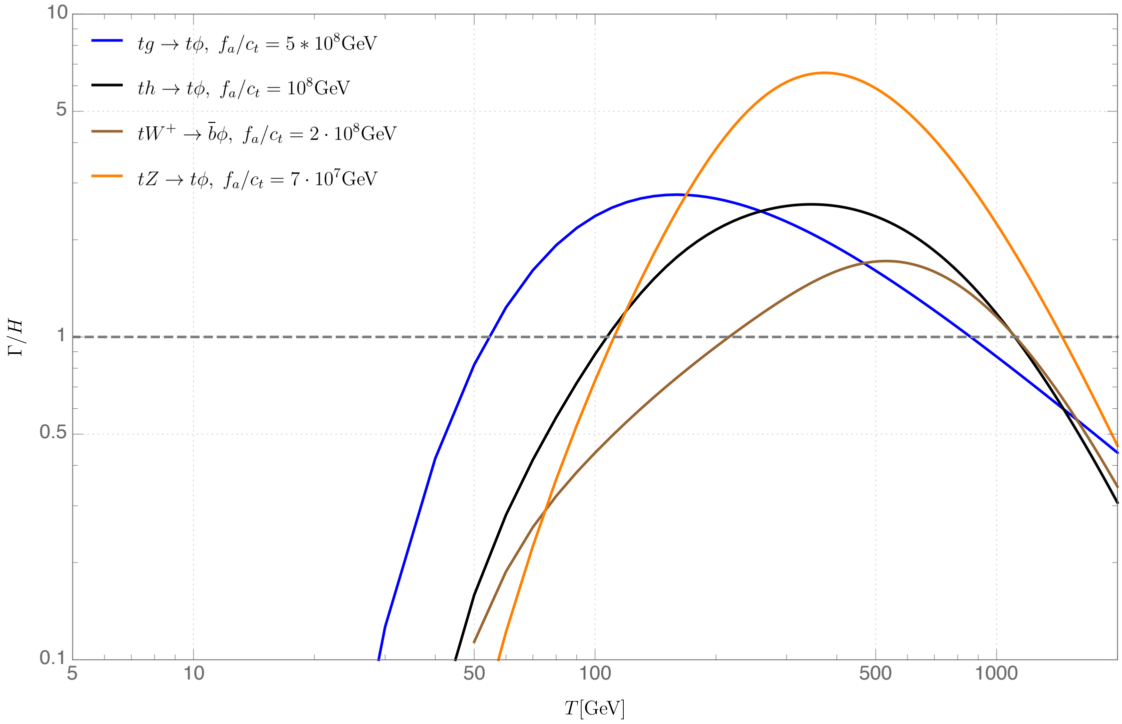

Figure 4.4: Log-Log graph of the *scattering* processes at the EW scale involving the Z, W^+ and h bosons. In addition we also plotted the process with gluons in order to compare them.

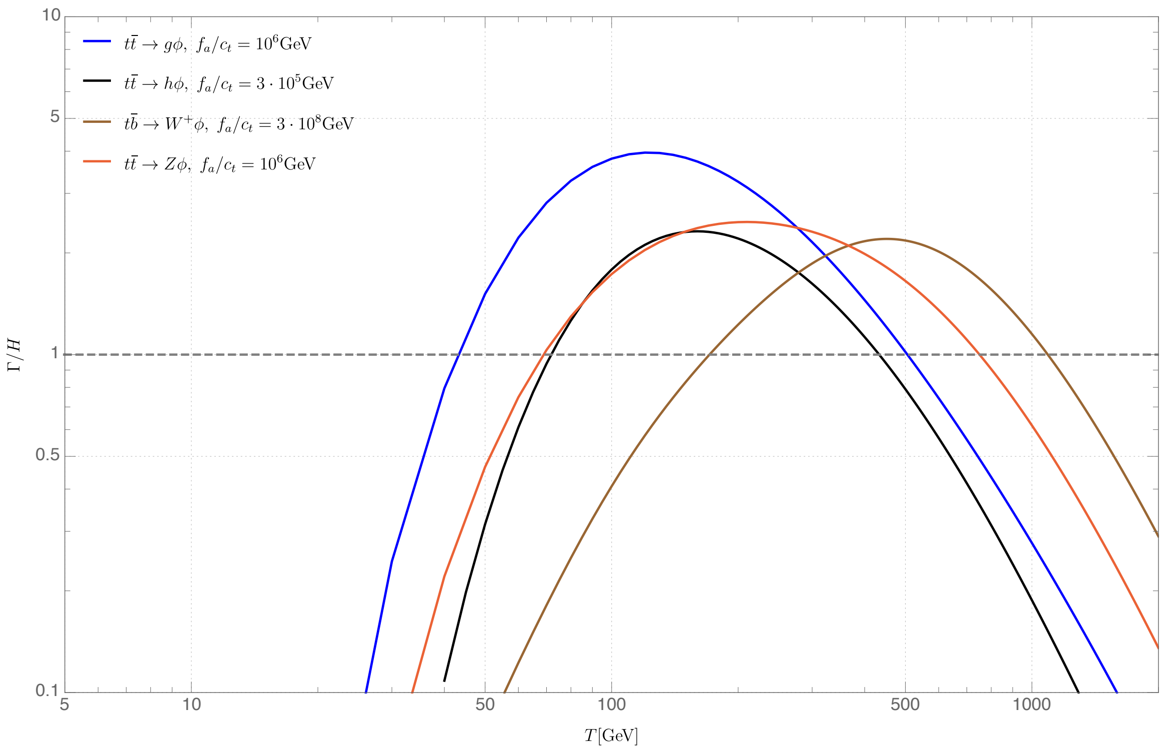

Figure 4.5: Log-Log graph of the *annihilation* processes at the EW scale involving the Z, W^+ and h bosons. In addition we also plotted the process with gluons in order to compare them.

KSVZ model

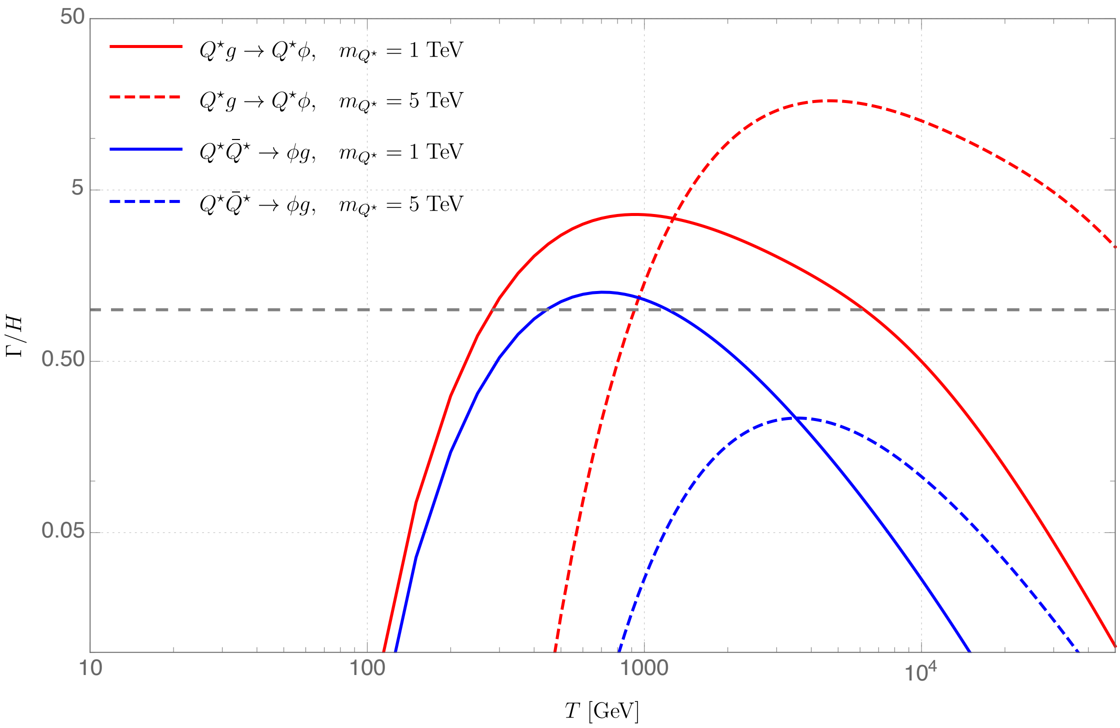

Figure 4.6: Scattering (red) and annihilation (blue) production rates with heavy quarks in the KSVZ model. We here plotted for the values $m_{Q^{\star}} = 1$ TeV and $m_{Q^{\star}} = 5$ TeV. The scattering curves are evaluated at $f_a/c_{Q^{\star}} = 2 \cdot 10^9$ GeV, while the annihilation at $f_a/c_{Q^{\star}} = 10^6$ GeV.

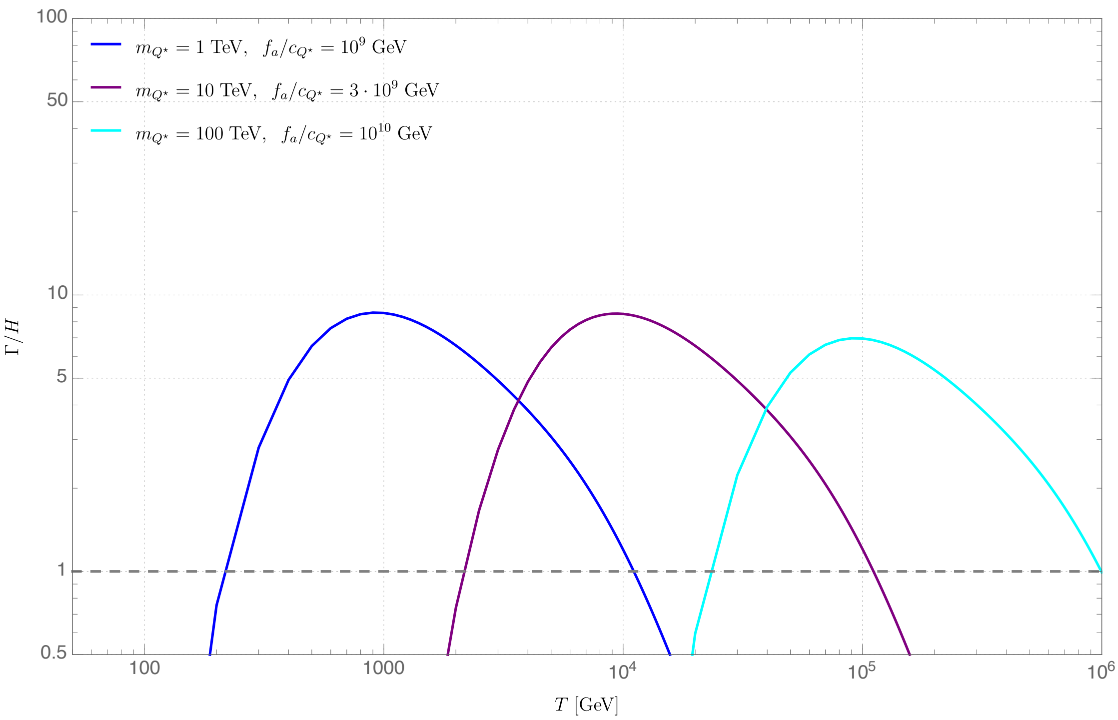

Figure 4.7: Scattering rates with new heavy quarks, for different values of the quark mass.

4.2 Axion thermal abundance

Once we numerally we computed the rates Γ_i we can determine the axion abundance that every process will produce in the scatterings and annihilations. We need to solve Boltzmann equation 2.12

$$sHx\frac{dY_\phi}{dx} = \left(1 - \frac{1}{3}\frac{d\ln g_{*s}}{d\ln x}\right)\gamma_a\left(1 - \frac{Y_\phi}{Y_\phi^{eq}}\right), \tag{4.9}$$

but the latter can be also written as

$$x\frac{dY_\phi}{dx} = \frac{0.277}{g_{*s}}\frac{\Gamma}{H}\left(1 - \frac{1}{3}\frac{x}{g_{*s}}\frac{dg_{*s}}{dx}\right)\left(1 - \frac{g_{*s}Y_\phi}{0.277}\right), \tag{4.10}$$

as we recalled the relation $Y_\phi^{eq} = n_\phi^{eq}/s \equiv 0.277/g_{*s}$. Now we can numerically solve the differential equations using the software *Mathematica*, by putting as input the Γ/H ratio of the process computed and providing the function g_{*s} that has a non-trivial dependence on the temperature. The curve in the following plots will refer to the use of g_{*s} taken from two different works, and the bands between the curves can be used as an uncertainty in the number of relativistic degrees of freedom. The upper line, labelled $g_*^{(1)}$ is taken from [45], while the lower $g_*^{(2)}$ from [46]. When not specified it is implied $g_*^{(1)}$. For the sake of brevity we leave all the plots of the abundances for every process studied and we leave the leading top-gluon processes as a numerical example, in figure 4.8.

4.2.1 Top-Axion

Up to now we considered single processes of axion production, in order to understand for what values of f_a the axion can reach thermal equilibrium. It is important therefore to combine the results that we found into something that can be related to a real thermal production mechanism. As a matter of fact, if we look at our main lagrangian (3.1), we shouldn't consider single scattering processes, but operators that appear in the lagrangian.

As we already discussed in section 3.3.5 the top-axion coupling is our best shot for thermalization, the operator reads

$$\mathcal{L}_{\bar{t}t\phi} = \frac{ic_t m_t}{f_a}\phi\bar{t}\gamma_5 t, \tag{4.11}$$

and every process that contains this interaction should be considered in the thermalization and therefore in the Boltzmann equation. In the latter we should therefore put the total axion-top rate $\Gamma_{t\phi}$:

$$x\frac{dY_\phi}{dx} = \frac{\Gamma_{t\phi}}{H}f(Y_\phi, g_{*s}, x), \tag{4.12}$$

$$\Gamma_{t\phi} = \Gamma_{tg\to t\phi} + \Gamma_{th\to t\phi} + \Gamma_{tZ\to t\phi} + \Gamma_{tW^+\to\bar{b}\phi} + \Gamma_{t\bar{b}\to W^+\phi}, \tag{4.13}$$

neglecting the subdominants annihilation processes, due to thermal average in cross sections. In the computation of the axion abundance the rate in (4.13) is taking into account the presence of the additional model dependent (DFSZ) coupling that we considered in our work. In figure 4.9 it is depicted the axion abundance with the total top-axion rate at different values of f_a/c_t. In section 4.4 we also plotted the comparison with the abundances of the leading process $tg \to t\phi$ and the scattering $th \to t\phi$.

4.2.2 Subdominant couplings

In a totally analogous way we recall the bottom-axion coupling that we consider in our lagrangian

$$\mathcal{L}_{\bar{b}b\phi} = \frac{ic_b m_b}{f_a}\phi\bar{b}\gamma_5 b, \tag{4.14}$$

and we solve Boltzmann equation with the total rate

$$\Gamma_{b\phi} = \Gamma_{bg\to t\phi} + \Gamma_{bh\to t\phi} + \Gamma_{bZ\to t\phi}, \tag{4.15}$$

neglecting all the annihilations and the processes with the W bosons, as we have calculated their cross sections in the massless bottom limit. The yield from this coupling is much less effective, due to small ratio m_b^2/m_t^2, and that is why we leave the plots with the bottom quark in appendix C. The other process we are left to consider are the ones with the leptons

$$\mathcal{L}_{\mu\phi} = \frac{ic_\mu m_\mu}{f_a}\phi\bar{\mu}\gamma_5\mu, \qquad \mathcal{L}_{\tau\phi} = \frac{ic_\tau m_\tau}{f_a}\phi\bar{\tau}\gamma_5\tau, \tag{4.16}$$

that are even more suppressed because of the lepton masses and the electromagnetic coupling constant α_{em}.

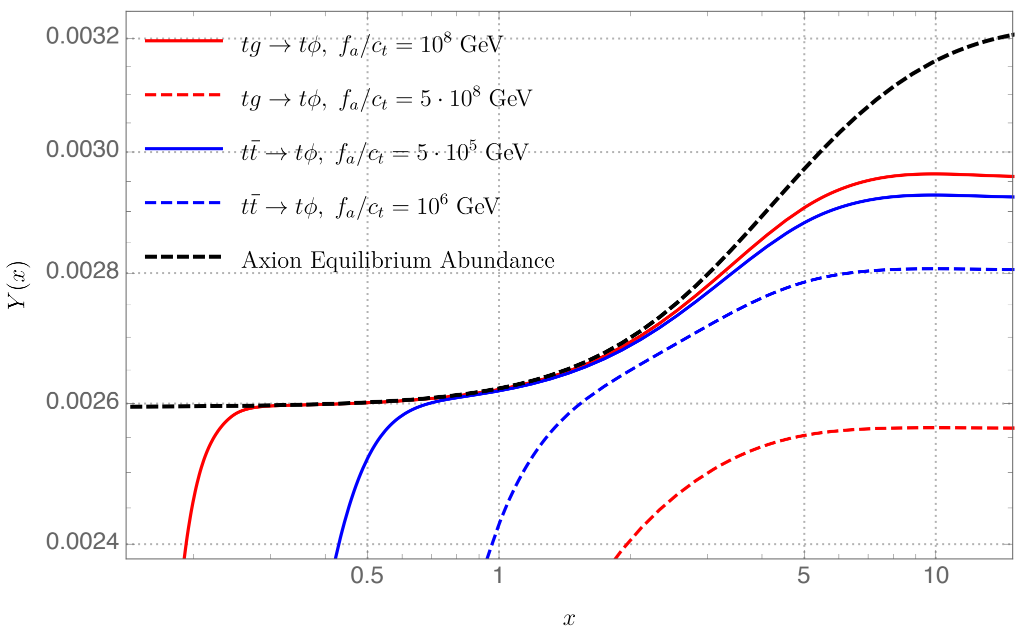

Figure 4.8: Numerical solutions of the scattering (red) and annihilation (blue) processes with top quarks and gluons. The black dotted line represents thermal equilibrium.

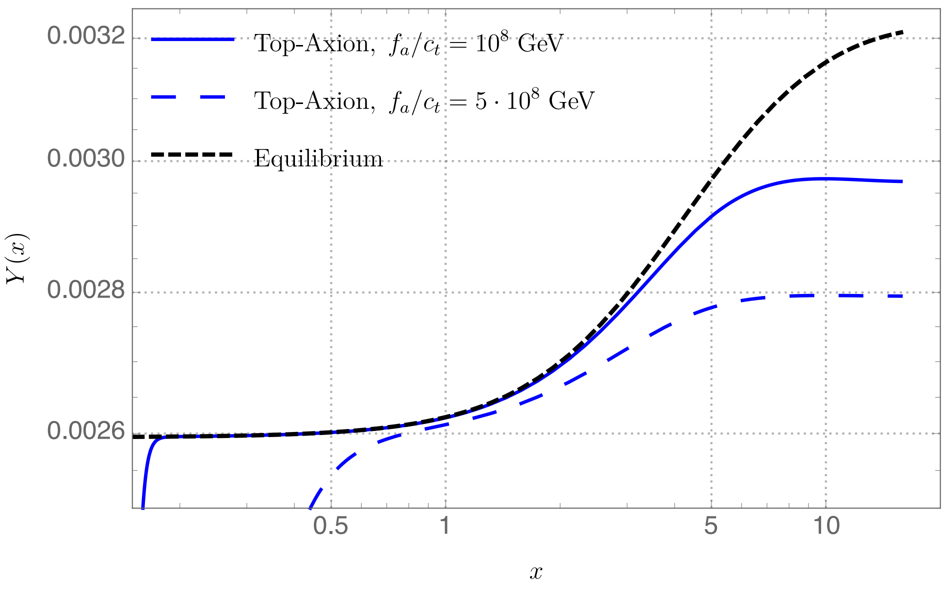

Figure 4.9: Numerical axion abundance using the top-axion coupling and the total rate 4.13. The black dotted line represents thermal equilibrium.

4.2.3 $Q^\star$-Axion

In the KSVZ model we have the additional coupling

$$\mathcal{L}_{\bar{Q}^\star Q^\star \phi} = \frac{i c_{Q^\star} m_{Q^\star}}{f_a} \phi \bar{Q}^\star \gamma_5 Q^\star, \tag{4.17}$$

and we have the annihilation and scattering calculated in section 3.4. Of course, as in the other cases, the scattering is the dominant process, and the abundance obtained with the latter is depicted in figure 4.14 for different values of $f_a/c_{Q^\star}$ or for the value $m_{Q^\star} = 1$ TeV. In this case we can see that thermalization can be reached for values of $f_a/c_{Q^\star} \sim 10^9$ GeV.

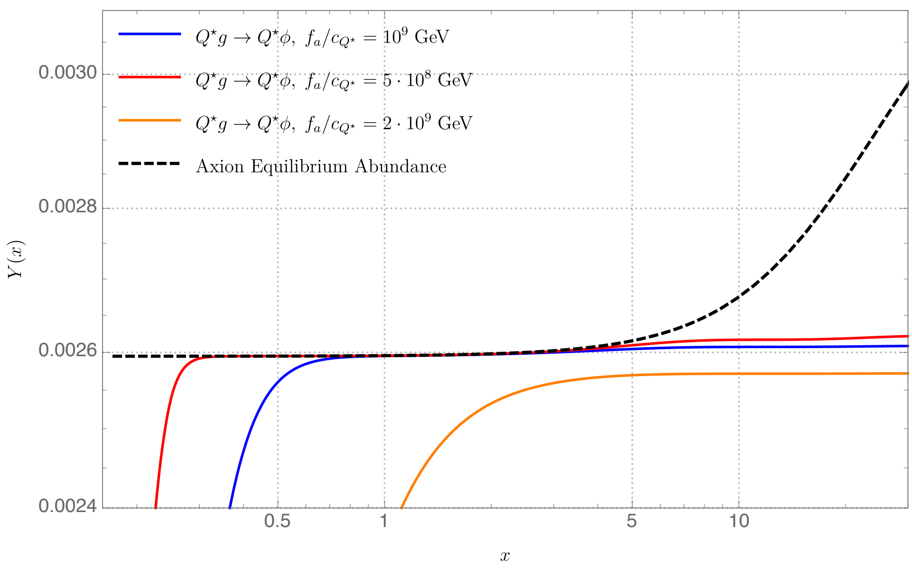

Figure 4.10: Numerical solutions of the scattering (red) and annihilation (blue) processes with top quarks and gluons. The black dotted line represents thermal equilibrium.

4.3 CMB signatures

Once we computed the abundance for every single process and later on for the operators considered in the lagrangian we can calculate the dark radiation contribution, namely the deviation ΔN_{eff} from the predicted $N_{\text{eff}}^{(SM)} = 3.046$ as we discussed in the first chapters. First of all, we want to check the large f_a approximation that we found in (2.29)

$$\Delta N_{\text{eff}} \sim f_a^{-8/3}, \tag{4.18}$$

and it is verified in the plots by comparing the signatures of a single process with a gray dotted line. Nevertheless, as we computed the full numerical Boltzmann equation, we can exploit the relation (2.25)

$$\Delta N_{\text{eff}} \simeq 74.82(Y_\phi)^{4/3}, \tag{4.19}$$

with Y_ϕ the solution of the Boltzmann equation. We therefore plot the dark radiation contribution of thermal axions for different values of f_a/c_i, where i indicate the fermion in the process. Our goal is to infer if there are reasonable values of f_a (i.e. not excluded by experiments and observational data) that can at the same time being possibly detected by the future experiment CMB-S4. The previous experiment Planck 2015 had a sensitivity up to $\Delta N_{\text{eff}} \simeq 0.19$, which is a huge number compared to our expected results. On the other hand, as listed in table 4.1, the new experiment CMB-S4, that is expected to run within a few years, can remarkably reach down to our target sensitivity $\Delta N_{\text{eff}} \sim 0.01$ [17, 44], while for values below this threshold we will refer to futuristic sensitivity of even next generation CMB probes.

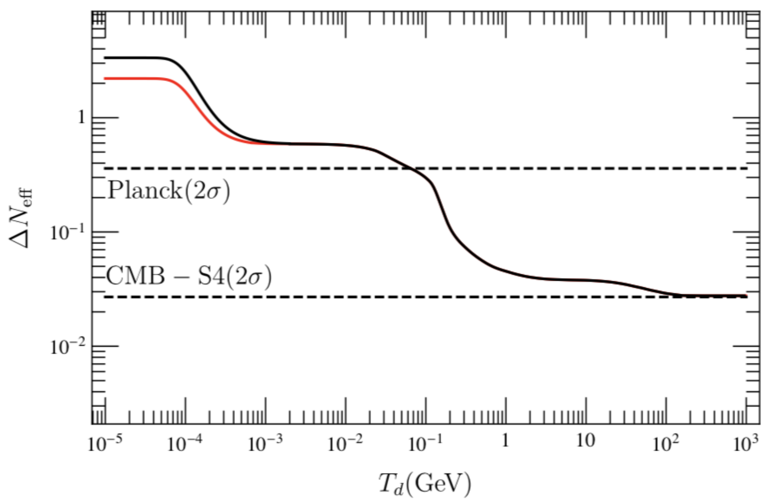

Figure 4.11: Value of ΔN_{eff} versus the decoupling temperature and the sensitivity of CMB probes [17].

Figure 4.11 also shows the sensitivity bands, in the graph where the dark radiation is plotted for different decoupling temperatures, provided that the axion production reaches thermal equilibrium and the contribution only depends on g_{*s}

$$\Delta N_{\text{eff}} \sim g_{*s}^{-4/3}, \qquad \text{for } \Gamma/H \gg 1, \tag{4.20}$$

Experiment	$\sigma(N_{\text{eff}})$
Planck 2015	0.30
	0.19
CMB-S4	0.048
	0.013

Table 4.1: Sensitivity in the CMB experiments [44].

For single processes the decoupling temperature is in direct correspondence with the fermion mass, as the production rates are peaked around it, and therefore for production closer and closer to the EWPT we expect to reach asymptotically the value $\Delta N_{\text{eff}} = 0.027$ predicted above the EW scale, as figure 4.11 shows. As we commented earlier, production with leptons, especially the scattering $\mu^{\pm}\gamma \to \mu^{\pm}\phi$ can produce high deviation in the dark radiation observable N_{eff}, but at the price of a small, i.e. excluded, axion decay constant, based on the Astrophysical bounds (details in section 5.1). This means that we want to focus on processes with top-axion coupling, depicted in figure 4.12.

4.3.1 Single process

In the following graphs we will show the single process plots in the plane $(f_a/c_i - \Delta N_{\text{eff}})$ for the scattering at the EW scale (and therefore with the top-axion coupling) and the KSVZ model. We also plotted in orange the CMB-S4 sensitivity band (up to 1 σ) and in red the futuristic band. The leading $tg \to t\phi$ scattering falls in the CMB-S4 sensitivity for values $f_a/c_t \lesssim 10^9$ GeV, for the W processes the possible values are $f_a/c_t \lesssim 7 \cdot 10^8$ GeV, for the Higgs scattering $f_a/c_t \lesssim 4 \cdot 10^8$ GeV and the Z scattering $f_a/c_t \lesssim 4 \cdot 10^8$ GeV. The other DFSZ single process contributions are plotted in appendix C.

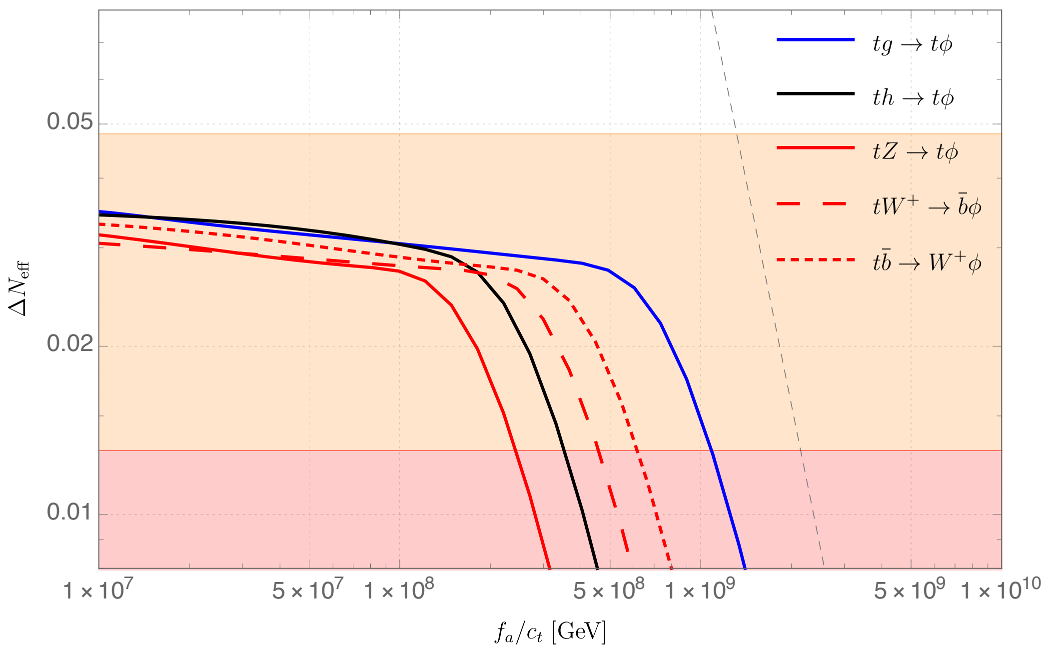

Figure 4.12: Dark radiation signatures from thermal production at different f_a/c_t for the scattering process with the top-axion coupling at the EW scale.

In the KSVZ model the decoupling temperature is just above the EW scale, and all the curves are asymptotically reaching this values for low f_a scales. In figure 4.13 we simulated the contribution for masses $m_{Q^\star} = 1, 5, 10$ and 100 TeV, and the maximum sensitivity of CMB-S4 can be reached for values $f_a/c_t \lesssim 4 \cdot 10^9$ GeV in the first case and $f_a/c_t \lesssim 4 \cdot 10^8$ GeV for the more massive $m_{Q^\star} = 100$ TeV case.

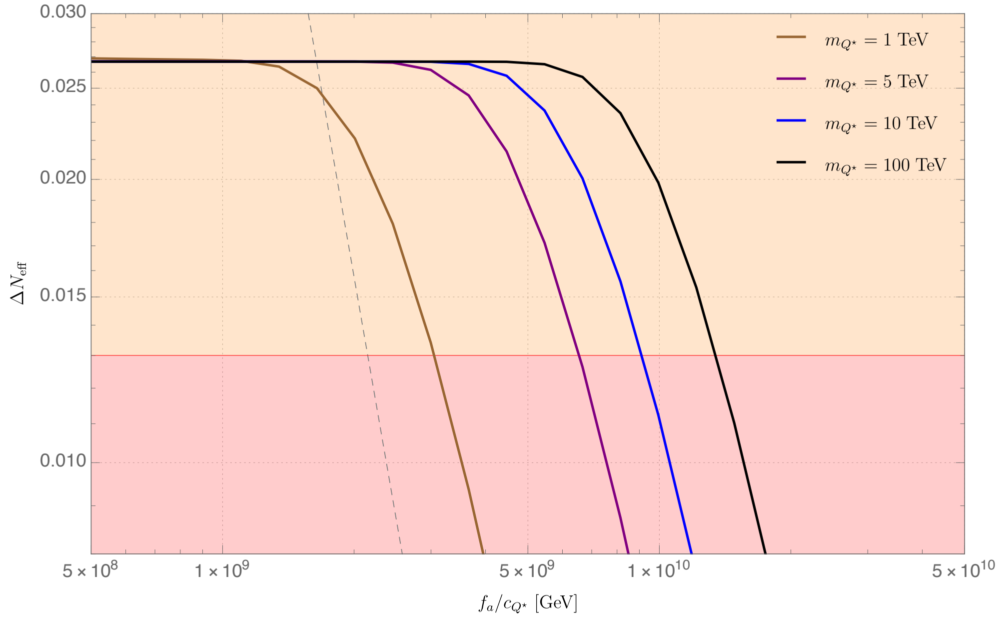

Figure 4.13: Dark radiation signatures from thermal production at different f_a scales and values of $m_{Q^\star}$ for the scattering process in the KSVZ model.

4.4 Final Results

We here present our final results.

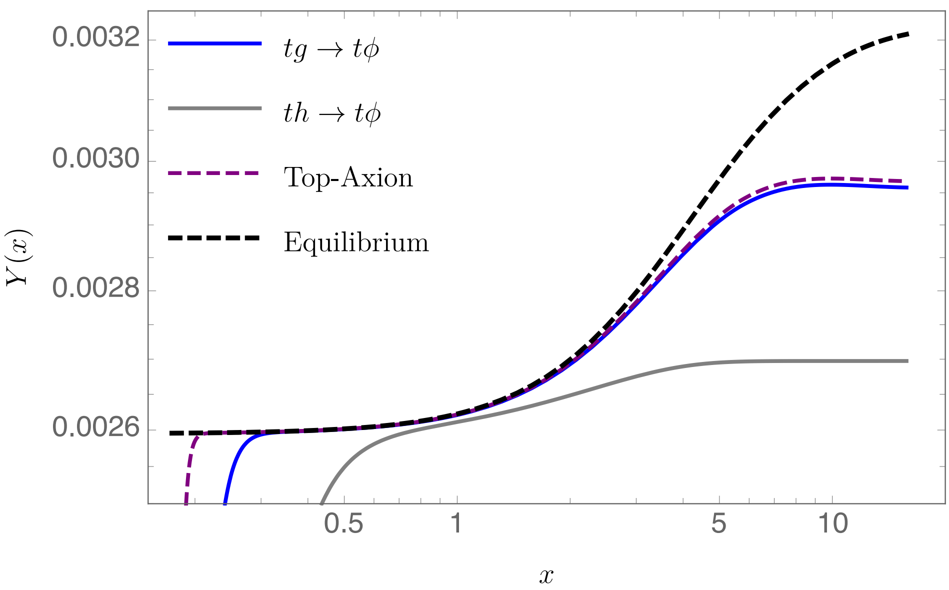

Figure 4.14: Relic comoving abunandance of the top-axion processes combined, in comparison to single processes, for the value $f_a/c_t = 10^8$ GeV.

Figure 4.14 shows the final relic abundance computed for all the processes with the top-axion coupling, compared to the leading scattering $tg \to t\phi$ and the Higgs scattering. The correction due to EW bosons slightly uplifts the abundance Y_ϕ^{tot} (purple dotted line), and this will also change the predicted dark radiation contribution. In figure 4.15 we plot indeed the values of ΔN_{eff} for reasonable values of f_a/c in the case of leading top-axion coupling for the DFSZ model and the hadronic KSVZ for $Q^\star$ masses up to 5 TeV. It is reasonable to assume that new physics would arise at the TeV scale, as we recently started to probe this energy region at the LHC. Our results for the non-hadronic model with the top-axion coupling show a detectable region in the near future in the range

$$f_a/c_t \lesssim 1.5 \times 10^9 \text{ GeV}, \tag{4.21}$$

while for the hadronic model the minimum value of ΔN_{eff} is reached in the region

$$3 \times 10^9 \text{ GeV} \lesssim f_a/c_{Q^\star} \lesssim 1.5 \times 10^{10} \text{ GeV}. \tag{4.22}$$

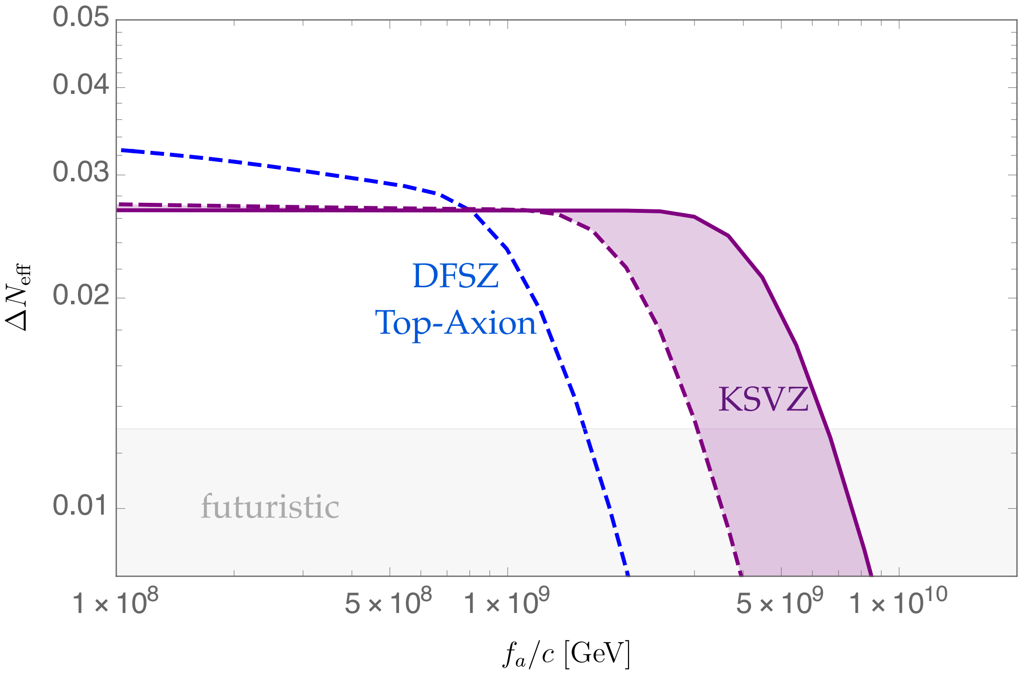

Figure 4.15: Our prediction of dark radiation contribution, for the DFSZ model using the top-axion coupling and the KSVZ model for $Q^\star$ masses up to 5 TeV.

The top-axion coupling for low values $f_a \lesssim 10^8$ GeV gives more promising contributions $\Delta N_{\text{eff}} \sim 0.032$, while in the KSVZ the decoupling temperature is slightly above the EW phase transition, meaning that even for very low values of f_a the maximum contribution is the value obtained in [30] $\Delta N_{\text{eff}} = 0.027$. The presence of the EW bosons in our discussion will open to larger window in the f_a parameter space of possible detectable thermal productions. Nevertheless the variation from the leading scattering with the gluons is expected to be less than 10%, in agreement with our ΔN_{eff} final results.

Extending our work to the bottom-axion coupling and higher $Q^\star$ masses (up to 500 TeV) the range of observable values are

$$f_a/c_b \lesssim 2 \times 10^8 \text{ GeV} \tag{4.23}$$

for the former and

$$f_a/c_{Q^\star} \lesssim 6 \times 10^{10}\ \text{GeV} \tag{4.24}$$

for the latter, as they are both depicted in figure 4.16.

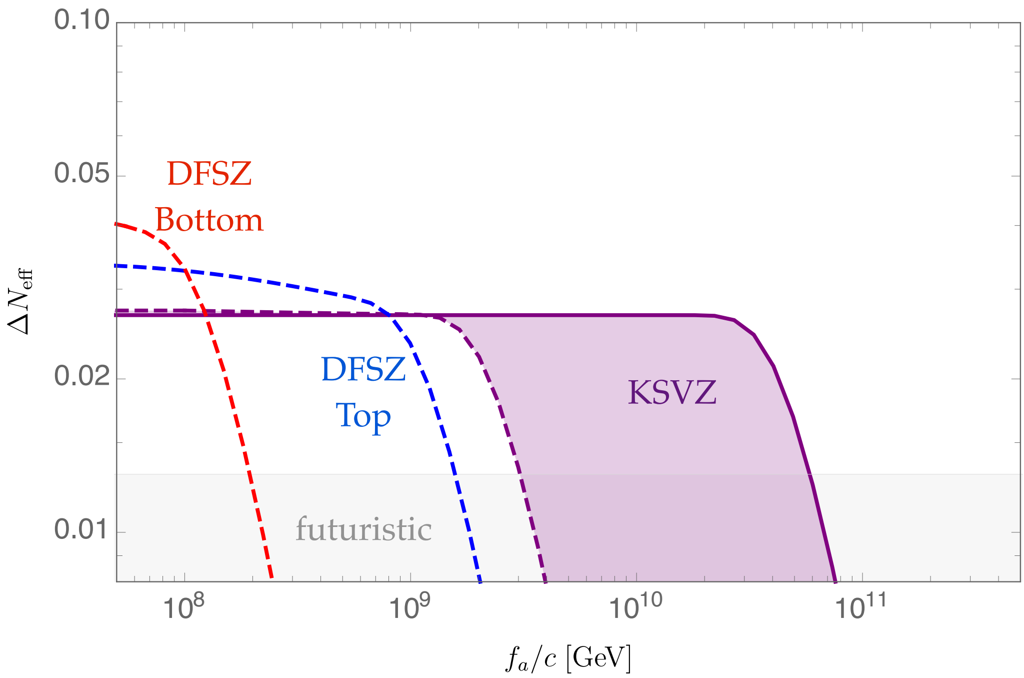

Figure 4.16: Our prediction for the DFSZ the top-axion and bottom-axion couplings and the KSVZ model for $Q^\star$ masses up to 500 TeV.

Chapter 5

Future prospects

In this final chapter we are going to briefly review the observational and experimental point of views in axion physics. We want to establish the current exclusion bands in the parametric space of the axion decay constant and the status of the experiments. We finally want to discuss what are the possible values of f_a that could give rise to detectable populations of both hot and cold axions.

5.1 Astrophysical bounds

Astrophysical bounds refer to what we can learn about low-mass and weakly interacting particles, such as axions, from the observed properties of stars. Indeed, a hot and dense stellar plasma will emit axion particles, that subsequently escape from the stellar interior directly, without further interactions due to weakness of the coupling, providing a local energy sink for the stellar medium. Astronomical observables can therefore set powerful limits on the properties axions, and also other particles. A natural starting point would be considering the best-known star: our Sun, that is powered by nuclear fusion and the burning of hydrogen. The solar energy loss has to take into account the observed ν_e flux, coming from the fusion reactions, but also the possibility of producing new particles, axions in our case. This particular type of production is called Primakoff effect and is based on the axion-photon coupling $g_{\phi\gamma}$: a photon is converted into an axion thanks to the electromagnetic field (virtual photon) of the charged particles in the Sun, see figure 5.1. But if we want to compute the energy-loss rate from stellar plasmas we should specify all the interactions with the medium constituents [38]. For example in the case of the DFSZ model the interaction with a fermion ψ of mass m_ψ is generically

$$\mathscr{L}_{int} = \frac{c_\psi}{2f_a}\partial_\mu\phi\bar{\psi}\gamma^\mu\gamma_5\psi \qquad \text{or} \qquad \mathscr{L}_{int} = \frac{ic_\psi m_\psi}{f_a}\phi\bar{\psi}\gamma_5\psi, \tag{5.1}$$

and c_ψ is model dependent coefficient of order unity (the PQ charge in the DFSZ). We can define the quantity $g_{\phi\psi}$, that will play the role of the Yukawa and therefore a coupling constant, and the "axionic fine structure constant" $\alpha_{\phi\psi}$:

$$g_{\phi\psi} = \frac{c_\psi m_\psi}{f_a}, \qquad \alpha_{\phi\psi} = \frac{g_{\phi\psi}^2}{4\pi}. \tag{5.2}$$

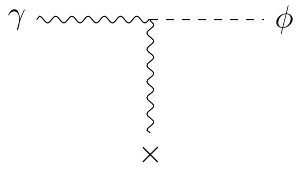

Figure 5.1: Feynman diagram of the Primakoff production, the photon with the $\times$ symbol is virtual and coming from a nucleus.

In the KSVZ model instead, no tree-level couplings to quarks and leptons arise, but axions still couple to couple to nucleons ($c_{\phi p}, c_{\phi n}$) due to their mixing with the neutral pion, as explained in the first chapter. We can therefore divide the observational bounds using the coupling with two photons $g_{\phi\gamma}$, for both DFSZ and KSVZ models and the coupling with electrons $g_{\phi e}$, only for DFSZ.

5.1.1 Photons

The lagrangian of the interaction between photons and axions can be written as

$$\mathcal{L}_{int} = \frac{1}{4} g_{\phi\gamma} \phi \tilde{F}_{\mu\nu} F^{\mu\nu} = -g_{\phi\gamma} \phi \mathbf{E} \cdot \mathbf{B}, \tag{5.3}$$

where we recall

$$g_{\phi\gamma} = \frac{\alpha}{2\pi f_a} c_{\phi\gamma} = \frac{\alpha}{2\pi f_a} \left(\frac{E}{N} - 1.92 \right), \tag{5.4}$$

and we explicitly write it in table 5.1* for our models.

Model	N_{DW}	E/N	$c_{\phi\gamma}$
DFSZ	6,3	8/3	0.75
KSVZ	6,3	0	-1.92

Table 5.1: Axion-photon couplings for the invisible models.

According to [38] the most important limit on the axion-photon coupling is coming from the helium-burning lifetime of HB (*horizontal branch*) stars in globular clusters

$$g_{\phi\gamma} \lesssim 0.6 \times 10^{-10} \text{ GeV}^{-1}, \tag{5.5}$$

that for the axion decay constant becomes from relation (5.4)

$$f_a / c_{\phi\gamma} \gtrsim 2 \times 10^7 \text{ GeV}. \tag{5.6}$$

For example in the DFSZ model, where $c_{\phi\gamma} \approx 0.75$ the bound can be written as

$$f_a \gtrsim 1.5 \times 10^7 \text{ GeV}. \tag{5.7}$$

5.1.2 Electrons and Nucleons

Axions that couple to electrons can be produced by Compton scatterings $e^- + \gamma \to e^- + \phi$ and electron Bremsstrahlung and the most restrictive limit comes from the delay of helium ignition in low-mass red-giants in globular clusters [38]

$$g_{\phi e} \lesssim 2.5 \times 10^{-13}, \qquad f_a / c_{\phi e} \gtrsim 6.7 \times 10^8 \text{ GeV}. \tag{5.8}$$

*The DFSZ we put on the table is usually called in the literature as type I [17].

The coupling to nucleons creates axion emission from nuclear transitions in low mass stars, however it has a better constraint considering the supernovae SN1987A neutrino pulse duration measured on Earth [17]

$$g_{\phi p} < 0.9 \times 10^{-9}. \tag{5.9}$$

Finally the coupling with neutrons $g_{\phi n}$ shows an experimental bound due to neutron stars (NS) cooling probes

$$g_{\phi n} < 0.8 \times 10^{-9}. \tag{5.10}$$

Coupling	Bound	f_a (DFSZ)	f_a (KSVZ)	Observable
$g_{\phi\gamma}$	0.6×10^{10} GeV^{-1}	1.5×10^7 GeV	4×10^7 GeV	HB/RG in 39 GCs
$g_{\phi e}$	2.5×10^{-13}	6.7×10^9 GeV	$\times$	WD cooling+GCs
$g_{\phi p}$	0.9×10^{-9}	6×10^8 GeV	5×10^8 GeV	SN1987A
$g_{\phi n}$	0.8×10^{-9}	2×10^7 GeV	2×10^7 GeV	NS cooling

Table 5.2: Numerical bounds on axion couplings taken from the complete review [17]. Notes: RG means red giants stars, GC global clusters, WD white dwarfs stars.

Table 5.2 gives a summary of the current observational astrophysical bounds on f_a, based on some of the axion couplings. The bounds for the two different invisible models are calculated using the values of the order 1 c_ψ couplings, also taken from the review [17]. In the case of the $g_{\phi e}$ coupling, there is no tree-level coupling in the hadronic KSVZ model, while the other couplings can set limits for both models. We also depicted in figure 5.2 the current situation of exclusion, in comparison with the two DM scenarios. The strongest limit is set by the same $g_{\phi e}$ coupling, but as we said is only valid for the DFSZ model.

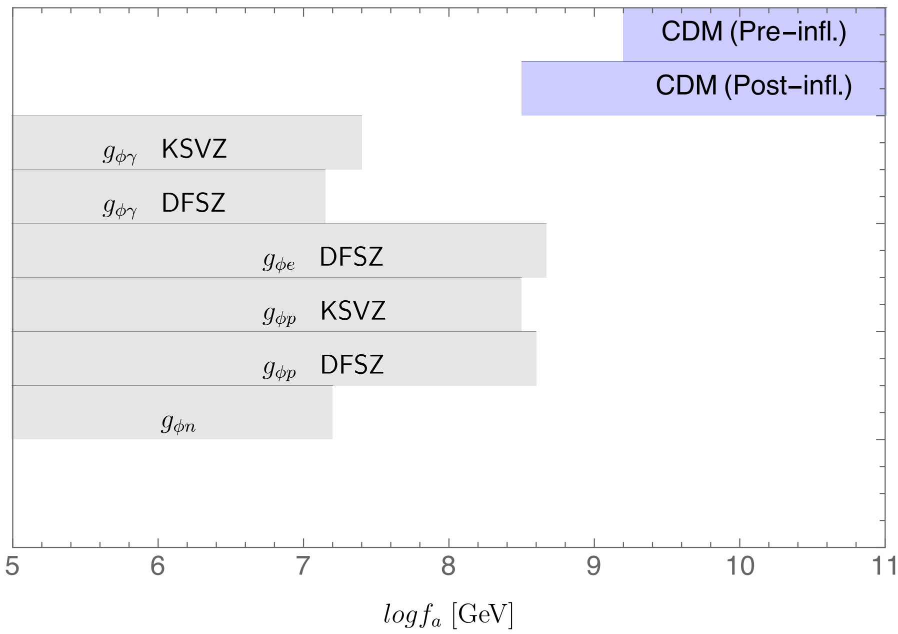

Figure 5.2: Exclusion bounds from Astrophysics observations in the f_a parameter space, based on the values of table 5.2, compared with the dark matter models.

5.2 Search for axions

We will discuss in this section the current experiments searching for all type of axions: produced in the stars, in laboratories and the cold axion population that could account for dark matter. Before discussing the experiments and their exclusion bands we briefly discuss how the axion couplings enter classical dynamics and axions can be detected.

5.2.1 Effects of the axion couplings

Due to the existence of new axion couplings with SM particles the equation of motion for the axion field $\phi(x)$ can be written

$$(\Box + m_a^2)\phi = g_{\phi\gamma}\mathbf{E}\cdot\mathbf{B} - \sum_{\psi}(g_{\phi\psi}j^5_\psi), \qquad j^5_\psi = \langle i\bar{\psi}\gamma_5\psi\rangle\,, \tag{5.11}$$

where we have used $\tilde{F}_{\mu\nu}F^{\mu\nu} = -4\mathbf{E}\cdot\mathbf{B}$. The couplings will affect not only the dynamics of the axion field, but also classical electrodynamics: for instance the presence of the $g_{\phi\gamma}$ coupling changes Maxwell's equations and thereofore wave equation for the photon gauge field $A_\mu = (A_0, \mathbf{A})$

$$\Box\mathbf{A} = g_{\phi\gamma}\mathbf{B}\partial_t\phi. \tag{5.12}$$

The propagation of photons is affected by the presence of the axions and viceversa and equations (5.11) and (5.12) reflect the nature of the system as an oscillation between two physical states: in a background magnetic field neither photons nor axions freely propagates because $(\mathbf{E}\cdot\mathbf{B})\phi$ quantum mechanically mixes them, along the polarization of the $\mathbf{B}$-field. Let's look at one example, we consider a wave that propagates along the z-direction with frequency ω and we split the photon polarization into parallel and transverse to the magnetic field. The system of equations (5.11) and (5.12) reads

$$\left[-\omega^2 - \partial_z^2 + \begin{pmatrix} 0 & 0 & 0 \\ 0 & 0 & ig_{\phi\gamma}B\omega \\ 0 & -ig_{\phi\gamma}B\omega & m_a^2 \end{pmatrix}\right]\begin{pmatrix} A_\perp \\ A_\parallel \\ \phi \end{pmatrix} = 0, \tag{5.13}$$

where the off-diagonal part represents the mixing. This means that a purely EM wave polarized along a transverse $\mathbf{B}$-field must be interpreted as a superposition of a photon-like (k_γ) and an ALP-like wave (k_a) and since the waves have different wavenumbers, they necessarily become out of phase after some distance. Therefore, like in the neutrino case, we have an oscillation pattern:

$$\mathcal{P}(\phi \leftrightarrow \gamma)(L) = g_{\phi\gamma}^2 B^2\left[\frac{\sin(qL/2)}{q}\right]^2, \qquad q \propto k_\gamma - k_\phi. \tag{5.14}$$

This formula is the most important result that every experiment has to take into account if it is to detect physical axions, via the $g_{\phi\gamma}$ coupling of course. The oscillation probability is proportional to the coupling squared and the external field squared; moreover it features the typical pattern of oscillation phenomena, meaning that a coherence effect can be exploited as long as $qL \ll 1$, obtaining $P \propto L^2$, where L is the length of the magnetic field region. It is important to notice that for symmetry reasons the probability of an axion turning into a photon is exactly the same of the reversed process. The $g_{\phi\gamma}$ coupling is used in most of the experiments: direct detection of solar axions and dark matter axions, but also laboratory searches (LSW, *Light-Shining-Through-Walls* [17]).

The coupling $g_{\phi\psi}$ can be used instead for the detection of axion fields sourced by a macroscopic object by NMR techniques: fermions into an axion field will behave as magnetic dipoles into an effective magnetic field

$$\mathbf{B}_\phi = -\frac{g_{\phi\psi}}{m_\psi \gamma_\psi} \nabla \phi, \tag{5.15}$$

with γ_ψ the gyromagnetic ratio. This interaction is used for the search of dark matter axions, that can be described as a "wind" passing trough our planet. If we parametrise the axion DM field as a non-relativistic field

$$\phi \sim \phi_0 \cos(\omega t - \mathbf{k} \cdot \mathbf{x}), \tag{5.16}$$

then the $\mathbf{B}_\phi$-field at a given point is

$$\mathbf{B}_\phi \sim -\frac{g_{\phi\psi}}{m_\psi \gamma_\psi} m_a \mathbf{v} \phi_0 \sin(\omega t), \tag{5.17}$$

but due to local DM constraints† [17], the magnitude of the magnetic field only depends on the ratio $g_{\phi\gamma}/m_\psi \gamma_\psi$ and can be detected with NMR techniques.

5.2.2 Outline of the experiments

We want to briefly review the current status of experimental searches, especially for low values of f_a if we consider the DFSZ model. The most relevant approach for the detection of solar axions is the so-called axion *helioscope*: we are expecting a flux of axions in the keV range (most of the energy will be kinetic) coming from the Sun because of Primakoff conversion. Up to now the most restrictive experimental limit is given by the CAST experiment at CERN, that features a dipole magnet pointing to the Sun and trying to convert solar axions. In other words the apparatus is trying to detected a flux made of X-rays, as the axions will be converted into photons thanks to the magnetic field. The coherence condition relies on the dimension of the detector and the strength of the magnet, if we look back at the conversion probability (5.14). In the case of the CAST experiment the coherence is satisfied for the values

$$m_a \lesssim 10^{-2} \text{ eV}, \qquad f_a \gtrsim 6 \times 10^8 \text{ GeV}. \tag{5.18}$$

However, given that we are exploiting the $g_{\phi\gamma}$ coupling, we should check the sensitivity of the experiments regarding this quantity: as a matter of fact, the CAST bound on the coupling, for masses (5.18) is [17]

$$g_{\phi\gamma} < 0.66 \times 10^{-10} \text{ GeV}^{-1}, \tag{5.19}$$

and it is much higher (see figure 5.3) than the coupling values describing promising axion models, such as QCD models DFSZ and KSVZ. In other words, the fact that the CAST experiment didn't detect solar axions is reasonable, at least according to QCD axion models.

†The product $m_a \phi_0$ is fixed [17] and $\mathbf{v}$ can be observed.

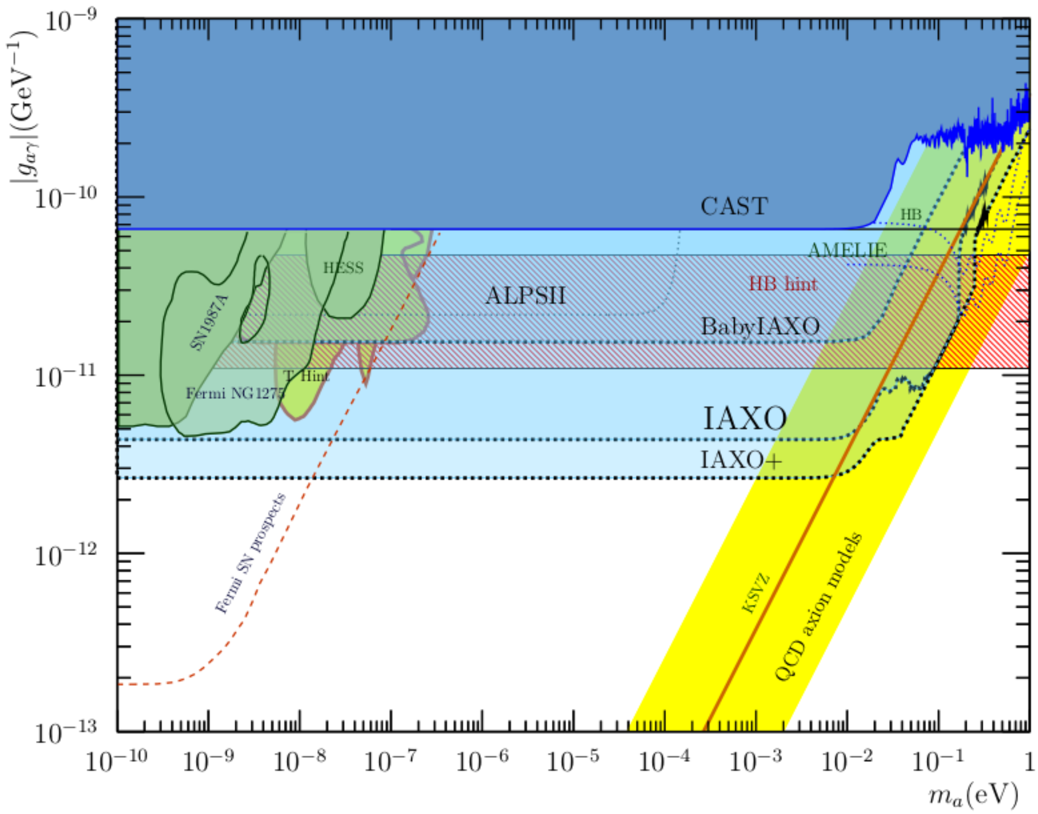

Figure 5.3: Exclusion bands for wide-bands experiments, such as helioscopes, in the mass-coupling plane. The KSVZ model of the QCD axion is also highlighted.

The proposed next generation axion helioscope, dubbed the International AXion Observatory (IAXO), promises to be the most sensitive detector for solar axions ever built [52], and the sensitivity to the axion-photon coupling is expected to surpass the best current limits set by CAST by at least a factor 10, as seen in figure 5.3. Moreover, IAXO is expected to supersede astrophysical limits on $g_{\phi e}$ of table 5.2, opening the possibility to probe an interesting set of non-hadronic axion models, like the DFSZ. However, due to loss of coherence the limit on f_a of IAXO will be the same of CAST

$$f_a \gtrsim 6 \times 10^8 \text{ GeV}. \tag{5.20}$$

The latter is very close (see figure 4.15) to our predictions in the thermal production using the DFSZ top-axion coupling. If we consider instead the hadronic KSVZ model, figure 4.15 suggests an arbitrarily higher range on f_a, as we can theoretically accept new heavy quark masses $m_{Q^\star} > 1$ TeV. The maximum value will be $\Delta N_{\text{eff}} \simeq 0.027$, but we could obtain observable values in the near future, in the range (4.22) up to $m_{Q^\star} = 100$ TeV and in the range

$$f_a/c_{Q^\star} \lesssim 6 \times 10^{10} \text{ GeV}, \tag{5.21}$$

for values up to $m_{Q^\star} = 500$ TeV. Therefore we need to check the experimental status of experiments for high values of f_a as well. The latter are aimed to detect CDM axions, mostly in the post-inflationary scenario, where plausible values of are between 10^{10} GeV and 10^{12} GeV. The most relevant experiment in CDM axion detection is ADMX [17], using the famous *haloscope* technique, first proposed by Sikivie in 1983 [56]. However, even if reaches the sensitivity of the QCD axion

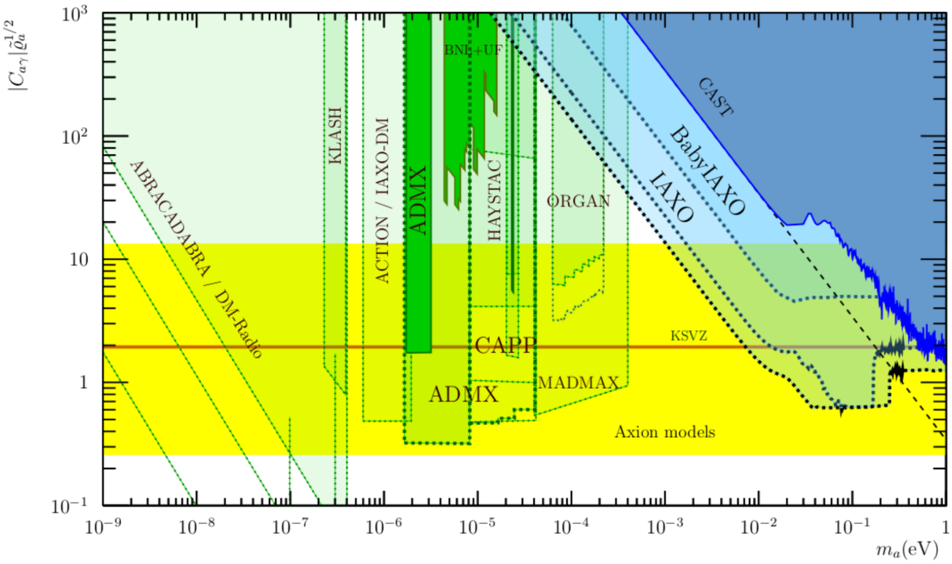

Figure 5.4: Exclusion bands for narrow-bands experiments, or haloscopes, in the mass-coupling plane. The light-green bands are describing sensitivies of upcoming experiments. The KSVZ model of the QCD axion is also highlighted.

models in the coupling $g_{\phi\gamma}$, it covers a very narrow band in the f_a parameter space, focusing on very high values $f_a \simeq 10^{12}$ GeV. Consequently, as we will see in detail in the last section, the post inflationary scenario is untouched by current experiments [54]. The recent proposal of the MADMAX experiment presents a new concept [54, 55] to cover this region of interest, and it is capable of discovering $\sim 100\ \mu$eV mass axions. In other words, as we can see from figure 5.4, MADMAX will cover the range of interest for the KSVZ model

$$1.5 \times 10^{10}\ \text{GeV} \lesssim f_a \lesssim 1.5 \times 10^{11}\ \text{GeV}. \tag{5.22}$$

For DFSZ models we also have to check the experiments using the $g_{\phi\psi}$ couplings. The QUAX proposal relies on the axion-electron coupling and can detect DM axions using NMR techniques and the relation (5.17). It will cover the small region

$$2 \times 10^{10}\ \text{GeV} \lesssim f_a \lesssim 3.5 \times 10^{11}\ \text{GeV}. \tag{5.23}$$

It is however important to make a comment: within the DFSZ model we developed our calculations of thermal production using only axion coupling to heavy fermions, that belong to the third generation. As it turns out, only the top-axion coupling can give detectable contributions to dark radiation (ΔN_{eff}) for reasonable values of f_a. Nevertheless the bounds from astrophysics and the QUAX experiment both use the DFSZ coupling to electrons, which are fermions of the first generation. In principle these kind of limitations are not valid for the coupling $g_{\phi t} = c_t m_t/f_a$, and this why we actually started computing before looking at exclusion bounds. It is also true that we want to compare our thermal production results with the ones of CDM discussed in the second chapter, as both population of axions are expected to exist. In the following last section we therefore summarize the observational and experimental bounds, the computations of thermal axions and the CDM scenarios both for the DFSZ and the KSVZ models.

5.3 Possible windows of f_a

In this final section we summarize and discuss all the computations and considerations that we exposed in the work. We want to combine all the informations on the f_a parameter in order to find a window where all the following conditions have to be satisfied: an observable contribution to dark radiation given by thermal production of hot axions and an agreement with the CDM models and observations/experiments. In detail:

- **Thermal production**: our main focus is to discuss quantitatively the possible processes of thermal axion production that could be detectable through the ΔN_{eff} contribution, at least in the near future (CMB-S4). We extended the work of [26, 27] including corrections from EW bosons $Z, W^{\pm}$ and h for the coupling $g_{\phi t}$ in the DFSZ model. In addition we discussed the KSVZ model, introducing new and massive (TeV) heavy quarks, for the production of thermal axions above the EW phase transition. The top-axion coupling certainly gives slightly higher contributions to N_{eff} than the limit (2.30), as its total rate decouples at temperatures around m_t; the possible observable values, including the EW correction of $\approx 6\%$, lie in the range $f_a/c_t \lesssim 2 \times 10^9$ GeV, where we typically assume an order one PQ charge c_t. The contribution instead in the KSVZ is exactly the one calculated in [30] (2.30), but the range of possible scales that can reach it is bigger. For $c_{Q^\star} \sim \mathcal{O}(1)$ we find $f_a \lesssim 1.5 \cdot 10^{10}$ GeV.

- **Axion cold dark matter**: we want to include the theoretical calculations that expect a cold population of axions that can account for the observed and dominating dark matter. The post-inflationary scenario seems more reasonable for different reasons but all its effects are hard to compute with enough precision, especially topological defects. Our best guess, based on simulations [41,50], approximately give the possible window $f_a \in [10^9; 10^{11}]$ GeV, as for higher values we have too much dark matter. In the pre-inflationary scenario the windows is extended arbitrarily because of the fine-tuning scenario $\bar{\theta}_i \to 0$, giving only a lower bound $f_a \gtrsim 10^9$ GeV.

- **Astrophysical bounds**: we have to consider possible exclusions due to astrophysical observations. The best limit is given by the $g_{\phi p}$ coupling for the KSVZ model and by $g_{\phi e}$ for the DFSZ model. However the latter coupling uses a first generation fermion, and in principle the top-axion and bottom-axion couplings used in this work should not be affected by this bound. The numerical values are in table 5.2.

- **Experimental exclusions**: the search of axions is developing really fast in the last years and will be even more present in the near future. The current experiments for wide range of f_a (helioscopes) didn't yet probe the plausible QCD axion models, but will try to do it the next years. The most relevant experiment that probed the QCD axion band is ADMX, but the haloscope technique focuses or very specific and high values of f_a. We would have to wait for new generation experiments, such as MADMAX, in order to cover the still very large and untouched window of possibles values of f_a.

Finally, the possible windows that are in agreement with these arguments, are for the DFSZ and KSVZ model, respectively:

$$6 \times 10^8\ \text{GeV} \lesssim f_a^{\mathsf{DFSZ}} \lesssim 2 \times 10^9\ \text{GeV}, \tag{5.24}$$

$$5 \times 10^8\ \text{GeV} \lesssim f_a^{\mathsf{KSVZ}} \lesssim 2 \times 10^{10}\ \text{GeV}. \tag{5.25}$$

All the contributions and numerical values discussed are qualitatively presented in figures 5.5 and 5.6.

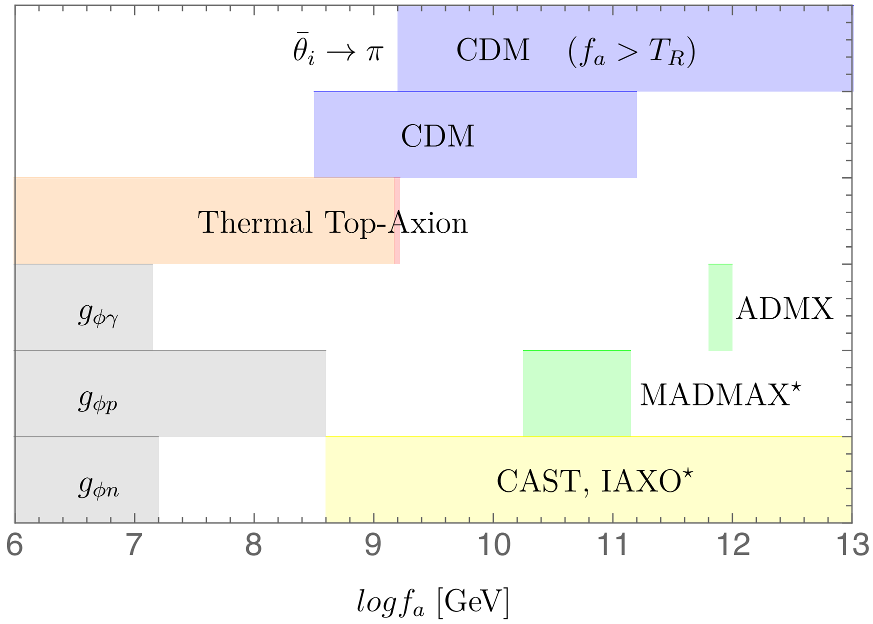

Figure 5.5: Summary of possible windows of f_a in the DFSZ model using the top-axion coupling.

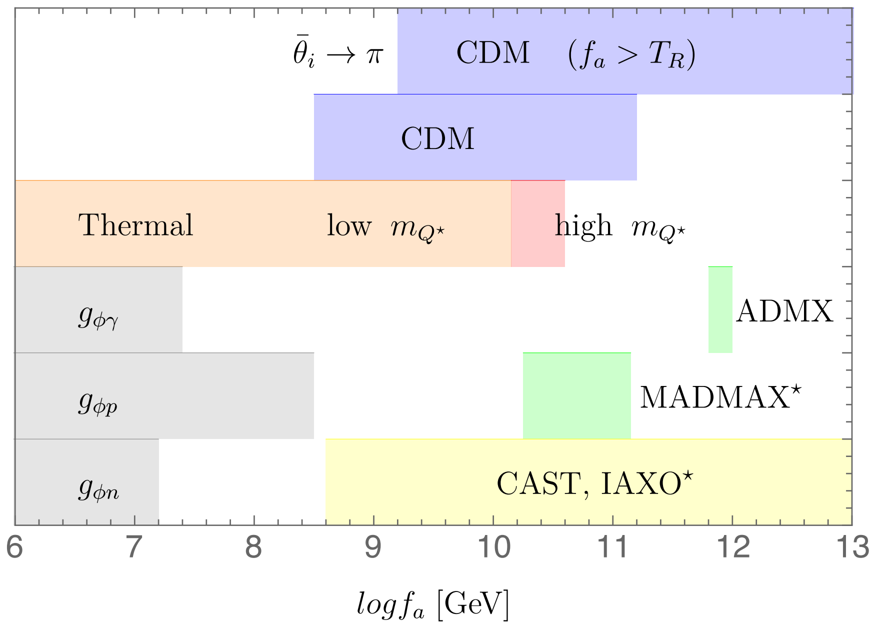

Figure 5.6: Summary of possible windows of f_a in the KSVZ model using the top-axion coupling.

Acknowledgements

I want to thank all the people that were close to me during all these years, family and friends.

I would like to thank my supervisors Francesco D'Eramo and Alessio Notari for the possibility of developing the work, the guidance and for sharing interest in the topics. I also thank the University of Padova for giving me the appropriate educational background for five years and the Heidelberg University for my Erasmus stay. I finally thank F. D'Eramo, the INFN and the Galileo Galilei Institute for Theoretical Physics in Florence for hosting me while writing the last part of the work.

Appendix A

Standard Model physics

A.0.1 Lagrangian and couplings

In this appendix we report with full detail the SM lagrangian, with a particular emphasis on the couplings relevant for our work. It also helps the reader follow the notation and the conventions. The entire lagrangian is invariant under the gauge symmetry $SU(3)_C \times SU(2)_L \times U(1)_Y$ can be written in a compact form in only one line:

$$\mathscr{L}_{SM} = \mathscr{L}_{SSB} + \mathscr{L}_{gauge} + \mathscr{L}_{Yukawa},$$

let us describe the terms.

SSB: the first term is the Higgs sector responsible for the spontaneous symmetry breaking of the electroweak interactions $SU(2)_L \times U(1)_Y \to U(1)_{em}$. Its lagrangian reads

$$\mathscr{L}_{SSB} = (D_\mu \Phi)^\dagger (D^\mu \Phi) - V(\Phi^\dagger \Phi). \tag{A.1}$$

Here $\Phi = (\varphi^+, \varphi^0)^T$ is a complex doublet field (it therefore has 4 degrees of freedom) and is invariant under both the transformations of $SU(2)_L$ and $U(1)_Y$m respectively:

$$\Phi \to e^{-ig\alpha_a \tau_a/2}\Phi, \qquad \Phi \to e^{-ig'Y\alpha}\Phi,$$

where τ_a are the Pauli matrices, Y is the hypercharge of the field and α, α_a are real parameters that depends on spacetime. It interacts with electroweak gauge bosons via the covariant derivative

$$D_\mu \Phi = \left(\partial_\mu + \frac{ig}{2} W_\mu + \frac{ig'}{2} B_\mu\right)\Phi, \qquad W_\mu = W_\mu^a \tau_a.$$

From the first term of eq. (A.1) we can extract the mass spectrum of the gauge bosons and the interactions between the Higgs bosons h and the the EW bosons, using a particular choice of the vacuum and exploiting the *unitary gauge*. The interactions can be written in the lagrangian

$$\mathscr{L}_{int}^h = \left(\frac{m_W}{v}\right)^2 [2vhW^+W^- + h^2W^+W^-] + \frac{1}{2}\left(\frac{m_Z}{v}\right)^2 [2vhZZ + h^2ZZ].$$

The potential needed for the Higgs mechanism can be written as

$$V(\Phi^\dagger\Phi) = \lambda(\Phi^\dagger\Phi - v^2)^2,$$

where $v^2 = -\mu^2/\lambda$. In order to have SSB the quadratic parameter μ^2 has to be negative.

GAUGE: the gauge sector includes the pure gauge theory and the matter content, namely vector gauge bosons and fermions.

$$\mathscr{L}_{gauge} = -\frac{1}{4}G^a_{\mu\nu}G^{\mu\nu}_a - \frac{1}{4}W^i_{\mu\nu}W^{\mu\nu}_i - \frac{1}{4}B_{\mu\nu}B^{\mu\nu} + i\sum_f \bar{\Psi}_f \not{D}\Psi_f.$$

The contracted index a represents a trace in colour space where $SU(3)$ is the gauge symmetry, $G^a_{\mu\nu}$ is the gluon field strength and represents the gluons. The index i is for the gauge group $SU(2)_L$ and the $W^i_{\mu\nu}$ and $B_{\mu\nu}$ are the electroweak massless bosons. After SSB three of them becomes the $W^\pm, Z$ bosons and one of them the still massless photon. The last term is the represented by the the matter terms and their interactions with gauge bosons via the covariant derivative $\not{D} = D_\mu\gamma^\mu$, where γ^μ are the Dirac gamma matrices. The sum runs over the fermionic matter fields

$$\Psi_f \in \{q_L, l_L, u_R, d_R, e_R\}, \qquad q_L = (u_L, d_L)^T, \qquad l_L = (\nu_L, e_L)^T,$$

and every fermion can be split in right handed an left handed (+1/2 or -1/2 helicity respectively) (the difference between Dirac and the Weyl spinors is later explained). Let us look up these terms explicitly.

Fermion-boson interaction

We are considering here the interactions of fermions, namely quarks, electrons and neutrinos with the gauge boson in the electroweak sector. We are considering the one flavour case, but the real case with $N_f = 3$ is easily derived. In the lagrangian term $\bar{\Psi}_f\not{D}\Psi_f$ we can neglect the kinetic term ($\bar{\Psi}_f\not{\partial}\Psi_f$) and consider only the interaction, therefore

$$\begin{aligned}\mathscr{L}_{int} =& \frac{1}{2}\bar{L}(g\not{W}_a\tau_a + g'Y_L\not{B})L + \frac{1}{2}\bar{e}_R(g'Y_{e_R}\not{B})e_R, \\ &+ \bar{Q}(g\not{W}_a\tau_a + g'Y_Q\not{B})Q + \frac{1}{2}\bar{u}_R(g'Y_{u_R}\not{B})u_R \\ &+ \frac{1}{2}\bar{d}_R(g'Y_{d_R}\not{B})d_R,\end{aligned} \tag{A.2}$$

where the hypercharges are $Y_L = -1/2$, $Y_{e_R} = -1$, $Y_{e_R} = 2/3$ and $Y_{e_R} = -1/3$ by construction. Now we remember that we can define the physical bosons as

$$W^\pm = \frac{W_1 \mp W_2}{\sqrt{2}}, \qquad \begin{pmatrix} Z_\mu \\ A_\mu \end{pmatrix} = \begin{pmatrix} \cos\theta_W & -\sin\theta_W \\ \sin\theta_W & \cos\theta_W \end{pmatrix}\begin{pmatrix} W_{3\mu} \\ B_\mu \end{pmatrix},$$

therefore we divide the interaction lagrangian into an off-diagonal charged current interaction (CC) and the diagonal neutral current interaction (NC). In the CC the electric charge is conserved because the $W^\pm$ bosons are charged

$$\mathscr{L}^{CC}_{int} = \frac{g}{\sqrt{2}}(\bar{\nu}_L\not{W}^+e_L + \bar{e}_L\not{W}^-\nu_L) + \frac{g}{\sqrt{2}}(\bar{u}_L\not{W}^+d_L + \bar{d}_L\not{W}^-u_L) \tag{A.3}$$

$$= \frac{g}{2\sqrt{2}}\left[W^+_\mu(\bar{\nu}\gamma^\mu(1-\gamma_5)e + \bar{u}\gamma^\mu(1-\gamma_5)d) + \text{h.c.}\right]. \tag{A.4}$$

This lagrangian describes the interactions of fermions with the $W^{\pm}$ bosons, but for the quarks in the $N_f = 3$ case we have to modify the interaction because of the quark mixing. This means that passing from the interaction basis to the mass basis we have to take into account of the appropriate mixing angle V_{ij} of the CKM matrix. We can draw the following diagram with the interactions

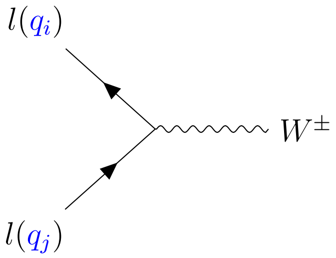

$$= \frac{-ig}{2\sqrt{2}}\gamma^{\mu}(1-\gamma_5)(V_{ij}).$$

In the NC interactions we have also to recall the relation $T_3 + Y = Q$, where T_3 is the third component of the isospin operator and Q is the electric charge. Expanding the lagrangian (A.2), we have to impose the condition $g \sin\theta_W + g' \cos\theta_W Y_L = 0$ because neutrinos have zero electric charge and $g \sin\theta_W = e = g' \cos\theta_W$, where e is the electric charge of the proton, for consistency with the electromagnetic interaction. We then obtain

$$\mathscr{L}_{int}^{NC} = -eQ_f \sum_{f=e,u,d} \bar{\psi}_f \not{A} \psi_f - \frac{g}{2\cos\theta_W} \sum_f \bar{\psi}_f \not{Z} (c_V - c_A\gamma_5)\psi_f,$$

where $c_V = T_{3L,f} - 2Q_f \sin^2\theta_W$ and $c_A = T_{3L,f}$. The first line represents the electromagnetic interactions of electrons (muons, tauons) and all the quarks with photons (A_μ field), in the vertex we have to consider the electric charge of the fermion Q_f, in units of e. The second part is neutral weak interaction mediated by the Z bosons.

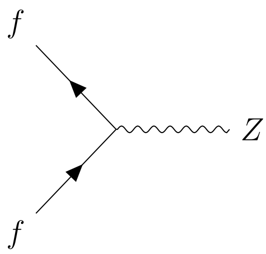

$$= \frac{-ig}{2\cos\theta_W}\gamma^{\mu}(c_V - c_A\gamma_5).$$

The remaining interaction is the one between quarks and gluons and it has the same structure of the electromagnetic interaction, with the addition of the colour structure. In the quark-gluon vertex we have to add the generator of the $SU(3)$ group (the Gell-Mann matrices λ_a), therefore the interaction can be written as $-ig_s\gamma^{\mu}(\lambda_a)^{\alpha\beta}/2$, where now α and β are the colour indices.

YUKAWA: the Yukawa lagrangian is the source of the fermion masses and their interaction with the Higgs field. It can be written as

$$\mathscr{L}_{Yukawa} = -(\bar{L}^i Y_e^{ij} \Phi e_R^j + \bar{Q}^i Y_d^{ij} \Phi d_R^j + \bar{Q}^i Y_u^{ij} \tilde{\Phi} u_R^j) + \text{h.c.},$$

where $\tilde{\Phi} = i\tau_2\Phi^* = (\varphi^{0*}, -\varphi^-)^T$ and the indices i, j live in flavour space if we are considering the three generations. Y_e, Y_d, Y_u are $N_f \times N_f$ complex matrices, but we can diagonalize them with a biunitary transformation. In this way is possible to write the in the unitary gauge fermion masses and the interactions. We find

$$m_{e,j} = (Y_e)^{jj}_{diag}\frac{v}{\sqrt{2}}, \qquad m_{u,j} = (Y_u)^{jj}_{diag}\frac{v}{\sqrt{2}}, \qquad m_{d,j} = (Y_d)^{jj}_{diag}\frac{v}{\sqrt{2}},$$

and the interactions

$$\mathscr{L}_Y = y_\psi h\bar{\psi}\psi. \tag{A.5}$$

Dirac and Weyl spinors

Given a Dirac field $\Psi(x)$ that satisfies the Dirac equation, see [2], we can split it into left-handed and a right-handed part

$$\Psi = \Psi_L + \Psi_R = \begin{pmatrix} \Psi_L \\ \Psi_R \end{pmatrix},$$

where

$$\Psi_L = P_L\Psi = \frac{1}{2}(1-\gamma_5)\Psi, \qquad \Psi_R = P_R\Psi = \frac{1}{2}(1+\gamma_5)\Psi$$

are Weyl spinors. P_L and P_R are called projectors and satisfy the relations: $P_{L,R}^2 = P_{L,R}$, $P_L P_R = P_R P_L = 0$. This is the definition of handedness, or *chirality*, which involves the presence of the γ_5 matrix. A general solution of the Dirac equation is not an irreducible representation of the Lorentz group, a Weyl fermion is. If we take two independent left-handed Weyl fields $\chi(x)$ and $\tilde{\chi}(x)$, their combination

$$\Psi(x) = \chi_1(x) + \tilde{\chi}^c(x), \qquad \tilde{\chi}^c(x) = C\tilde{\chi}(x)$$

form a Dirac spinor, meaning that Dirac spinor field Ψ and its conjugate $\bar{\Psi}$ are equivalent to two left-handed Weyl spinors χ and $\tilde{\chi}$ (or equivalently their right-handed conjugates $\chi^\dagger$ and $\tilde{\chi}^\dagger$). The operator C is the charge conjugation [2]. Now we are going to show how an axial current current (e.g. for anomalous $U(1)_A$) of Dirac spinors is defined

$$\begin{aligned} j_5^\mu &= \bar{\Psi}\gamma^\mu\gamma_5\Psi = \frac{1}{2}\bar{\Psi}\gamma^\mu(1+\gamma_5)\Psi - \frac{1}{2}\bar{\Psi}\gamma^\mu(1-\gamma_5)\Psi \\ &= \bar{\Psi}_R\gamma^\mu\Psi_R - \bar{\Psi}_L\gamma^\mu\Psi_L = j_R^\mu - j_L^\mu, \end{aligned}$$

where Ψ is a Dirac spinor, Ψ_L, Ψ_R are left-handed and right handed Weyl spinors, respectively. To sum the axial current (with γ_5) of Dirac spinors is the difference of the vector currents of Weyl fields

$$j^\mu_{5,\text{Dirac}} = j^\mu_{R,\text{Weyl}} - j^\mu_{L,\text{Weyl}}. \tag{A.6}$$

A.0.2 Running of the coupling constants

Within the SM framework it is known that the coupling constants assume different values as the energy scale μ^2 changes. In order to take into account this effect when computing the rate or solving the Boltzmann equations at different temperatures we have to solve the *Renormalization Group Equation* (RGE) for the couplings and consider them as functions. The RGE are differential equations that can schematically written as

$$\frac{d\alpha_i}{d\log\mu^2} = \beta(\alpha_i), \tag{A.7}$$

where $\alpha_i = g_i^2/(4\pi)$, also in the case of the Yukawa coupling we can define $\alpha_t = y_t^2/(4\pi)$. We show in this section the known results for the RGE equations up to

2 loop order in the $\beta(\alpha_i)$ functions for the SM couplings, g_1, g_2, g_3 and up to 1 loop order for the y_t coupling, in $\overline{\text{MS}}$ scheme [36]. The couplings g_1 is related to the electrical charge via the relation

$$e = \sqrt{\frac{5}{3}} g_1 \cos\theta_W, \tag{A.8}$$

while $g_2 = g$ and $g_3 = g_s$. We explicitly write the four differential equations [36]

$$\frac{dg_1^2}{d\log\mu^2} = \frac{g_1^4}{(4\pi)^2}\left(\frac{41}{10}\right) + \frac{g_1^4}{(4\pi)^4}\left(\frac{44g_3^2}{5} + \frac{27g_2^2}{10} + \frac{199g_1^2}{50} - \frac{17y_t^2}{10}\right), \tag{A.9}$$

$$\frac{dg_2^2}{d\log\mu^2} = \frac{g_2^4}{(4\pi)^2}\left(-\frac{19}{6}\right) + \frac{g_2^4}{(4\pi)^4}\left(12g_3^2 + \frac{35g_2^2}{6} + \frac{9g_1^2}{10} - \frac{3y_t^2}{2}\right), \tag{A.10}$$

$$\frac{dg_3^2}{d\log\mu^2} = \frac{g_3^4}{(4\pi)^2}(-7) + \frac{g_3^4}{(4\pi)^4}\left(-26g_3^2 + \frac{9g_2^2}{2} + \frac{11g_1^2}{10} - 2y_t^2\right), \tag{A.11}$$

$$\frac{dy_t^2}{d\log\mu^2} = \frac{y_t^4}{(4\pi)^2}\left(\frac{9y_t^2}{2} - 8g_3^2 - \frac{9g_2^2}{4} - \frac{17g_1^2}{20}\right). \tag{A.12}$$

For the numerical solution, done with *Mathematica*, we used as conditions the values of the couplings at $T = m_t$ [36]:

$$g_1(m_t) = 0.3583, \tag{A.13}$$

$$g_2(m_t) = 0.6478, \tag{A.14}$$

$$g_3(m_t) = 1.1666, \tag{A.15}$$

$$y_t(m_t) = 0.9402. \tag{A.16}$$

We finally show a graph with the couplings we used in the computation (e, g, g_s, y_t), using the relation (A.8).

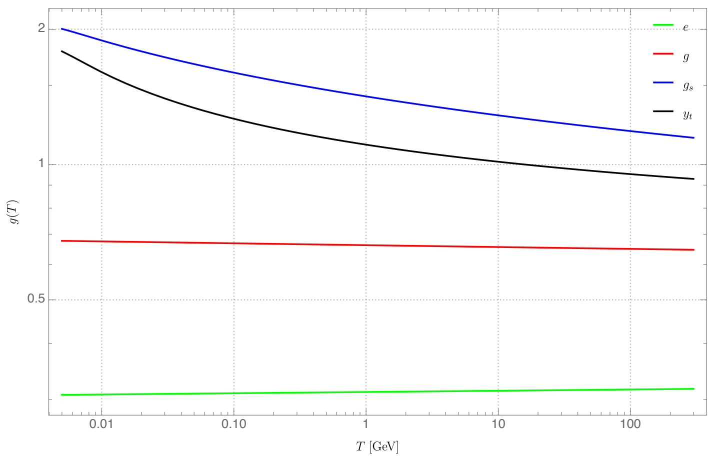

Figure A.1: Running of the coupling constants in the GeV range.

Appendix B

Computation of cross sections

Cross section of $q\bar{q} \to \phi g$

The matrix element is the sum of the of the u-channel and t-channel diagrams

$$\mathcal{M}_{q\bar{q}\to\phi g} = \mathcal{M}^{(t)}_{q\bar{q}\to\phi g} + \mathcal{M}^{(u)}_{q\bar{q}\to\phi g},$$

written explicitly in the Yukawa basis

$$i\mathcal{M}^{(t)}_{q\bar{q}\to\phi g} = \frac{ic_q m_q g_s}{f_a}\epsilon^*_\mu(p_3,\lambda)\bar{v}(p_2)c_i^\dagger\gamma_5\frac{i(\not{p}_1 - \not{p}_3 + m_q)}{t - m_q^2}(i\gamma^\mu t^a)u(p_1)c_j$$

$$i\mathcal{M}^{(u)}_{q\bar{q}\to\phi g} = \frac{ic_q m_q g_s}{f_a}\epsilon^*_\mu(p_3,\lambda)\bar{v}(p_2)c_i^\dagger(i\gamma^\mu t^a)\frac{i(\not{p}_1 - \not{k} + m_q)}{u - m_q^2}\gamma_5 u(p_1)c_j,$$

where c_k is the colour of the quark q_k and t_a the $SU(3)$ generators. The colour factor can be factorized independently of the Lorentz structure and written as $t^a_{ij} = c_i^\dagger t^a c_j$. Also, g_s is the strong coupling constant and λ is the helicity of the gluon. The squared amplitude is obtained by squaring the sum, giving four contributions, and averaged over the initial polarizations

$$|\bar{\mathcal{M}}|^2 = \frac{1}{4}\left(\frac{c_q m_q g_s}{f_a}\right)^2 |t^a_{ij}|^2 g_{\mu\alpha}\mathcal{J}^{\mu\alpha},$$

$$\begin{aligned}\mathcal{J}^{\mu\alpha} = \mathrm{tr}\Bigg[(\not{p}_1 + m_q)\left(\frac{\gamma^\alpha(\not{p}_1 - \not{p}_3 + m_q)\gamma_5}{t - m_q^2} + \frac{\gamma_5(\not{p}_1 - \not{k} + m_q)\gamma^\alpha}{u - m_q^2}\right)\times \\ (\not{p}_2 - m_q)\left(\frac{\gamma_5(\not{p}_1 - \not{p}_3 + m_q)\gamma^\mu}{t - m_q^2} + \frac{\gamma^\mu(\not{p}_1 - \not{k} + m_q)\gamma_5}{u - m_q^2}\right)\Bigg].\end{aligned}$$

Because of the symmetry of the system the mixed terms are equal, leaving us with the contracted squared amplitude

$$|\bar{\mathcal{M}}|^2 = \frac{1}{4}\left(\frac{c_q m_q g_s}{f_a}\right)^2 |t^a_{ij}|^2\left[\frac{T^2}{A^2} + \frac{U^2}{B^2} + \frac{2UT}{AB}\right],$$

where $A = t - m_q^2$ and $B = u - m_q^2$. We are left we compute T^2, U^2 and the mixed term TU.

$$\begin{aligned}
T^2 &= \mathrm{tr}\Big[(\not{p}_1 + m_q)\gamma_\mu(\not{p}_1 - \not{p}_3 + m_q)\gamma_5(\not{p}_2 - m_q)\gamma_5(\not{p}_1 - \not{p}_3 + m_q)\gamma^\mu\Big] \\
&= \mathrm{tr}\Big[\not{p}_1\gamma_\mu(\not{p}_1 - \not{p}_3)\gamma_5\not{p}_2\gamma_5(\not{p}_1 - \not{p}_3)\gamma^\mu\Big] + m_q^2\mathrm{tr}\Big[\gamma_\mu\gamma_5\not{p}_2\gamma_5(\not{p}_1 - \not{p}_3)\gamma^\mu\Big] - \\
&\quad m_q^2\mathrm{tr}\Big[\gamma_\mu(\not{p}_1 - \not{p}_3)\gamma_5\gamma_5(\not{p}_1 - \not{p}_3)\gamma^\mu\Big] + m_q^2\mathrm{tr}\Big[\gamma_\mu(\not{p}_1 - \not{p}_3)\gamma_5\not{p}_2\gamma_5\gamma^\mu\Big] - \\
&\quad m_q^2\mathrm{tr}\Big[\not{p}_1\gamma_\mu\gamma_5\gamma_5(\not{p}_1 - \not{p}_3)\gamma^\mu\Big] + m_q^2\mathrm{tr}\Big[\not{p}_1\gamma_\mu\gamma_5\not{p}_2\gamma_5\gamma^\mu\Big] - \\
&\quad m_q^2\mathrm{tr}\Big[\not{p}_1\gamma_\mu(\not{p}_1 - \not{p}_3)\gamma_5\gamma_5\gamma^\mu\Big] - m_q^4\mathrm{tr}\Big[\gamma_\mu\gamma_5\gamma_5\gamma^\mu\Big] \\
&= 2\mathrm{tr}\Big[\not{p}_1(\not{p}_1 - \not{p}_3)\not{p}_2(\not{p}_1 - \not{p}_3)\Big] - 8m_q^2\, p_2\cdot(p_1 - p_3)\mathrm{tr}\big[\mathbb{1}_4\big] - 4tm_q^2\mathrm{tr}[\mathbb{1}_4] + \\
&\quad 4m_q^2\mathrm{tr}\Big[\not{p}_1(\not{p}_1 - \not{p}_3)\Big] + 2m_q^2\mathrm{tr}\Big[\not{p}_1\not{p}_2\Big] - 4m_q^4\mathrm{tr}[\mathbb{1}_4] \\
&= 4\Big[(s - 2m_q^2)(m_q^2 - t) + (m_q^2 + t)(-m_q^2 - t + 2m_q^2)\Big] = 4(u - m_q^2)(t - m_q^2)
\end{aligned}$$

$$\begin{aligned}
U^2 &= \mathrm{tr}\Big[(\not{p}_1 + m_q)\gamma_5(\not{p}_1 - \not{k} + m_q)\gamma_\mu(\not{p}_2 - m_q)\gamma^\mu(\not{p}_1 - \not{k} + m_q)\gamma_5\Big] \\
&= T^2(s \to s, t \to u, u \to t) = 4(t - m_q^2)(u - m_q^2)
\end{aligned}$$

$$\begin{aligned}
UT &= \mathrm{tr}\Big[(\not{p}_1 + m_q)\gamma_5(\not{p}_1 - \not{k} + m_q)\gamma_\mu(\not{p}_2 - m_q)\gamma_5(\not{p}_1 - \not{p}_3 + m_q)\gamma^\mu\Big] \\
&= \mathrm{tr}\Big[\not{p}_1\gamma_5(\not{p}_1 - \not{k})\gamma_\mu\not{p}_2\gamma_5(\not{p}_1 - \not{p}_3)\gamma^\mu\Big] + m_q^2\mathrm{tr}\Big[\gamma_5\gamma_\mu\not{p}_2\gamma_5(\not{p}_1 - \not{p}_3)\gamma^\mu\Big] - \\
&\quad m_q^2\mathrm{tr}\Big[\gamma_5(\not{p}_1 - \not{k})\gamma_\mu\gamma_5(\not{p}_1 - \not{p}_3)\gamma^\mu\Big] + m_q^2\mathrm{tr}\Big[\gamma_5(\not{p}_1 - \not{k})\gamma_\mu\not{p}_2\gamma_5\gamma^\mu\Big] - \\
&\quad m_q^2\mathrm{tr}\Big[\not{p}_1\gamma_5\gamma_\mu\gamma_5(\not{p}_1 - \not{p}_3)\gamma^\mu\Big] + m_q^2\mathrm{tr}\Big[\not{p}_1\gamma_5\gamma_\mu\not{p}_2\gamma_5\gamma^\mu\Big] - \\
&\quad m_q^2\mathrm{tr}\Big[\not{p}_1\gamma_5(\not{p}_1 - \not{k})\gamma_\mu\gamma_5\gamma^\mu\Big] - m_q^4\mathrm{tr}\Big[\gamma_5\gamma_\mu\gamma_5\gamma^\mu\Big] \\
&= -4p_2\cdot(p_1 - p_3)\mathrm{tr}\Big[\not{p}_1(\not{p}_1 - \not{k})\Big] + 4m_q^2\, p_2\cdot(p_1 - p_3)\mathrm{tr}[\mathbb{1}_4] + \\
&\quad 2m_q^2\mathrm{tr}\Big[(\not{p}_1 - \not{k})(\not{p}_1 - \not{p}_3)\Big] - 2m_q^2\mathrm{tr}\Big[\not{p}_1\not{p}_2\Big] + 2m_q^2\mathrm{tr}\Big[(\not{p}_1 - \not{k})\not{p}_2\Big] - \\
&\quad 2m_q^2\mathrm{tr}\Big[\not{p}_1(\not{p}_1 - \not{p}_3)\Big] - 4m_q^2\mathrm{tr}\Big[\not{p}_1(\not{p}_1 - \not{k})\Big] + 4m_q^4\mathrm{tr}[\mathbb{1}_4] \\
&= 4\Big[(m_q^2 + t)(m_q^2 + u) - 3m_q^2(m_q^2 + t) - 3m_q^2(m_q^2 + u) - m_q^2(s - 2m_q^2) + 6m_q^4\Big] \\
&= 4\Big[m_q^2(2t + s - m_q^2) - t(t + s)\Big]
\end{aligned}$$

Therefore the sum of the three contributions is

$$\frac{T^2}{A^2} + \frac{U^2}{B^2} + \frac{2UT}{AB} = 4\left[\frac{u - m_q^2}{t - m_q^2} + \frac{t - m_q^2}{u - m_q^2} + 2\frac{m_q^2(2t + s - m_q^2) - t(t + s)}{(t - m_q^2)(u - m_q^2)}\right]$$
$$= \frac{4s^2}{(s + t - m_q^2)(m_q^2 - t)},$$

and the total squared amplitude reads

$$|\bar{\mathcal{M}}|^2_{q\bar{q}\to\phi g} = \left(\frac{c_q m_q g_s}{f_a}\right)^2 |t^a_{ij}|^2 \frac{s^2}{(s + t - m_q^2)(m_q^2 - t)}. \tag{B.1}$$

Cross section of $q\bar{q} \to Z\phi$

The full expression of the trace computation lead to the squared amplitude (we used $m_q \equiv m$ and $M_Z \equiv M$ for simplicity)

$$\begin{aligned}
|\bar{\mathcal{M}}|^2_{q\bar{q}\to Z\phi} = -\frac{1}{4}\left(\frac{c_q m_q g_W}{2\cos\theta_W f_a}\right)^2 \Bigg[& 4(c_V^2 + c_A^2)\Bigg(\frac{2m^6 - 3m^4M^2 - m^4t - m^4u +}{M^2(m^2 - t)(m^2 - u)} \\
& \frac{+3m^2M^2t + 3m^2M^2u - 2m^2tu - M^2t^2 - M^2tu - M^2u^2 + t^2u + tu^2}{M^2(m^2 - t)(m^2 - u)}\Bigg) \\
& - 4(c_V^2 - c_A^2)\Bigg(\frac{2m^8 + 3m^6M^2 - m^6t - 3m^6u - 7m^4M^2t +}{M^2(m^2 - t)(m^2 - u)^2} \\
& \frac{-2m^4M^2u - m^4tu + m^4u^2 + 4m^2M^2t^2 + 2m^2M^2tu +}{M^2(m^2 - t)(m^2 - u)^2} \\
& \frac{+3m^2M^2u^2 + m^2t^2u + 3m^2tu^2 - 3M^2tu^2 - t^2u^2 - tu^3}{M^2(m^2 - t)(m^2 - u)^2}\Bigg)\Bigg].
\end{aligned} \tag{B.2}$$

The computation of the cross section has to be done with the software *Mathematica*. The result is too long to be put here and for the sake of brevity we don't write it.

List of functions in the cross sections

The functions $F_5(s)$ and $F_6(s)$ involving the Z boson are not present.

$$F_1(s) = \frac{\tanh^{-1}(L(s))}{4\pi(s - 4m_q^2)}, \tag{B.3}$$

$$F_2(s) = \frac{2s^2\log(s/m_q^2) - 3s^2 + 4m_q^2 s - m_q^4}{32\pi s^2(s - m_q^2)}, \tag{B.4}$$

$$\begin{aligned}
F_3(s) = {} & 2\tanh^{-1}(L(s))\left[m_t^2\left(4M_W^2 + s\right) + 8M_W^2\left(M_W^2 - s\right)\right] + \\
& + L(s)s\left(8M_W^2 - s\right),
\end{aligned} \tag{B.5}$$

$$F_4(s) = m_t^2\left(-2s - 8\pi M_W^2\right) + 8m_t^2 M_W^2 \log\left(\frac{s}{m_t^2 + M_W^2} - 1\right) + \\ + 2\left(m_t^4 + m_t^2\left(M_W^2 - s\right) + 8M_W^2 s\right)\log\left(\frac{m_t^2 + M_W^2}{m_t^2 + M_W^2 - s}\right) - s^2 \tag{B.6}$$

$$F_7(s) = \left(8m_t^4 - 2m_t^2\left(2m_h^2 + s\right) + m_h^4 - m_h^2 s + s^2\right) \times \\ \times \log\left(\frac{(L+1)\left(Ls - 2m_h^2 + s\right)}{(L-1)\left((L-1)s + 2m_h^2\right)}\right) \tag{B.7}$$

$$F_8(s) = \left(m_h^2 - s\right)\Bigg[2Ls\left(2m_t^2 - 2m_h^2 + 3s\right) - 2\left(2m_h^2 - s\right)\left(2m_t^2 - 2m_h^2 + 3s\right) \times \\ \times \tanh^{-1}\left(\frac{Ls}{2m_t^2 - s}\right) + \left(32m_t^4 + 4m_t^2\left(s - 6m_h^2\right) + 4m_h^4 - 2m_h^2 s + s^2\right) \times \\ \times \log\left(\frac{-Ls - 2m_t^2 + s}{Ls - 2m_t^2 + s}\right)\Bigg] \tag{B.8}$$

Appendix C

Numerics and plots

We here leave the additional graphs of production rates, abundance and ΔN_{eff}, for single production process and for both annihilation and scattering.

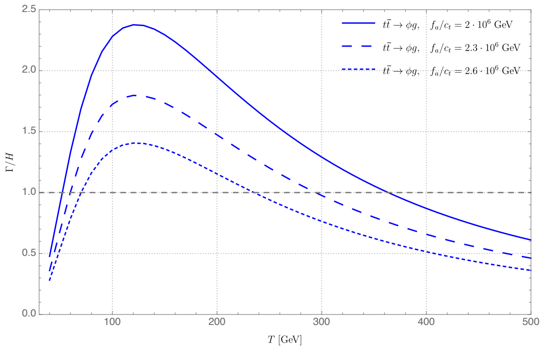

(a) $t\bar{t} \to g\phi$ *process.*

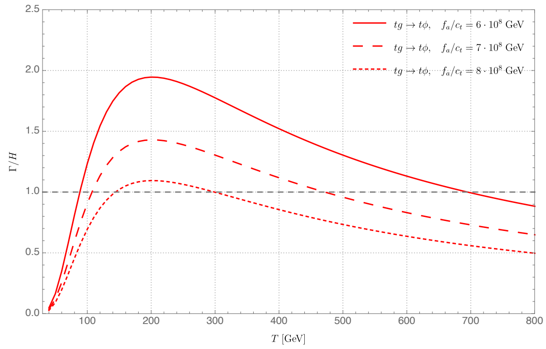

(b) $t(\bar{t})g \to t(\bar{t})\phi$ *process.*

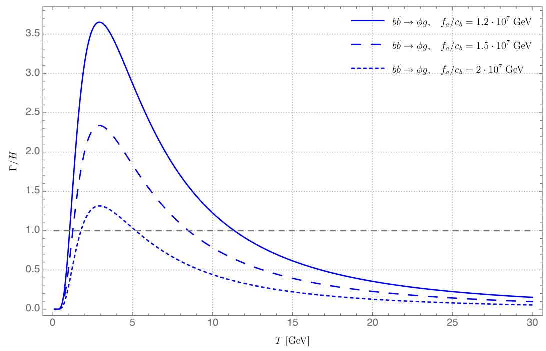

(c) $b\bar{b} \to g\phi$ *process.*

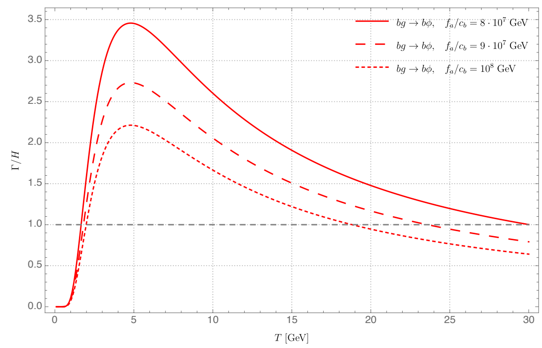

(d) $b(\bar{b})g \to b(\bar{b})\phi$ *process.*

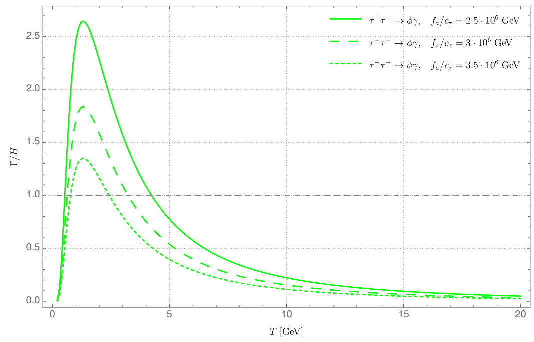

(a) $\tau^+\tau^- \to \gamma\phi$ *process.*

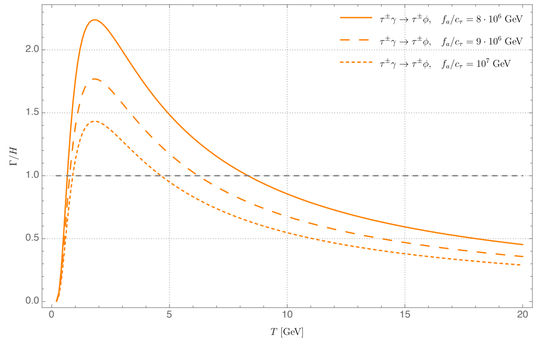

(b) $\tau^\pm\gamma \to \tau^\pm\phi$ *process.*

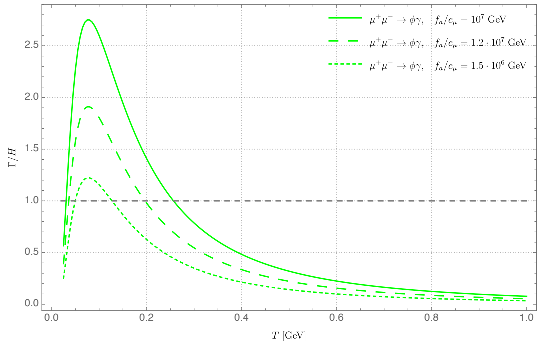

(c) $\mu^+\mu^- \to \gamma\phi$ *process.*

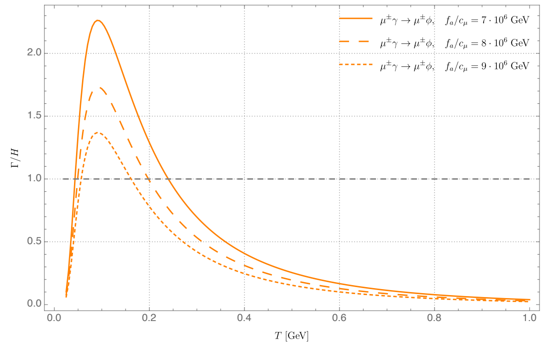

(d) $\mu^\pm\gamma \to \mu^\pm\phi$ *process.*

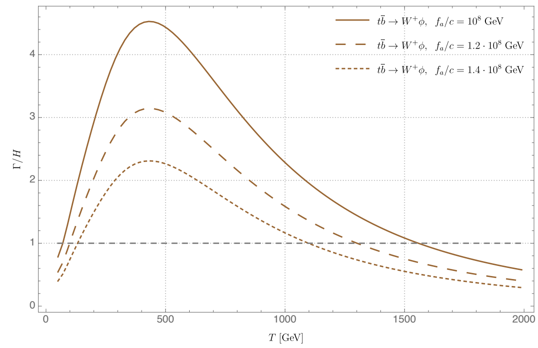

(a) $t\bar{b} \to W^+\phi$ *process.*

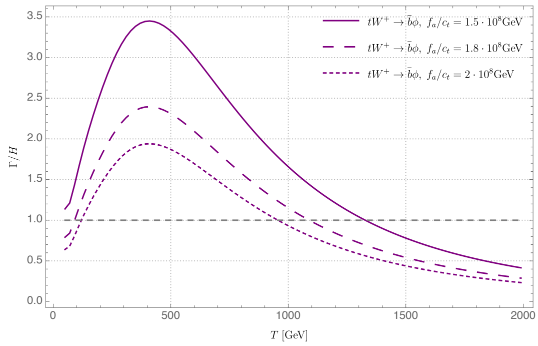

(b) $tW^+ \to \bar{b}\phi$ *process.*

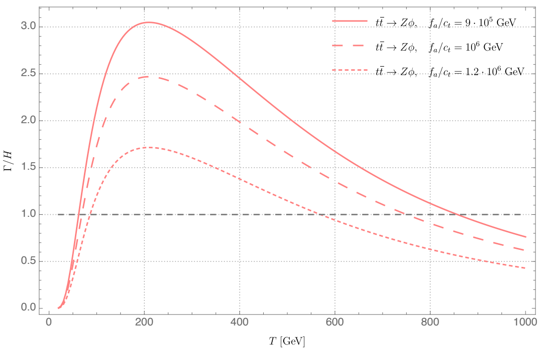

(c) $t\bar{t} \to Z\phi$ *process.*

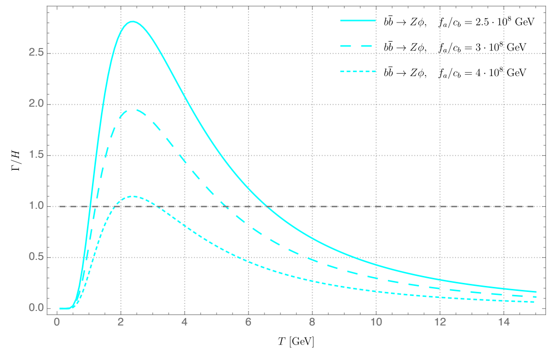

(d) $b\bar{b} \to Z\phi$ *process.*

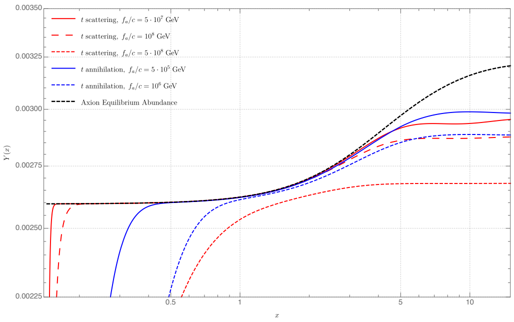

(a) *Top-gluon processes.*

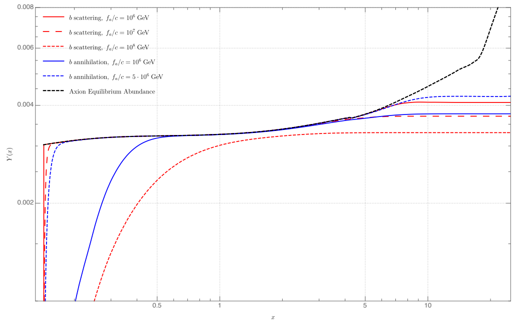

(b) *Bottom-gluon process.*

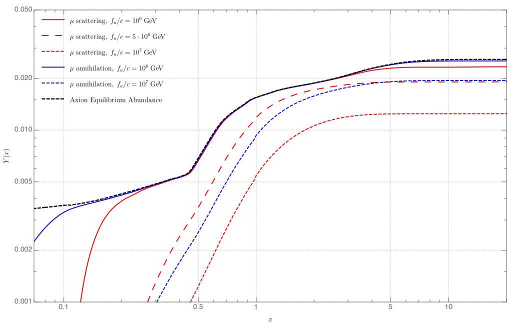

(a) *Muon-photon processes.*

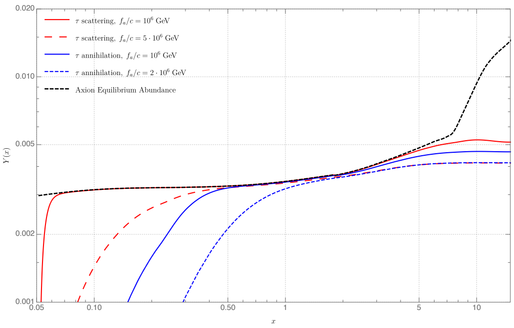

(b) *Tau-photon processes.*

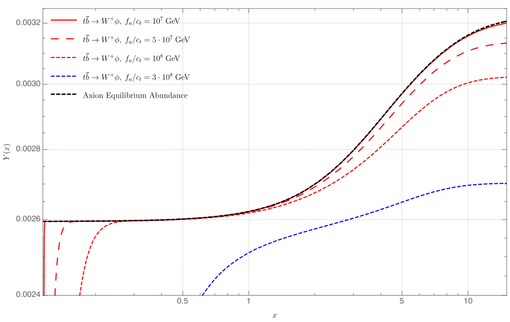

(a) $t\bar{b} \to W^+\phi$ *process.*

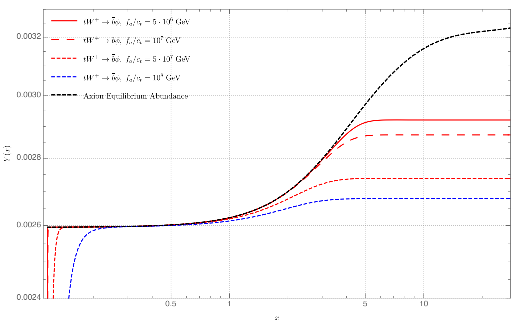

(b) $tW^+ \to \bar{b}\phi$ *process.*

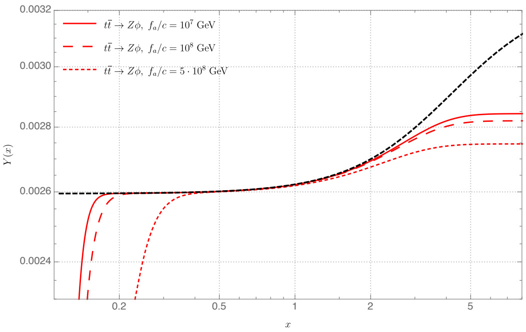

(a) $t\bar{t} \to Z\phi$ *process.*

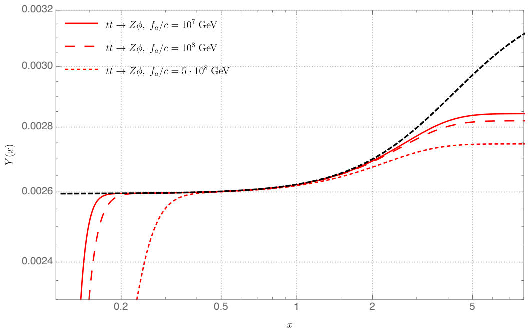

(b) $b\bar{b} \to Z\phi$ *process.*

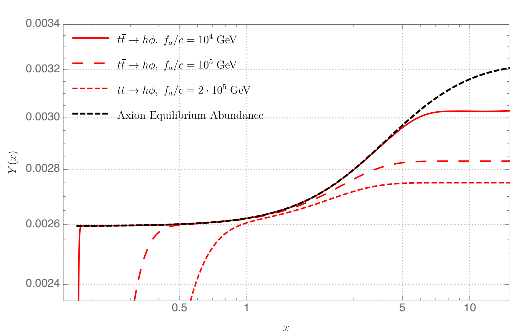

(a) $t\bar{t} \to h\phi$ *process.*

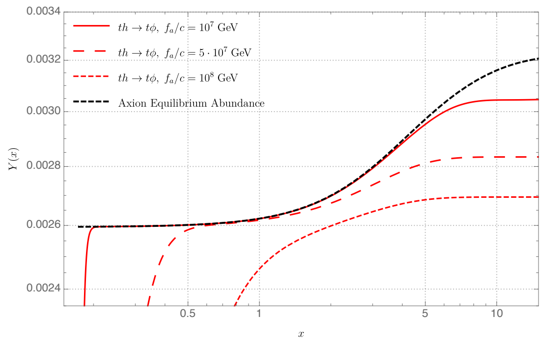

(b) $th \to t\phi$ *process.*

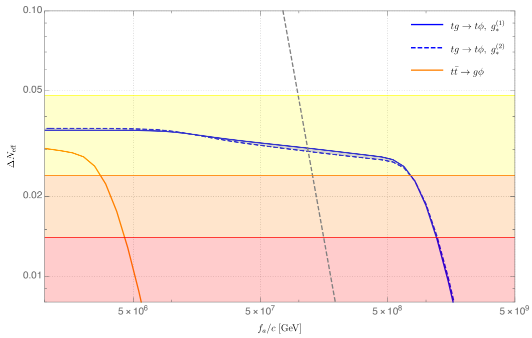

(a) *Top-Gluons.*

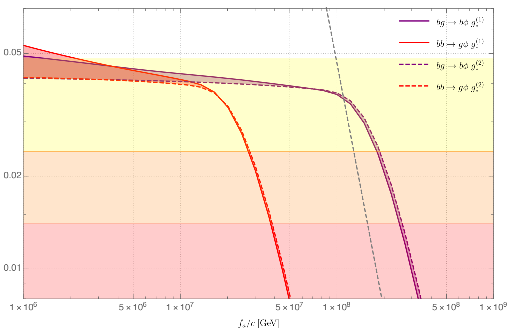

(b) *Bottom-Gluons.*

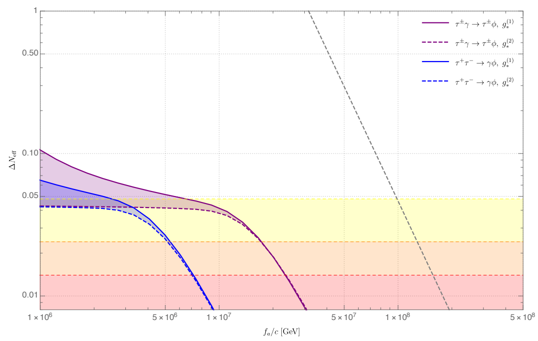

(a) *Tau-Photons.*

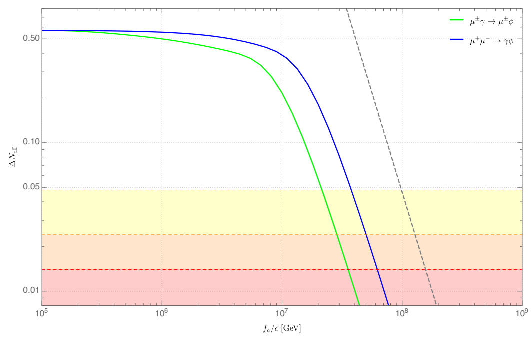

(b) *Muon-Photons.*

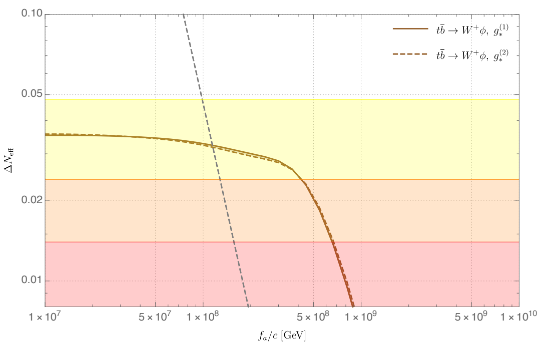

(a) $t\bar{b} \to W^{+}\phi$ *process.*

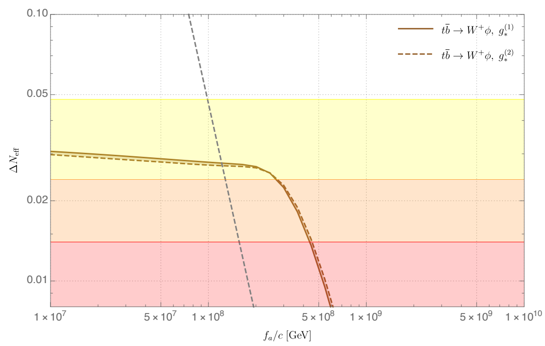

(b) $tW^{+} \to \bar{b}\phi$ *process.*

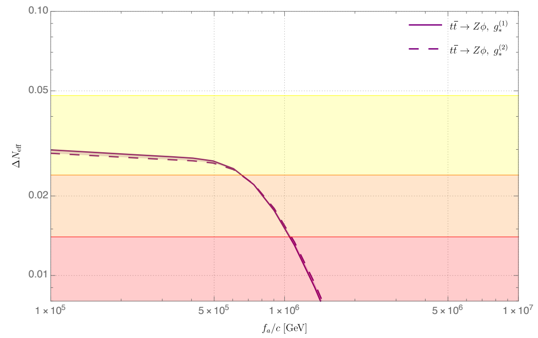

(a) *Top-Z annihilation.*

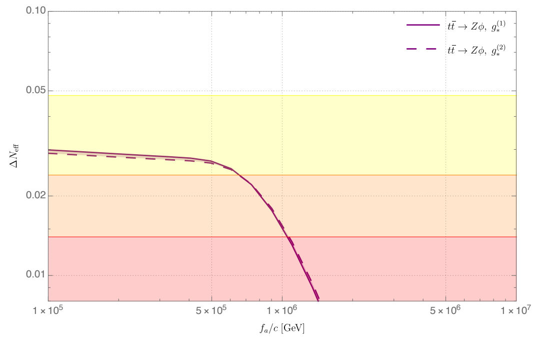

(b) *Bottom-Z annihilation.*

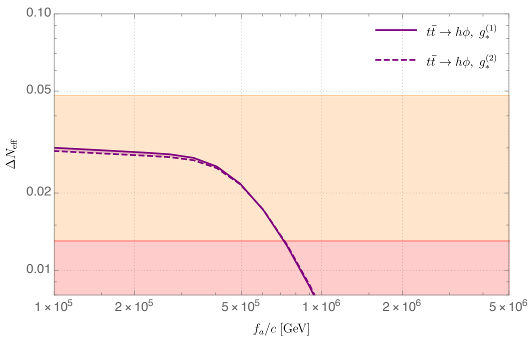

(c) *Top-h annihilation.*

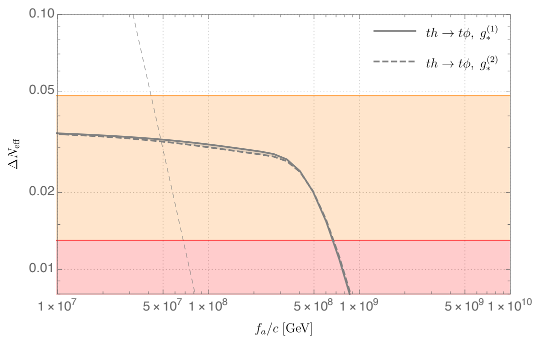

(d) *Bottom-h annihilation.*

Bibliography

[1] Edward W. Kolb, Michael S. Turner, *The early Universe*, Taylor & Francis Inc, 1994.

[2] Michael E. Peskin, Daniel V. Schroeder, *An Introduction To Quantum Field Theory*, Taylor & Francis Inc, 1995.

[3] S. Coleman, *Aspects of symmetry*, Cambridge University Press, 1985.

[4] V. Rubakov, *Classical theory of gauge fields*, Princeton University Press, 2002.

[5] A. Vilenkin, E.P.S. Shellard, *Cosmic strings and other topological defects*, Cambridge University Press, 1994.

[6] Kuster, Markus, Raffelt, Georg, Beltrán, Berta (Eds.), *Axions: Theory, Cosmology, and Experimental Searches*, Springer, 2008.

[7] G. 't Hooft, *How Instantons Solve the U(1) Problem*, [Phys. Rept. 142 357-387 (1986)]

[8] S. Weinberg, *U(1) problem*, [Phys. Rev. D 11, 3583]

[9] R. D. Peccei, H. R. Quinn, *CP Conservation in the Presence of Pseudoparticles*, [Phys. Rev. Lett. 38, 1440]

[10] R.D. Peccei, *The strong CP problem and axions*, [arXiv:hep-ph/0607268]

[11] Michael Dine, *TASI lectures on the strong CP problem*, [arXiv:hep-ph/0011376]

[12] Stefan Scherer, Matthias R. Schindler, *A Chiral Perturbation Theory Primer*, [arXiv:hep-ph/0505265]

[13] Gilberto Colangelo, Gino Isidori, *An introduction to CHPT*, [arXiv:hep-ph/0101264]

[14] Anees V. Manohar, *Effective field theories*, [arXiv:hep-ph/9508245]

[15] C. Amsler et al., *Particle Data Group* (2008), [PL B667]

[16] M. Tanabashi et al., *Particle Data Group* (2018), [Phys. Rev. D 98, 030001]

[17] I. G. Irastorza, J. Redondo, *New experimental approaches in the search for axion-like particles*, [arXiv:1801.08127]

[18] David J. Gross, Robert D. Pisarski, Laurence G. Yaffe, *QCD and instantons at finite temperature*, [Rev. Mod. Phys. 53, 43]

[19] Giovanni Grilli di Cortona, Edward Hardy, Javier Pardo Vega, Giovanni Villadoro, *The QCD axion, precisely*, [arXiv:1511.02867]

[20] T. Schaefer, E. Shuryak, *Instantons in QCD*, [arXiv:hep-ph/9610451]

[21] S.-H. Henry Tye, Sam S.C. Wong, *The Chern-Simons Number as a Dynamical Variable*, [arXiv:1601.00418]

[22] Adel Bilal, *Lectures on Anomalies*, [arXiv:0802.0634]

[23] David J. E. Marsh, *Axion Cosmology*, [arXiv:1510.07633]

[24] Olivier Wantz, E.P.S. Shellard, *Axion Cosmology Revisited*, [arXiv:0910.1066]

[25] Particle data group, *Axions and other similar particles*, [PDG Rev.]

[26] Ricardo Z. Ferreira, Alessio Notari, *Observable windows for the QCD axion through N_{eff}*, [arXiv:1801.06090]

[27] Francesco D'Eramo, Ricardo Z. Ferreira, Alessio Notari, José Luis Bernal, *Hot Axions and the H_0 tension*, [arXiv:1808.07430]

[28] E. Masso, F. Rota, G. Zsembinszki, *On Axion Thermalization in the Early Universe*, [arXiv:hep-ph/0203221]

[29] Peter Graf, Frank Daniel Steffen, *Thermal axion production in the primordial quark-gluon plasma*, [arXiv:1008.4528]

[30] Alberto Salvio, Alessandro Strumia, Wei Xue, *Thermal axion production*, [arXiv:1310.6982]

[31] Lars Husdal, *On Effective Degrees of Freedom in the Early Universe*, [arXiv:1609.04979]

[32] P. Sikivie, *Axion Cosmology*, [arXiv:astro-ph/0610440]

[33] R.L.Davis, *Cosmic axions from cosmic strings*, [Physics Letters B Volume 180, Issue 3]

[34] D. Harari, P. Sikivie, *On the Evolution of Global Strings in the Early Universe*, [Phys. Lett. B195 (1987)]

[35] S. Profumo, *An introduction to particle dark matter*, World Scientific, 2017.

[36] Dario Buttazzo, Giuseppe Degrassi, Pier Paolo Giardino, Gian F. Giudice, Filippo Sala, Alberto Salvio, Alessandro Strumia, *Investigating the near-criticality of the Higgs boson*, [arXiv:1307.3536]

[37] S. Hannestad, A. Mirizzi, G. Raffelt, *New cosmological mass limit on thermal relic axions*, [arXiv:hep-ph/0504059]

[38] G. Raffelt, *Particle Physics from Stars*, [arXiv:hep-ph/9903472]

[39] Sanghyeon Chang, Kiwoon Choi, *Hadronic axion window and the big-bang nucleosynthesis*, [arXiv:hep-ph/9306216]

[40] Yvonne Y.Y. Wong, *Axions*, Lecture slides from COSMO2011, Porto (2011), [COSMO2011]

[41] K. Saikawa et al., *Production and Evolution of Dark Matter Axions in the Early Universe*.

[42] CMB-S4 Collaboration, *CMB-S4 Science Book, First Edition*, [arXiv:1610.02743]

[43] Günther Dissertori, *The Determination of the Strong Coupling Constant*, [arXiv:1506.05407]

[44] D. Baumann, D. Green, J. Meyers, B. Wallisch, *Phases of New Physics in the CMB*, [arXiv:1508.06342]

[45] M. Laine and Y. Schroder, *Quark mass thresholds in QCD thermodynamics*, [arXiv:hep-ph/0603048]

[46] S. Borsanyi et al., *Lattice QCD for Cosmology*, [arXiv:1606.07494]

[47] W. L. K. Wu, J. Errard, C. Dvorkin, C. L. Kuo, A. T. Lee, P. McDonald, A. Slosar, O. Zahn, *A Guide to Designing Future Ground-based CMB Experiments*, [arXiv:1402.4108]

[48] K.N. Abazajian et al., *Neutrino Physics from the Cosmic Microwave Background and Large Scale Structure*, [arXiv:1309.5383]

[49] Georg G. Raffelt, *Astrophysical Axion Bounds*, [arXiv:hep-ph/0611350]

[50] C. Hagmann, S. Chang, P. Sikivie, *Axion Radiation from Strings*, [arXiv:hep-ph/0012361]

[51] R. Barbieri, C. Braggio et al., *Searching for galactic axions through magnetized media: the QUAX proposal*, [arXiv:1606.02201]

[52] I. G. Irastorza et al., *Towards a new generation axion helioscope*, [arXiv:1103.5334]

[53] J. K. Vogel et al., *IAXO-The International Axion Observatory*, [arXiv:1302.3273]

[54] MADMAX Working Group, *Dielectric Haloscopes: A New Way to Detect Axion Dark Matter*, [arXiv:1611.05865]

[55] B. Majorovits, J. Redondo, *MADMAX: A new Dark Matter Axion Search using a Dielectric Haloscope*, [arXiv:1611.04549]

[56] P. Sikivie, *Experimental Tests of the "Invisible" Axion*, [Phys. Rev. Lett. 51, 1415]